# Energy Management System Design for Plug-in Hybrid Electric Vehicle Based on the Battery Management System Applications

Ning Ding

A thesis submitted to

Auckland University of Technology

In fulfilment of the requirements for the degree of

**Doctor of Philosophy (PhD)**

**2020**

School of Engineering

# Abstract

The Energy Management System (EMS) applied in battery management system (BMS) plays the decisive role in effectiveness and proper operation of any hybrid energy storage system. Without significant advances in the state-of-the-art of BMS techniques, the future uptake of hybrid electric/electric vehicle applications are not feasible. Therefore, this thesis aims to provide a coherent body of work on the enhancement of the most important tasks performed by a modern BMS, which includes the hybrid EMS design and State of Charge (SoC) estimation.

The premeditated EMS adopted groups of rules to determine the operation state of different components. The main advantage of premeditated EMS is less computational burden and easy to apply. A novel rule-based control strategy is proposed throughout this thesis to decrease the emission and increase the fuel economy. Then, an optimization using genetic algorithm (GA) is applied on the designed rule-based control strategy to improve the vehicle performance and achieve reduction of fuel consumption and emissions at the same time. This hybrid EMS combined the rule-based control strategy and its optimization is verified through a bi-directional simulation. The hybrid electric vehicle (HEV) model and the input of load condition adopted in the simulation are based on the real data to close to the practical implementations. In addition, an improved extended Kalman Filter (iEKF) is designed to provide high-accuracy SoC estimation of battery. The SoC estimation is considered as a dynamic identification process of the parameters of battery model and it significantly relies on the battery model. This estimator with iEKF algorithm adopts a composite battery model, which combines the method of open-circuit voltage (OCV) (to obtain an initial value of parameters), Amp-hour (Ah) method (to dynamically

identify the parameters), and the extended Kalman Filter (to improve the accuracy) . There are five groups of experiments conducted on Lithium-based cell, to provide the data for parameters identification. Finally, the proposed estimator with iEKF algorithm is simulated in MATLAB_Simulink to show the effectiveness of the proposed SoC estimation in BMS.

# Acknowledgement

With the sincerest gratitude in my heart, I would like to thank my academic supervisors, Professor Krishnamachar Prasad and Professor Tek Tjing Lie. I would not have been able to complete this thesis without their generous support and encouragement. I would like to acknowledge the patience and commitment from Professor Prasad in guiding me to nudge my ideas towards clear and mature research throughout these years. Also, big thanks to my secondary supervisor Professor Tek Tjing Lie for his valuable and heuristic suggestions regarding the work despite his busy schedule.

This research could never have been possible without the everlasting moral support from my family and friends around me, who have always created a positive environment for me to complete my PhD studies. I wish to give my special thanks to AUT and the School of Engineering, Computer and Mathematical Sciences staff who have blessed me with their technical and moral support throughout my research. Finally, I would like to acknowledge the technical supporting from CRRC Corporation limited.

# Attestation of Authorship

I hereby declare that this submission is my own work and that, to the best of my knowledge and belief, it contains no material previously published or written by another person (except where explicitly defined in the acknowledgements), nor material which to a substantial extent has been submitted for the award of any other degree or diploma of a university or other institution of higher learning.

Signed

Date 03/03/2020

# Table of Contents

# List of Figures

# List of Tables

# Lists of Abbreviations

Accumulator (ACC)

Adaptive unscented Kalman Filter (AUKF)

Advanced Vehicle SimulatOR (ADVISOR)

Alternating Current (AC)

Artificial Intelligence (AI)

Adaptive Kalman Filter (AKF)

Brushed DC (BDC)

Battery Electric Vehicles (BEVs)

Brushless induction (BLI)

Brushless permanent magnet (BLPM)

Battery Management System (BMS)

Battery Management Units (BMU)

Brushless switched reluctance (BLSR)

Controller Area Network (CAN)

Carbon dioxide ($CO_2$)

Charge Depletion (CD)

Crossover Probability ($P_c$)

Charge Sustaining (CS)

Cell Supervising Sensor Units (CSSU)

Direct Current (DC)

Direct Current Resistance (DCR)

Dual Kalman Filter (DKF)

Depth-of-discharge (DOD)

Dynamic Programming (DP)

Electronic Control Units (ECU)

Equivalent Circuit Model (ECM)

Equivalent Consumption Minimization Strategy (ECMS)

Electrochemical Impedance Spectroscopy (EIS)

Electric Motor (EM)

Energy Management System (EMS)

Energy Storage Unit (ESU)

Extended Kalman Filter (EKF)

Extreme Learning Machine (ELM)

Enhanced self-correcting (ESC)

Electric Vehicle (EV) Electric Vehicles (EVs)

Fuel Consumption (FC)

Fuel cells (FCs)

Fuel Cell Electric Vehicles (FCEVs)

Fuel Economy (FE)

Genetic Algorithm (GA)

Genetic-based bacteria foraging (GBF)

General Non-linear (GNL)

Hybrid Electric Vehicles (HEVs)

Hybrid Dynamic System (HDS)

Hybrid Pulse Power Characterization (HPPC)

Hydraulic Hybrid Vehicle (HHV)

Internal Combustion Engine (ICE)

improved Extended Kalman Filter (iEKF)

Insulate Gate Bipolar Transistor (IGBT)

Kalman Filter (KF)

Lithium Iron Phosphate ($LiFePO_4$)

Lithium Nickel-Cobalt Manganite (NCM)

Lithium Titanite ($Li_2TiO_3$/LTO)

Learning Vector Quantization (LVQ)

Miles per Gallon (MPG)

Motor Control Unit (MCU)

Model Predictive Control (MPC)

Mutation Probability ($P_m$)

Nitrogen-oxide compounds ($NO_x$)

New Generation of Vehicles (PNGV)

Nickel-metal hybrid (NiMH)

Neural Networks (NN)

Number (size) of Population (NP)

Open Circuit Voltage (OCV)

Particle Swarm Optimization (PSO)

Plug-in Battery Electric Vehicles (PBEVs)

Plug-in Electric Vehicle (PEVs)

Plug-in Hybrid Electric Vehicles (PHEVs)

Pontryagin's minimum principle (PMP)

Random Access Memory (RAM)

Range-extended Electric Vehicles (REVs)

Recursive Least Squares (RLS)

Stochastic Dynamic Programming (SDP)

State of Charge (SoC)

State of Health (SoH)

State of Power (SoP)

Selection Probability ($P_s$)

Signal-noise Ratio (SNR)

Sequential Quadratic Programming (SQP)

Support vector Machine (SVM)

U.S. Advanced Battery Consortium (USA BC)

Unscented Kalman Filter (UKF)

Vehicle Control Unit (VCU)

# Chapter 1 Introduction

This chapter briefly introduces the background and explains the motivation of this thesis. It presents an overview of the research issues and challenges in the field of electric vehicles (EVs), especially the energy management system (EMS) or battery management system (BMS) in EVs. This chapter also gives an outline for the structure of the thesis. The contributions and the novelty of work in this research is succinctly listed at the end of this chapter.

## 1.1 Background

Automobiles have become an indispensable means of transportation. The daily vehicle usage and the automotive manufacturing market are dominated by the traditional automobile. However, the high usage of internal combustion engine (ICE) in the traditional automobile will inevitably lead to more pollution. Petrol as the main power source in ICE of the traditional automobile aggravates the excessive consumption of resources, especially non-renewable energy, such as the fossil fuels. Various national governments have enforced vehicle emission regulations for environmental issues. The harmful components in the exhaust gas from individual units should be less than the prescribed threshold values under different regulations for vehicle emission in any country. The exhaust gas produced by burning of petrol from ICE is completely discharged into the atmosphere. The Carbon dioxide ($CO_2$) in the exhaust gas causes the Greenhouse Effect; the Nitrogen-oxide compounds ($NO_x$) destroy the Ozone layer; the sulphides lead to acid rain, which will seriously impact the ecological environment [1]. The reserves of fossil energy are decreasing at an alarming level and the

environmental pollution is getting worse with the social progress and economic development [2]. For energy conservation and environmental protection, the development of an eco-friendly vehicle has become mandatory.

The EV refers to a vehicle driven by an electric motor and powered by an on-board battery package [3]. The general classifications of the EVs mainly include the Hybrid Electric Vehicles (HEVs), Battery Electric Vehicles (BEVs) and Fuel Cell Electric Vehicles (FCEVs). Compared to the conventional ICE automobile, there are serval advantages for EVs. The battery powers the electric motor (EM) to drive the vehicle and there is no pollution in the process. The motor works smoothly with little or no noise. Compared to the ICE, the working efficiency of the EM is higher. The EVs could be charged at night to take advantage of the 'valley power' of the grid. In addition, the maintenance of EM is simple and convenient. The ICE regularly requires replacing the engine oil and filter, while the EM needs only a lubricant [3, 4].

### 1.1.1 The Global Trend of EVs

The development of renewable-EVs is a primary task for worldwide automotive manufacturers. The data released by EV sales indicate that the rapid progress of EV market in recent years is mainly due to the surge of EV-related industries in Europe, United States and Asian markets dominated by China [5]. Various countries have formulated relevant laws and regulations to promote the development of renewable-energy vehicles [6]. The Paris Agreement was signed by approximately 200 parties in United Nations Framework Convention on Climate Change in 2015, which plans to deploy 100 million EVs by 2030 [7]. International Energy Agency proposed that the market of EVs will grow to 150 million by 2030 and 1 billion by 2050 [8].

The governments of various countries proposed incentives for EVs, which have promoted the sales growth and the development of technologies related to EVs. Major auto producers are steadily pushing forward the energy transformation in the field of transportation. According to the data collection reported by EV sales [9], in terms of the global market, the total number of EVs exceeded 2 million in 2018. At the same time, the sales of EVs accounted for more than 2.1% of global auto sales. The sales of EVs in 2018 were up 72% compared to 2017. The main market of the EVs sales is dominated by plug-in electric vehicle (PEVs), which include the plug-in battery electric vehicles (PBEVs) and plug-in hybrid electric vehicles (PHEVs).

Norway is the main EV market in Europe and a pioneer in the field of Carbon-free transportation worldwide. The data published in International Energy Agency [10] showed the sale of PBEVs and PHEVs in Norway in 2018 increased by 31.2% and accounted for 32% of total vehicle sales compared to 2017. According to the report from Nordic Energy Research [11], the Norwegian EV market share is expected to exceed 50% in 2019. The EV market share in Norway has reached the highest level in the world. Norway plans to ban traditional fuel vehicles by 2025. Similarly, France has announced the prohibition of fuel car by 2040. France is vigorously building the supporting construction of charging piles. The French government levies taxes on vehicles based on Carbon: when the Carbon emissions are less than 60g/km, a subsidy is granted (up to 6000 euros): otherwise, a tax is levied [12]. The German government implements a tax reduction policy for the owners of “zero-emission” vehicles to promote the new energy vehicles. Germany expects to reach one million new energy vehicle population by 2020 [12].

The US government lists the development of new energy vehicles as a national strategy. Both the customers and the new energy vehicle manufactures could receive certain amounts of subsidies from the US government. Meanwhile, the US government encourages investment in the battery technology industry and the purchase of the new energy vehicles. The main incentives include exempting the emission test and expanding the privilege of EVs [13, 14].

In Asia [15], Japan attaches importance to the new energy vehicles. In 2020, the market share of EVs and HEVs will reach 15% in Japan. The Japanese government encourages research institutions to conduct research on the power battery of EVs. The major auto companies have launched corresponding development plans [16] for EVs such as Toyota, Honda and Nissan. South Korea has increased research and investment in the batteries to meet the increasing needs of new energy vehicles. Automobile industry is the pillar of the national economy in China. The production and sales of the new energy vehicles in China have continued to grow in the last five years. The sales of new energy vehicles increased to 40% in 2018 [17]. The Chinese government has implemented subsidies and tax reduction polices for customers and manufactures of new energy vehicles since 2008 [12]. China plans to exceed five million units of PEVs by 2020, while the sales of new energy vehicles have accounted for 10% of the total vehicle sales [18].

### 1.1.2 The Current EV Technology

With the progress of the EV-related technologies, the performance of EVs is improving and gradually meeting the demands of most customers. Meanwhile, the manufacturing cost of EVs is continuously decreasing. As the representative of the

advanced technologies/products in the PBEVs industry, the charging system of Tesla Model S [19] supports three charging methods- Direct Current (DC) fast charging on the super charging pile, high power wall hanging charging and 220 V household socket charging. The battery pack (85 kWh) is composed of more than 7000 individual battery units in a series and parallel connection configuration. The battery equalization adopts the passive equalization approach and the equalization current is 0.1 A. The representative of range-extended electric vehicles (REVs) is BMW i3 [20]. The BMW i3 [20, 21] is also using Lithium battery pack to power the vehicle. The maximum endurance mileage of the BMW i3 is 271 kms under full charge, while the highest speed can reach 150 km/h. Meanwhile, the BMW i3 realized fast charging function, from 0% to about 80% in one hour. Nissan Leaf is reported as one of the most popular PBEV in recent EV market [22]. Two different types of battery cell have been adopted in Nissan Leaf for the versions released in the Asian and the European markets, respectively. The battery cell for European market uses the Nickel Cobalt Manganite (NCM266) - the battery pack consists of 24 modules and each module includes 8 cells, 192 cells in total. The rated terminal voltage is 360 V and the weight is 249 kg. The output power of the EM is 80 kW, the maximum torque is 280 Nm and the range is 160 kms. The fast charging function achieves 80% charging within half an hour. The version for the Asian market uses the ternary Lithium. The constant speed range enables the range to be 389 kms. The Asian Nissan Leaf has fast and slow charging modes - the fast charging mode is the same as the European version while the slow charging mode can achieve full charge in 8 hours. The Toyota Prius is reported as the one of the most popular of PHEVs [23-25]. In terms of the propulsion, Toyota Prius

adopts both ICE (1.8 L) and EM. The THS-III system achieved an effective series-parallel drive based on power split. The power of ICE is divided by the THS-III system - one part is directly used to drive the vehicle while another part is used to generate the electricity to drive the EM. The ratio of the divided power can be adjusted arbitrarily according to the different working conditions. 8.8 kWh Lithium battery pack singly supplies the power to the pure-electric driving mode of Toyota Prius, which has a maximum range of 35 kms and the highest speed of 135 km/h. Because of hybrid propulsion, the battery with small capacity of Toyota Prius can be fully charged in a short time [23-25].

With the rapid development of EV technology and related industries, the battery technology, as the leading force for the EV development, has made significant progress globally. The commonly used battery for EVs mainly includes the Lead-acid batteries, NiMH batteries, Lithium Iron Phosphate ($LiFePO_4$) batteries, ternary Lithium batteries and Lithium Titanite ($Li_2TiO_3$/LTO) batteries [26]. Table 1.1 lists the performance of the different mainstream battery types in common usage for EVs in the current era [27, 28]. It is defined as the discharge current divided by the theoretical current draw under which the battery would deliver its nominal rated capacity in one hour.

Table 1.1 Performance comparison of common battery types.

| **Battery types** | Lead-acid | NiMH | $LiFePO_4$ | Ternary Lithium | LTO |
|---|---|---|---|---|---|
| Energy density (Wh/kg) | 40 ~ 60 | 60 ~ 100 | 70 ~ 120 | 150 ~ 250 | 70 ~ 80 |
| Discharge rate | 2 C | 3 C | 5 C | 2 C | 6 C |
| Cycle life (times) | 300 | 400 | 2000 | 500 ~ 1000 | 25000 |

Battery is the decisive factor in the performance of EVs. However, existing battery materials still have limitations in energy/power density, which affect the charging/discharging performance. According to the information listed in Table 1.1, the energy density, discharge rate and lifetime of the vehicle batteries are gradually increasing with more extensive battery material research and applications. Lithium-based batteries are increasingly popular due to the advantages of high energy/power density, longer lifetime, less self-discharge and wide temperature range [29, 30]. The $LiFePO_4$ and ternary Lithium batteries are the most commonly used in EVs now [31, 32]. The $LiFePO_4$ battery has good safety performance. The $LiFePO_4$ battery such as BYD Song DM and BJEV EC180 has been widely used in passenger vehicles because of high power density and high temperature resistance [33]. The anode material of ternary Lithium battery is Nickel-Cobalt Manganite (NCM). The high energy density of ternary Lithium shows advantages in higher cruising range [34]. The BEVs produced by Tesla are powered by ternary Lithium battery in type 18650 [35]. Similarly, BMWi3, Volkswagen E-Golf and BJEV EV200 use the ternary Lithium battery to achieve higher cruising range [36, 37]. The LTO battery is commonly used in electric bus because of the wide temperature range, good safety performance and fast charging characteristics.

In terms of the vehicle battery manufactures, significant progress has been made by Samsung SDI battery industry from South Korea [20, 38]. Several SDI battery plants located overseas are into large scale production. The LG Chem as one of the dominant battery suppliers has cooperated with several manufactures involved in EVs, such as Renault S.A. and AUDI. Besides, the SK Innovation and the PolyPlus Battery

Company from South Korea cooperatively researched and developed a Lithium metal battery with high energy density and longer lifecycle [39]. There are major breakthroughs in battery technology in China [40]. The development of EVs in China is mainly based on ternary Lithium battery [41]. Since 2012, China has vigorously developed the power battery for EVs, which has tripled the energy density of the Lithium-battery cell and the price dropped by 70% in 2017.

The main difference between the EV and traditional car is the use of electricity to drive the EV. Lithium-based batteries have higher energy/power density among many types of rechargeable batteries. The Lithium-based battery is tipped to be the dominant player in the current battery market. There are still many restrictions on the use of the battery. The Lithium-based battery without protection is prone to excessive charge/discharge and overheating, which will have a great impact on the performance of the battery [42]. According to the characteristics of the different types of Lithium-based batteries, the effective management of the different working modes and states of battery pack poses a significant issue. The normal operation of vehicular Lithium-based battery pack partially depends on a matched BMS. The coordinative works between the battery pack, the EM, and the engine are mainly achieved by the BMS or EMS [43].

Figure 1.1 shows a summary of general BMS for EVs [44, 45]. The function of monitoring is to collect the voltage, current and temperature information of the battery. The battery information monitoring should be accurate and reliable because it is the basis for all the other works of the BMS, for example the State of Charge (SoC)

estimation. The protection function is mainly to avoid overcharge/discharge and over-temperature working. In particular, Lithium-based battery is prone to damage in the case of overcharge/discharge such as capacity attenuation and can lead to burning to explosion [46].

The EMS plays an important role in BMS, which determines the different working states (charge/discharge) between the battery and other components such as the EM or the engine. At the same time, due to the electrochemical characteristics of the battery, the voltage of the cells is changing dynamically during the energy transfer.

The high difference among the cell voltage decreases both stability and safety. Therefore, the equalization control of the battery plays a significant part in the EMS. The main purpose of the EMS is to maximize the efficiency of the battery without any damage, which will depend on the different pathways of the control strategy [47, 48]. However, the control strategy is limited by the practical conditions during the EV running process. The optimization control is required to work cooperatively with the control strategy to improve the working efficiency of the battery.

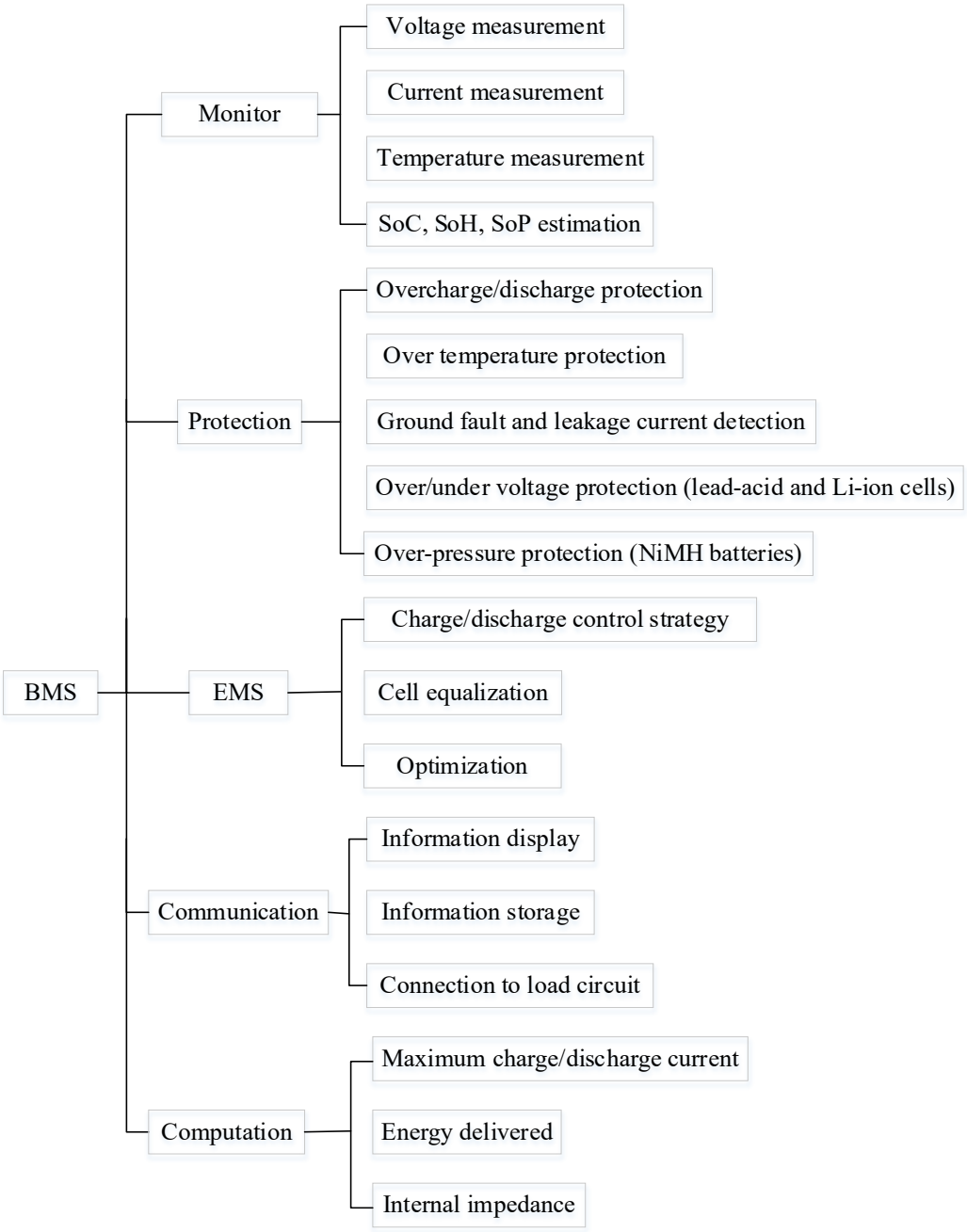


Figure 1.1 General functions of BMS.

The communication between various elements is essential. The different functions of BMS are achieved by different modules. The hardware, which includes the cell-controller (modular architecture) and controller-controller (distributed architecture), is properly managed by internal communication [47-49]. The external communication

connects the BMS and other electronic control systems; different types of communications such as the Controller Area Network (CAN) bus and wireless communications are often used [49]. In addition, the regular operation of the BMS requires some necessary calculations such as maximum charge/discharge current, number of cycles, the operating time of the battery, the internal impedance and the energy delivered in one charge cycle and the total energy delivered since the first use.

For the BMS related products, many EV companies mainly in the US, Germany and Japan are involved in the BMS research and production. The SmartGuard system developed by Aerovironment in the US is an early representative product of BMS [50]. An integrated chip is used in the SmartGuard system to measure the voltage and temperature of the battery. The BatOpt designed by AC Propulsion Company collects the battery information through a bussing technique. The majority of the research institutions in the US focus on the battery performance for the BMS design [51]. For example, the designed BMS based on the battery decay effectively avoids the working mode which can lead to rapid battery deterioration [51]. The basic functions of different BMS design are similar. However, the implementation is different. Germany, which dominates the European market for EVs, has developed sophisticated BMS of its own. A BMS of BATTMAN manages different types of batteries by setting up both the hardware and software. The BMS of BADICHEQ and BADICOACH was designed by Electronic GmbH and Werner Retzlaff [52, 53]. In terms of the battery equalization, the BADICHEQ includes an additional EM to charge the cell to decrease the difference. The BADICOACH is an improvement on the BADICHEQ, which enhances the functions of monitor and communication to obtain a faster response. The

Preh Company from Germany has spent years developing vehicular components and control systems [54]. They designed an effective BMS for the BEV of BMW i3, which includes the electronic control unit (ECU) of the battery management unit (BMU) and cell supervising sensor unit (CSSU). The CSSU monitors the voltage and temperature of the battery in real-time while the measured data is processed by the BMU. In Japan, research related to BMS has been conducted since 1990s [55]. Toyota began researching on the BMS for EVs more than a decade ago [56]. Their research studied different types of batteries and compared the control strategies based on many groups of contrast tests. The BMS design in Prius of Toyota has an advanced thermal management system - the temperature distribution of the battery can be balanced by evacuating the excess heat to keep a reasonable temperature environment [57].

## 1.2 Motivation

From the background information provided in section 1.1, it can be seen that the global popularity of EVs is an irresistible trend. However, the open and pressing issues in efficiency, cost and safety for the EVs are significant in terms of research. The current challenges of EV related technologies includes three main aspects:

- The vehicle control technology:

  The vehicle control unit (VCU) is the core unit to decide the different working modes by collecting the signals from the accelerator pedal, the brake pedal and the gear, which respond to the driving requirements in different operating conditions. The operating modes of different types of the EVs vary from each other and strongly rely on the battery pack. For example, the power demands and energy transmission of the electric bus are different from that of small-size

passenger vehicle. The challenge of the VCU technology is to seek an optimal control strategy amongst the battery pack, the driving system and the vehicle, which achieve the purpose of energy conservation and emission reduction when meeting the driving demands.

- The motor control technology:

  The motor control unit (MCU) controls the energy transmission between the battery pack and the EM. The controlled objects mainly include the EM, DC/DC converter, vehicle-mounted charger and the electric air-conditioning system. To control the voltage, current, phase sequence and frequency of the three-phase input AC, the MCU adjusts the performance of EM to obtain an appropriate speed, torque, steering and to increase the efficiency of the braking energy recovery system. The MCU is the core component for motor driving, which is facing the issues of high integrated and high voltage design. The voltage endurance capability of the insulated gate bipolar transistor (IGBT) for the MCU is currently developing systems in the range of 650 V to 750 V and even up to 1200 V.

- The BMS technology:

  The BMS is the core technology of the power battery pack to work with VCU and MCU cooperatively. The current difficulties of the BMS technology mainly include an accurate SoC estimation which is required to build a reliable battery model, the optimization of battery charge/discharge control algorithm which can improve the efficiency and provide a friendly working environment for the battery, an efficient control strategy of battery equalization which is

required for transferring from energy dissipative type to non-energy dissipative type, a sensitive temperature protection system which requires a cooling method with faster cooling speeds compared to the cold air system such as liquid cooling technology and an advanced self-diagnostic technology for BMS which prevents the failure of the BMS in advance.

Recognising the main technical issues listed above, the difficulties and challenges faced by the researchers to promote the EV technical industry are interdisciplinary. The main areas include control engineering, materials science, hardware/software design, optimization algorithms, *etc*.. The current material technology and production process of the battery have many limitations which reflect in the low charging rate, poor safety performance, low instantaneous power, low power/energy density and high cost. Moreover, there are many uncertainties and impact factors in the electrochemical reaction when the battery is in operation and the safety issues cannot be ignored. The BEVs strongly rely on the dynamic performance of the battery, while the PBEVs replenish battery power in the plug-in rechargeable method. This means an extensive establishment of the charging station is necessary, which brings a heavy economic burden. The widespread popularity of either BEVs or PBEVs seems difficult to achieve due to the limitations of the current vehicular battery and the huge investment of charging facility. HEVs are seen as a short-term transition from the traditional ICE automobile to BEVs. Both the engine and the battery provide the driving force while the HEVs do not entirely rely on the battery. The HEVs have the potential to ensure a good driving experience while saving energy and reducing emission. There are two types of energy transmission - mechanical and electric energy transmissions, which

demand an appropriate EMS to effectively engage the different working modes of the engine, EM and the battery.

## 1.3 Thesis Contribution

This thesis focuses on the EMS/BMS to control and monitor the battery aspects of the EV operation. The research presents a novel control strategy for PHEVs - an optimization based on genetic algorithm (GA) achieved significant reduction of the emission. The design and optimization of the EMS is verified by modelling and simulation according to the value of harmful gases emissions and fuel consumption. Meanwhile, the implementations of the designed and optimized EMS significantly rely on the SoC estimation. To increase the reliability and feasibility of the designed and optimized EMS, an improved extended Kalman filter (iEKF) has been designed to obtain an accurate SoC estimation. The battery model used in SoC estimation is based on real experimental data of Lithium Iron Phosphate ($LiFePO_4$) battery. The research presented in this thesis has resulted in three journal and one conference publications, with another journal paper currently under review.

**Journal publications:**

- Ding, N., Prasad, K. and Lie, T. T. (2017). The electric vehicle: a review. *International Journal of Electric and Hybrid Vehicles*, *9*(1), 49-66.
- Ding, N., Lie, T. and Prasad, K. (2017). The Design of Control Strategy for Blended Series-Parallel Power-Split PHEV–a Simulation Study. *International Journal of Transportation Systems*, *2*, 21-24.

- Ding, N., Prasad, K., Lie, T. T. and Cui, J. (2019). State of Charge Estimation of a Composite Lithium-Based Battery Model Based on an Improved Extended Kalman Filter Algorithm. *Inventions*, *4*(4), 66.

**Conference publication:**

- Ding, N., Prasad, K. and Lie, T. T. (2017, November). The potential Li 4 Ti 5 O 12 battery products applications for New Zealand electric buses. In *2017 24th International Conference on Mechatronics and Machine Vision in Practice (M2VIP)* (pp. 1-7). IEEE.

## 1.4 Aims and Objectives of the Thesis

The main aims and objectives of the thesis can be itemized as follows：

- To develop an efficient energy management system firstly using a rule-based control strategy. This is further improved by using Genetic Algorithms to achieve a better fuel economy and reduced emissions.

- To develop an accurate estimation of the State of Charge (SoC) of the battery. This is done by using improved Extended Kalman Filter (iEKF) approach. The approach also used real battery experimental data from a company which was used to build the battery model.

## 1.5 Thesis Organisation

This thesis is organized into several chapters.

**Chapter 1** gives the introduction of the thesis and discusses the motivations behind the research work for different objectives. Chapter 1 enables the readers to quickly understand the research difficulties and challenges in the field of EVs.

**Chapter 2** reviews the technologies in EVs, including the mainstream technologies of the battery models and energy transmission in various types of EVs. The background of the EMS is also provided, which is discretionary for developing an advanced control strategy for PHEVs. The modelling methods and experimental control for the characteristics of the different types of battery are discussed with a view to later development of the designed battery model. The optimization techniques are reviewed to form appropriate algorithms in EMS design, which can robustly optimize the designed control strategy to improve the performance such as the fuel economy. Finally, the state-of-art of the SoC estimation is reviewed to develop the monitoring function of BMS design in this thesis.

**Chapter 3** discusses the importance of the EMS for PHEVs. The control strategy as the core technology in EMS design mainly divided into adaptive algorithm and the control strategy with empiricism. A novel rule-based control strategy is demonstrated for the purpose of decreasing the fuel consumption and the emissions. Also, simulation studies of the design rule-based control strategy are proposed. The rule-based control strategy is implemented in a practical vehicle model using MATLAB.

**Chapter 4** presents and discusses a Genetic Algorithm (GA) for optimization. The algorithm will be used to optimize designed rule-based control strategy demonstrated in Chapter 3. The GA mathematical model built considering the scenarios in PHEVs.

The fitness functions are set based on the optimizing objectives of reducing the fuel consumption and emission. The group of the solutions in GA mathematical model is decided by a logical and mechanical controlling. The reasons for setting the parameter values is explained, which includes the initial population and genetic operator selection, crossover and mutation. A simulation study is conducted with same vehicle model and input of working conditions to compare the optimization results.

**Chapter 5** describes the battery models and estimation algorithm for the monitoring function in BMS. The different battery models are evaluated in terms of model complexity, ability of the voltage tracking and the model development efficiency. A novel composite battery model is developed according to the electrochemical empirical models. The composite battery model based on the real experimental data of the $LiFePO_4$ is built. The composite battery model showed an accurate voltage tracking and used to build the estimator. An iEKF algorithm is described for SoC estimation, which combined the Open Circuit Voltage (OCV), Ah counting method and the EKF methods. The simulation results showed that the iEKF is capable of an accurate online parameter identification based on the composite model, even under varying operating conditions. Moreover, the significant issues for SoC estimation applications in monitoring module for BMS are analysed at the end of this chapter. A comparative and improved SoC estimation model is proposed for these issues, which include a second-order RC equivalent circuit model (ECM) and Thevenin battery model.

**Chapter 6** draws a number of conclusions and summaries the contributions of this research work in terms of EMS and BMS. It also presents the scope for any future work in the areas of EMS, BMS and EVs.

# Chapter 2 Literature Review

The implementations of EVs and related technologies have made significant progress in recent years, due to the urgent demand for energy saving and emission reduction. The EMS and BMS play a decisive role for the development of all types of EVs. Advanced techniques in EMS and BMS are constantly evolving. This chapter, therefore, targets at providing a review of the cutting-edge technologies in the field of EVs. The characteristics of different types of EVs are analysed and the advantages and disadvantages of each type of EVs are compared. Thereafter, a comprehensive review on the EMS and optimization approaches is undertaken. Finally, the monitoring methods for BMS are discussed to provide the readers with a deeper understanding of the topic. The review on the EVs topologies presented in section 2.1.1, has been successfully published as a review paper [58], while other technical reviews in the chapter are collected based on many issues in the research field of EVs.

## 2.1 A Review of Electric Vehicles

The invention of EVs in 1881 preceded the petrol- or diesel- driven ICEV. In the early stages, pure electric driven technique was only applied in small vehicles such as golf karts due to the then limitations in the battery technology. At that time, the EVs accounted for ~38% of the market share, only ~2% behind the steam-engine vehicles. The diesel- and petrol-powered ICEVs have dominated the vehicle market since 1905. At the end of 19$^{th}$ century and early of 20$^{th}$ century, the development of lead-acid batteries and rechargeable nickel-cadmium batteries brought new opportunities for the development of EVs. In the years 1990 and 1991, the development of nickel-metal

hydride (NiMH) and lithium-ion batteries with higher energy densities revolutionised the energy storage industries. The increased interests due to the issues of energy crisis and the environmental pollution accelerated the research and development of the EVs. The significant success in Toyota Prius HEV in 1997 showed that the promising and irreversible trend of turning from conventional ICEVs to the EVs. In 2008, the first BEV Roadster by US car manufacturer Tesla Motor company aroused the worldwide attention of the vehicle industries to the development of BEVs and related technologies [59, 60]. In recent years, major automotive manufactures such as BMW, Nissan and Mitsubishi, have vigorously developed the EVs as a result of technological progress in the battery field. In the following sections, some of the most advanced and most used technologies in EVs, PHEVs and BMS industry are discussed.

### 2.1.1 EV topologies [58]

Typically, the EV refers to any vehicle in which the electric power is responsible for the propulsion and at least one EM is used. As a general term in industry and academia, there is no specific distinction of the energy storage medium, such as supercapacitor or flywheel or the air compression energy storage unit (ESU), used in EVs. The term EVs in this thesis is used to describe vehicles that use battery as the energy storage medium.

Taking the power supplement and propulsion devices into account, Table 2.1 shows a brief classification of different EVs. The BEV is purely fed by electricity from the power storage unit, while the propulsion of BEV is solely provided by an electric motor. The driving system of HEV combines the electric motor and the engine, while the power sources involve both electricity and gasoline or diesel. FCEV is driven by an

electric motor and could be directly or indirectly powered using hydrogen, methanol, ethanol or gasoline [58].

Table 2.1 General comparison of EVs.

| Types | BEV | HEV | FCEV |
|---|---|---|---|
| Drive section | EM | EM and ICE | EM |
| Energy sources | ESU (battery) | ESU and petrol tank | Fuel cell |
| Energy supplements | Electricity and power system | Electricity and power system, gasoline station | Hydroge-nide |

**Battery Electric Vehicles (BEVs)**

In BEV, energy storage capacity fully depends on the battery technology. Zero discharge emission of BEV is a significant advantage because the electrical energy is solely supplied from the vehicle-mounted battery. On the other hand, the limitations on the present status of the on-board battery technology of BEV makes it less attractive than ICEV under similar economic and driving requirements. Batteries with high power densities but low energy densities result in longer charging time – even with fast charging technologies, one hour to several hours for full charging is necessary. Thus, main challenges of the BEV are limited driving range, high initial cost and lack of charging infrastructure [61]. For the practical implementation, the size and location of the battery inside the BEV should also be standardised [62].

**Fuel Cell Electric Vehicles (FCEVs)**

FCEVs are attractive because of zero roadside emissions. Even taking the overall emissions into account, which include the emission from chemical plants and on-

road reformers, the FCEV seems still competitive. Fuel cell (FC) is the main power supplier and the critical technology for FCEV is an electrochemical device that produces DC electrical energy through a chemical reaction. There are five main components in FC: anode, an anode layer, electrolyte, cathode and a cathode catalyst layer. With suitable parallel/series connection of FC sources, the required amount of power can be produced to drive the car. In terms of driving range, it is comparable to ICEV, thus resulting in a wide range of application of FCs from small scale plants of the order of 200 W to small power plants of the order of 500 kW. However, the high initial cost and lack of refuelling stations are still regarded as significant challenges for the success of FCEV [63]. Also, the supply electricity continuity of FCs is less reliable than conventional battery used in EVs.

The crucial advantage of BEV and FCEV is the 'zero emission' and hence reduced air pollution. However, the 'zero emission' of BEV and FCEV is not absolute considering the emissions during the whole processing. However, "what is critical as the main pollution-contributor and how" are the topics that are hardly discussed. For example, the pollution-contributors include chemical contamination when producing the fuel cell and the battery (or the electrochemical plant for FCs), the emissions during the vehicle manufacture, the pollution from scrap battery processing, *etc.*.

**Hybrid Electric Vehicles (HEVs)**

The HEV combines the properties of ICEV and BEV. Driving power sources of HEV include both gasoline/diesel and electricity; the propulsion relies on the engine and electric motor. According to different refuelling or recharging measures, HEVs can

be classified as either conventional HEVs or grid-able HEVs. Based on levels of the combination, the conventional HEV could be further developed to three types: micro, mild and full HEV. The grid-able HEV could be either PHEV or range-extended electric vehicle (REV) [62]. Table 2.2 shows different categories of EVs based on the energy source and propulsion device.

Table 2.2 Classification of EVs

| Energy Source | Vehicle Type | Propulsion Device |
|---|---|---|
| Gasoline | ICEV | Engine |
| | Micro HEV | |
| | Mild HEV | |
| | Full HEV | |
| | PHEV | |
| Electricity | REV | Electric Motor |
| | BEV | |
| | PBEV | |
| Hydrogen | FCEV | |

As both electricity and petrol propel the HEV, the driving range of HEV is comparable to that of ICEV. The economic practicality of HEV seems to take more advantages than BEV due to the status of present battery technology. However, the need for engine and gasoline is not eliminated in HEV – so there is no zero emission. The combination of electric generator and engine increases the complexity of the manufacturing process and the initial cost. Therefore, the challenges for HEV are the design of these two propulsion devices to achieve an optimal efficiency while reducing the design complexity at the same time [64]. Going through the overall development

of EVs and considering both the economy and the technology, HEV has the most potential to develop and is expected to dominate the next few decades.

EVs are fully or partially energised from the batteries, which themselves are directly or indirectly charged from either a power station and/or electrochemical reactions. Therefore, various renewable energy sources should be used to improve the overall emission of EVs. Figure 2.1 gives the energy diversification based on different feeding measures for the EV.

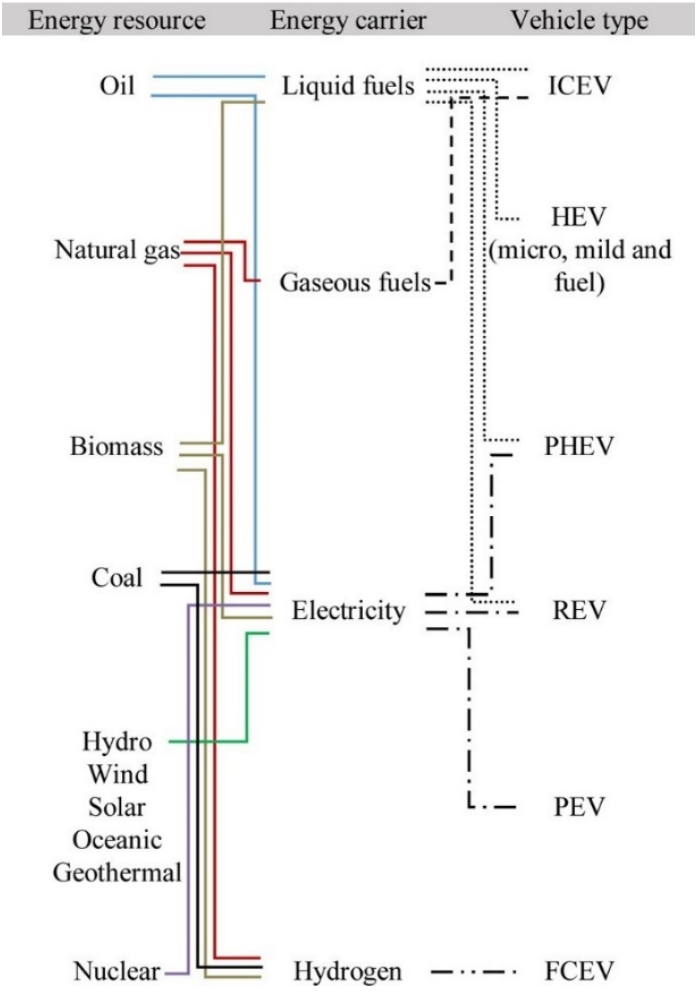


Figure 2.1 Energy diversification of EVs.

### 2.1.2 System Layout of HEVs

Since both ICE and EM provide the propulsion, there are two types of energy transmission in HEVs: electrical and mechanical energy transmissions. Figure 2.2 illustrates a typical system layout of the HEVs. The components shown in Figure 2.2 are generally divided into four systems and described in the following sections.

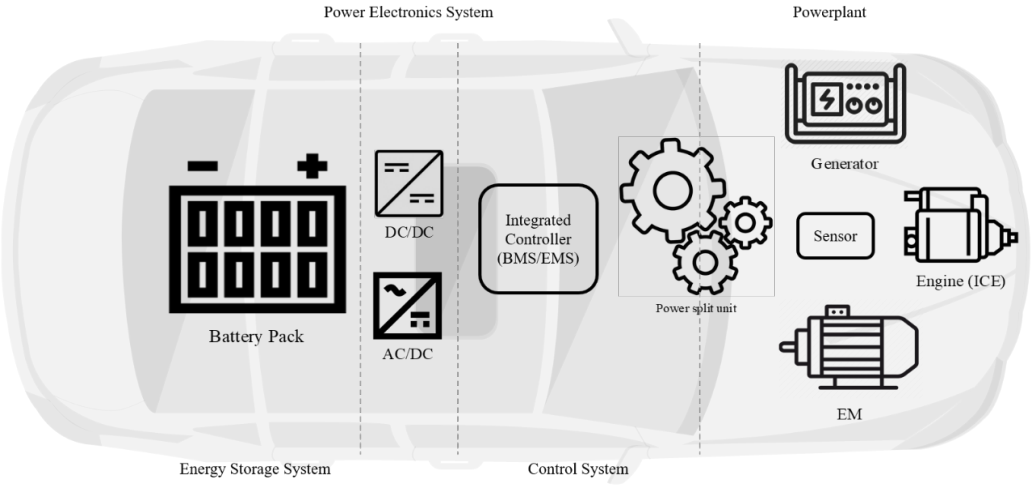


Figure 2.2 Typical system layout of HEVs.

**Energy storage system**

The energy storage system plays a significant role in EVs and HEVs to ensure a dynamic performance. The energy storage system can be classified into two types - baseload energy storage and peak energy storage [65]. The baseload energy storage technology is used in situations of large electricity demand, typically in BEVs. The peak energy storage technology is used in situations of high-rate charge/discharge cycle with little capacity degradation such as the supercapacitor or flywheel. The energy storage system includes the main battery pack and a back-up battery. The main battery pack is used to provide sufficient power for the normal operation of EVs/HEVs

[65, 66]. To avoid excessive consumption of the main battery pack, the main battery pack will be automatically shut down and isolated when the vehicle is turned off and not required to power the drivetrain. However, various other devices may continue working and require some amount of power. The back-up battery will be used to power such devices without depleting the main battery pack.

As discussed earlier in Chapter 1 (section 1.1 and Table 1.1), three main types of batteries are suitable for energy storage in EVs/HEVs - lead-acid battery, NiMH battery and lithium-based battery. Table 2.3 gives a more detailed performance comparison of the three main types of batteries used as the energy storage system in EVs/HEVs. In the table, DOD is an abbreviation for Depth-Of-Discharge [67].

Table 2.3 Performance comparison of three main types of batteries.

| **Performance of batteries** | **lead-acid** | **NiMH** | **lithium-based** |
|---|---|---|---|
| Common working voltage (V) | 2 | 1.2 | 3.2-3.7 |
| Energy density (Wh/kg) | 40-60 | 60-100 | 70-200+ |
| Charge/discharge cycle life @100%DOD | ≥300 times | ≥400 times | ≥600 times |
| Fast charging capability | ordinary | fairly good | good |
| Overcharge resistance | moderate | strong | weak |
| Environment performance | severe pollution | slight pollution | slight pollution |
| Operating temperature range (℃) | -20 to +50 | -20 to +50 | -20 to +55 |

From Table 2.2, it is clear that the lithium-based battery has distinct advantages over the other two types of batteries in terms of the working voltage, energy density, life cycle and the ability of overcharge resistance [43]. Selecting the lithium-based

batteries as the energy storage can reduce the weight of the battery pack and the vehicle because they offer higher energy density [42]. Meanwhile, lithium-based batteries, with their higher working voltages, can reduce the number of cell connection in series and hence provide a relief to any assembly difficulties of the battery pack. The main advantages of lead-acid and NiMH batteries are low cost and the technical maturity. It should be noted that there is no battery memory effect in all three types of the batteries.

**Power electronics system**

The power electronics system is mainly responsible for the operation of motor controllers and is the core of the EV drivetrains. The power electronics system converts the high voltage DC from the energy storage system to signals that meet the requirement of other motor controllers and sensors - for example, the electronics stability control and the hall-effect sensor [68]. For the grid-able EVs (PBEVs and PHEVs), the power electronics system design tends to include the control of various types of inverters and rectifiers. The battery can be charged or discharged to drive the vehicle and maintain a highly efficient working condition [69]. The power electronic system not only services the powertrain but also controls several vehicle components such as the step-down convertors, sensors and actuators of the lights, entertainment devices, *etc.*.

**Control system**

The control system refers to the integrated controller, which mainly includes the BMS and the EMS. The BMS plays an important role for a better safety performance and extended battery life. As the lead-acid batteries are gradually replaced by the lithium-based batteries, the design of the BMS can be complex. Table 2.4 lists the technology status and expectations of the BMS [70, 71]. The technology of EMS is also significant, especially for the HEVs with more than one type of energy transmission. The main purpose of EMS is achieving the control strategy working on the EM and ICE. The EMS is required to combine the power supply technology and motor control technology and collaboratively work with BMS in control system.

Table 2.4 The core technical status and development of the BMS [70,71].

| **Core functions** | **Last 5 years** | **Current difficulties** | **Indicators in 2020** | **Future expectation** |
|---|---|---|---|---|
| SoC estimation | Ah counting-based methods | Inaccurate and hard implementation | Ah counting-based methods | High estimation accuracy |
| Thermal management | Forced ventilation and runner structure design | Poor cooling effect with simple air cooling | Air cooling system with waste heat utilization | More sensitive to the temperature change for high safety and longer life |
| Power electronics | Three-stage chargers and pulse current charge | Lack of reliability on two-stage or three stage charging | The charging system with fast charging ability | Fast charging with better protection |
| Battery equalization | Dissipative charge and passive equalization | Hard to accomplish | Active equalization | Active equalization with low failure rate |

**Powerplant (EM/generator) [72, 73]**

There are four main types of electric motors (generators) used in the EVs:

*The brushed DC (BDC) motor* is one of the most common type of EMs, which has a permanent magnet in the stator and the armature windings and commutators mounted on the rotor. When the current is following through the brush and the commutator, the interaction between magnetic fields will generate electromagnetic torque so that the motor rotates to drive the load. There is less complexity in the control of BDC motor, because the communication is achieved by the mechanical brush. However, significant maintenance work due to mechanical contact cannot be ignored. Also, the efficiency of the EM is limited by the electrical contact of the brushes.

*Brushless permanent magnet (BLPM) motor* is seen as a reverse design of the BDC motor. There are no windings on the rotor. The rotor incorporates permanent magnets and creates the magnetic field while the stator has windings. The power electronic device in BLPM motor acts as the communicator without any mechanical connection, leading to an increase the complexity in control. The operation of the BLPM motor not only requires the power electronic devices to respond fast, but also an accurate decision from the position sensor and the processor. The Nissan Leaf and Chevrolet Spark have adopted the BLPM motor.

*Brushless induction (BLI) motor* is another common type of brushless motor. Compared to the BLPM motor, the BLI motor replaces the permanent magnet with a conductor mounted on the rotor. The conductor is inductively powered by the changing magnetic field around the stator. A concept of split in BLI motor is defined as the ratio

of the speed difference between the stator and rotor to the stator velocity. The BLI motor is widely used in the BEVs - for example, the Tesla Roadster uses a BLI motor.

*Brushless switched reluctance (BLSR) motor* has similar structure to the BLI motor - no permanent magnet on the rotor but stator mounted winding. To turn the rotor, certain sets of stator coils are powered such that the rotor responds by aligning sets of its teeth with these coils in order to minimise reluctance. The BLSR motor is a new type of speed-adjustable motor but has been developed for several applications such as household appliances, aviation and aerospace. The BLSR motor has a good performance when used in EVs.

## 2.2 A Review on EMS

The EMS, as the core control system in HEVs, decides the different operating modes of the ICE and EM. Based on the consideration of the fuel consumption, driving performance and the emission, the EMS is required to realize the optimization and complementarity among different energy sources in HEVs. A well performing EMS is required to adopt effective strategy for different control objectives. However, it is difficult to manage effectively for different objectives at the same time. The HEVs vary in the configurations and the degree of mixing of fuel consumption and electric energy consumption [74]. The different control methods applied in the EMS, therefore, have varying impacts on the vehicle performance.

The control methods of EMS for energy saving and efficiency optimization mainly consider the following four aspects: 1) a cooperative control of the EM and ICE which

ensures the ICE is working with high efficiency, 2) more use of pure electric mode (than fuel mode) reduces the fuel consumption under the premise of meeting the driving demand, 3) efficiently capture the energy loss in braking and then charging the battery through the motor with the captured energy and 4) take advantage of the fast start-stop characteristics of the EM to avoid the ICE in urban idle conditions. The energy sources structure and the energy transfer system of the HEVs are complex and nonlinear [75]. The control of the EMS is considered as a multi-objective comprehensive optimization problem. Figure 2.3 shows a process from design to practical implementation of the EMS.

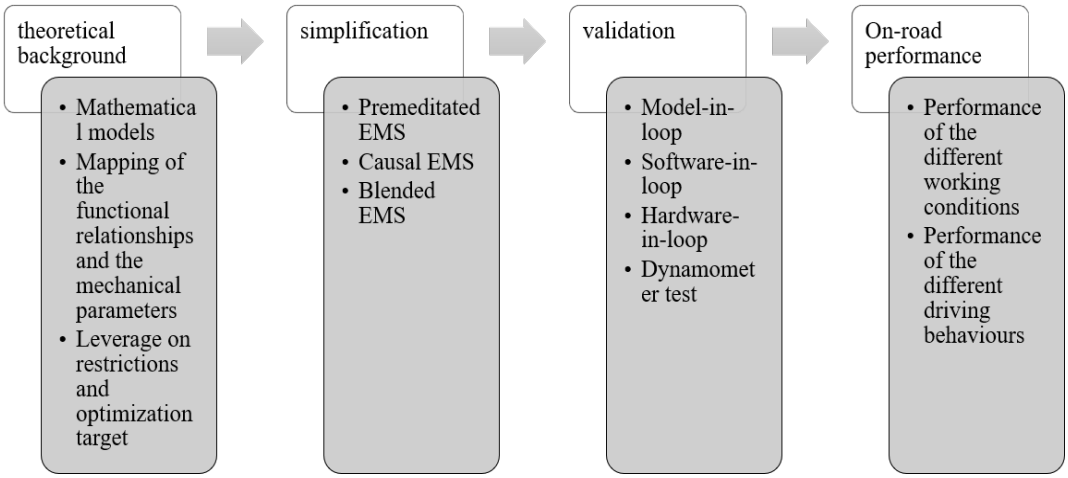


Figure 2.3 The implementation process of EMS.

In the first step of the theoretical background, the problem of energy management for HEVs could be solved by establishing mathematical models [76]:

$$\begin{cases} Continuity\ variable: \dot{x}(t) = f\big(x(t), u(t)\big), 0 \le t \le T \\ Discrete\ variable: x(k+1) = f\big(x(k), u(k)\big), k = 1,2,\cdots,N \\ mathematical\ model\ of\ the\ energy\ management: \min\limits_{\substack{x,u \\ s.t.G(x)\le 0}} J(x,u) \end{cases} \tag{2-1}$$

where $x \in X$ is the state variable and $u \in U$ is the control variable of the system and $G(x)$ is the constraint. Most of the control models use the SoC of the battery as the state variable while the distribution ratio of power demand or torque demand is generally set as the control variable. The constraints mainly include the maximum power and speed limits of the EM, the torque and speed limits of ICE, the upper and lower limits of battery SoC. According to the four control directions listed in the previous paragraph, five mathematical models are commonly used for solving the EMS problems. They are listed below:

1. Equivalent fuel consumption energy manage model:

$$\min_{u} J\,(t,u) = \Delta E_f(t,u) + s(t)\Delta E_e(t,u) \tag{2-2}$$

where the $\Delta E_f(t,u)$ and $\Delta E_e(t,u)$ are the fuel consumption and the electric energy consumption during the period $\Delta t$, respectively, which could be obtained through the map of ICE and EM. $s(t)$ is the energy conversion equivalent factor over the time. Musardo *et al*. [77] developed an adaptive model based on equation (2-2), which considers the change of the power demand and the equivalent factor during the charging/discharging process.

2. Energy management model considering the battery state:

$$\min_{u}: \int_0^T P_f(u,v,a,t)dt \tag{2-3}$$

$$\text{s.t.} \quad \dot{x}_1(t) = \frac{-P_i(u(t))}{Q_0\,(t)}$$

$$\dot{x}_2(t) = \frac{-\left|P_i(u(t))\right|}{\left(2 \cdot N\left(\left|P_i(u(t))\right|\right) \cdot Q_0(0)\right)}$$

$$x_1(0) = x_{1,0};\ x_2(0) = 1;\ x_1(T) \geq x_{1,0};\ x_2(T) \geq 0;$$

$$x(t) \in X, x = [x_1, x_2]^T; u(t) \in U\ .$$

where $P_f(u, v, a, t)dt$ is the energy consumption rate. $x_1(0)$, $x_2(0)$ and $x_1(T)$, $x_2(T)$ are the initial and stop values of SoC and the State of Health (SoH), respectively. $P_i\big(u(t)\big)$ is the output power of the battery. $x_{1,0}$ is the initial SoC, and $Q_0(0)$is the initial capacity. X and U are the state space and the control space, respectively. This mathematical model, which considers the capacity and the health of the battery, is discussed by Ebbesen *et al*. [78].

3. Energy management model considering the emission:

$$J = \sum_{k=0}^{N-1} \big[L\big(x(k), u(k)\big) + G\big(x(N)\big)\big]$$

$$L\big(x(k), u(k)\big) = fuel(k) + \mu NO_x(k) + \nu PM(k) \qquad (2\text{-}4)$$

$$G\big(x(N)\big) = \alpha\big(SoC(N) - SoC_f\big)^2$$

where *fuel(k)* is the fuel consumption during the period *k*. $NO_x(k)$and *PM(k)* are the emissions of $NO_x$ and PM, respectively. $SoC_f$is the expected stop value of SoC. $\mu, \nu$ and $\alpha$ are the weighting factors. $L\big(x(k), u(k)\big)$ is the fuel consumption and emission and *G(x(N))* is the impact of the change of SoC. The mathematical model described in equation (2-4) is used in various research works, for example, Nuesch *et al.* [79]. They incorporated the emissions into the function, which formed a compromise optimization problem of fuel consumption and emission control.

4. Energy management model considering both the steady and the unsteady state fuel consumptions:

$$J(k) = \alpha_1 \int_{t_k}^{t_k+t_p} \dot{m}_f(t)dt + \alpha_2\left[SoC(t_k) - SoC\left(t_k + t_p\right)\right]$$
$$+\alpha_3\left[1 - key_{on}\left(t_k + t_p\right)\right] \quad (2\text{-}5)$$
$$s.t.\ SoC_{low\_lim} \le SoC \le SoC_{up\_lim}$$

where $\dot{m}_f(t)$is the fuel consumption, $key_{on} \in \{0,1\}$ is the state of the ICE. $\alpha_i, i = 1,2,3$ is the weighting factor, $t_k$ is the time count at moment $k$, $t_p$ is predicted period of time and $SoC_{low\_lim}$ and $SoC_{up\_lim}$ are the upper and lower limits of the battery SoC, respectively. The mathematical model in equation (2-5) is discussed in great detail by *Yan et al.* [80]. They defined a cost function based on the fuel consumption, equivalent consumption of the electric energy with SoC change of the battery and the instantaneous fuel consumption when ICE is on or off. Moghbeli *et al.* [81] used a similar energy management model but included the fuel consumption when shifting gears.

5. Energy management model considering the structural parameters of the vehicle:

   - Cost function included the weight of the vehicle:

$$J = min\left(F \cdot \omega_f + W \cdot \omega_s\right) \quad (2\text{-}6)$$

   - Cost function considered the gear influence:

$$\min_{T_e(k),i(k)} J' = \sum_{k=0}^{N-1} D\left(T_e(k), i(k)\right) \cdot \Delta \quad (2\text{-}7)$$
$$D\left(T_e(k), i(k)\right) = \dot{m}\left(T_e(k), \omega_e(k), R\left(i(k)\right)\right)$$
$$s.t. T'_{e\_min}(k) \le T_e(k) \le T'_{e\_max}(k), i(k) \in I(k)$$
$$x(N) - x(0) = \Delta SoC = 0$$

where *F* in equation (2-6) is the fuel consumption, while *W* is the weight of the vehicle. $\omega_f$ and $\omega_s$ are the weighting factors of each item. Since the weight and the structure significantly impact the energy consumption of the vehicle, [81] used the model in equation (2-6) to solve the trade-off problems between the fuel consumption and the weight of the vehicle. Moreover, the mathematical model in equation (2-7) is discussed with great detail in [81], which deliberates the effect of changing gear on energy consumption. $\Delta$ in equation (2-7) is the sampling time, $D\big(T_e(k), i(k)\big)$ is the fuel consumption with a torque of $T_e(k)$, while $\dot{m}\left(T_e(k), \omega_e(k), R\big(i(k)\big)\right)$ is the fuel consumption when ICE is working at torque of $T_e(k)$, rotating speed of $\omega_e(k)$ and transmission ratio of $R(i(k))$, which could be calculated through the engine map. $T'_{e\_min}(k)$ and $T'_{e\_max}$ are the minimum and maximum output torques of the ICE and *x* is charge in the battery. In addition to the weight and gear influence of the vehicle, DiCariano *et al.* [82] proposed an energy management model based on the efficiency of the powertrain in a series HEV.

In terms of practical applications, the energy management model needs to be simplified when the EMS is implemented in the ECU. Taking the memory constraint and the computational capacity into account, some of the algorithms with high efficiency have been used in the established energy control models. The algorithms for EMS have been in development since 1992 [83]. These algorithms used in different scenarios range from offline to online applications and from local to global optimization. Figure 2.4 shows a general classification of the methods used in EMS.

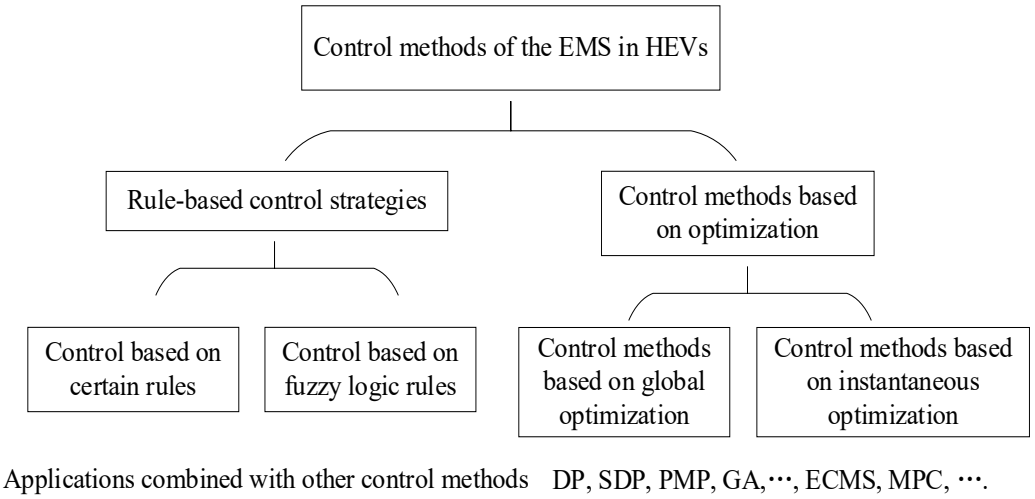


Figure 2.4 Control methods overview on the EMS in HEVs.

### 2.2.1 Rule-based control strategies applied for premeditated EMS

A premeditated EMS is also considered as the rule-based control strategy, which uses a deterministic rule or a group of fuzzy rules. The premeditated EMS uses a precalculated control policy, considers the values of inputs and the real-life driving conditions to produce an expected control. The premediated EMS is not encumbered with computational complexity. The premeditated EMS using the rule-based control strategy is commonly used to generate a simplified and offline control. On the other hand, a casual EMS uses algorithms with dynamic characteristics to produce the control in real-time/online during real-world driving scenarios. A blended EMS combines the premeditated EMS and the casual EMS. A premeditated decision and an instantaneous control are complementary to obtain a global and online optimization in blended EMS.

The rule-based control strategy used for premeditated EMS is often designed based on the empirical cognitions from the engineer, the division of different working modes in HEVs and a static energy efficiency map of the ICE and EM. The advantage of rule-based control is less calculation and easy implementation, but the drawback is its inability to adapt to complex operating conditions [84].

Compared to the rule-based control working separately, the fuzzy logic rules show strong robustness when addressing the nonlinear problem with uncertainty. Di Cairano *et al*. [82] used two controllers based on fuzzy logic rules to provide a fuzzy control on the battery SoC and the engine torque. Murphey *et al*. [85] adopted a hierarchical structure and fuzzy logic rules to control the engine torque to keep ICE working in an efficient workspace and improve the fuel economy. However, the fuzzy logic rules as one class of premeditated EMS methods, commonly rely on the engineering experience. Hence it is difficult to ensure an optimal solution.

The method of fuzzy logic rules is regularly used in conjunction with other algorithms to improve the adaptability of different operating conditions. Dynamic Programming (DP) and the fuzzy logic rules were combined to optimize five different working modes in HEV [81, 86]. Another method used fuzzy rules to control the equivalent factor in the Equivalent Consumption Minimization Strategy (ECMS) and produced an outstanding performance in fuel economy of a heavy HEV. Fuzzy logic control could also be combined with other intelligent algorithms [85]. For example, Vural *et al*. [87] combined the Genetic Algorithm (GA) to optimize the torque control, while Won and Langari [88] used Particle Swarm Optimization (PSO) instead of GA. In

addition, the fuzzy logic control was also combined with the learning vector quantization (LVQ) and Neural Networks (NN) for the optimization based on driving environment and status identification [68].

Compared to the single rule-based model, the fuzzy logic rules for EMS show strong robustness and are more suitable for the control of complex hybrid nonlinear systems that do not rely on the accuracy of the system. However, the fuzzy logic control cannot guarantee an optimal management; therefore, it is often combined with other algorithms to improve the performance of the system and then achieve the global optimization.

The control methods based on the optimization algorithms is another significant category for EMS, which define the energy consumption as a cost function and combined with the constraints. As shown in Figure 2.5, the control methods based on optimization can be divided into two categories - the EMS based on global optimization is formed on the static data table or historical data under specific operating conditions; the other is the online control based on real-time state or current parameters of the vehicle, which usually guarantees a local and instantaneous optimization.

The most representative methods for EMS based on the global optimization include the DP, Pontryagin's minimum principle (PMP) and GA, or some combinations of these methods [48]. The implementations of DP are highly targeted on the specific operating cycles, which require the information of the operating conditions in advance [89]. The main difficulties for DP applications in EMS are the large amount of

calculation and lengthy time consumption. A great number of researches have been devoted to the improvement of the DP algorithm used for EMS in HEVs. The improvement of DP implementation is mainly in three directions - reduce the computing time and memory requirements, recognition and prediction of the future information of operating conditions and integration with other technologies to improve the computational efficiency. The EMS for HEV could be considered as an optimal control problem for time-varying nonlinear systems with constrains. The method of PMP is appropriate to address the trade-off problem between the optimal control and the constraints. Compared to the DP-based control, the EMS using PMP significantly decreases the computation and is more adaptive to the real-time control.

In terms of the GA applications in EMS, the advantage of adaptive probabilistic iterative searching could provide faster convergence to multi-objective optimization. However, the EMS using GA method often demands to predict the driving cycle in advance and the amount of calculation is not significantly reduced; therefore, the practical application of EMS based on GA have some limits. A considerable number of published works used the GA in a hierarchical optimization model and in conjunction with other algorithms [65, 90, 91]. For example, Genetic-based bacteria foraging (GBF) proposed in [92] shown a good performance in fuel economy.

### 2.2.2 Control methods based on algorithms applied for casual EMS

With the development of real-time system technology, the instantaneous optimization has been gradually applied to the EMS of HEVs. The intention of the real-time control is to minimize the energy/power consumption in the current work state. According to

the optimum working curve of the ICE (the Map of fuel consumption, power and efficiency), algorithms are used to find the instantaneous optimal operating point and control the state variables for an effective dynamic energy distribution, such that the ICE and EM working at the instantaneous optimal point. The methods for causal EMS are optimal controls on the energy transmission in HEV under instantaneous working conditions, which will not be limited by the specific cycles and do not demand the prediction of the future driving information of the vehicles in advance. Moreover, compared to the rule-based control, the amount of the calculation in causal EMS is less and easier to implement.

The method of ECMS is one of the representative algorithms commonly used for a casual EMS. The principle of the ECMS is equivalent fuel consumption, which converts the energy consumption of EM under a transient condition into the fuel consumption of the ICE. The ECMS introduced an equivalent factor to build the cost function of total fuel consumption at each instantaneous state. Meanwhile, the weighting factor in ECMS could provide an optimization for different targets listed in the cost function. Therefore, the ECMS could achieve the real-time control and the compromised optimization among the dynamic performance, fuel economy and the emission of the HEVs.

However, the ECMS method is based on a hypothesis that the ICE compensates for the electricity in battery under the same condition, dynamic changes of the battery SoC are not considered. That means the ECMS cannot guarantee a global optimization. By way of illustration, Sciaretta *et al*. [93] used the ECMS for the real-time EMS without

the hypothesis of known driving cycle conditions and considered the difference of charging/discharging processes by using different weighting factors. Marano *et al*. [94] compared the EMS based on DP and ECMS. The EMS based on DP provided a higher fuel economy. However, the EMS based on ECMS is more real-time since there is no requirement of prior knowledge of the driving cycle. Ramadan *et al.* [95] combined the PMP and ECMS and achieved longer life battery with lower fuel consumption.

Model Predictive Control (MPC) is commonly used for online identification to optimize the dynamic parameters of the vehicles, which converts the global optimal control of fuel economy through the driving cycle into local optimal control in the prediction working area. The rolling optimization provided by MPC will update and predict the operating control state or the control parameters of the next time domain of the vehicle to obtain an optimization result. The method of MPC shows strong robustness and adaptability for the uncertain and nonlinear control system.

Moreover, the MPC could be used in combination with other algorithms such as NN, artificial intelligence (AI) and fuzzy logic control methods to obtain an excellent control performance [96]. The blended EMS used the model that includes both rule-based control strategies and optimization algorithms. Table 2.5 summarizes performance comparison of the different four energy management strategies.

Table 2.5 Performance comparison of main control methods for EMS.

| Performance | Rule-based control | Fuzzy logic control | Global optimization | Real-time optimization |
|---|---|---|---|---|
| Advantages | Simple and easy to implement. | Independent of the accuracy of the model; strong robustness and adaptability. | Good optimization performance and good adaptability with other algorithms. | Unconstrained on the cycling operating conditions; less calculations and instantaneous optimization. |
| Disadvantages | Depends on experience and static data; unable to adapt the dynamic changes of the operating conditions; unable to guarantee optimal control. | Depends on experience and unable to guarantee optimal control. | Depends on operating cycles and limits by great amount of calculation. | Unable to guarantee the global optimization. |

## 2.3 Monitoring Techniques for BMS

A good operation of the EMS is based on the current estimation and possible future predictions of the battery states from the monitoring module in BMS. With the progress of the battery technologies, the energy storage system in EVs often includes more than one type of battery. The monitoring module for composite energy storage system is more complicated. It is required to provide accurate battery states information and fastest response. Subsequently, the EMS will decide the appropriate actions on battery immediately to achieve optimal control and protection. Figure 2.6 gives a schematic of the basic functions of the battery monitoring module.

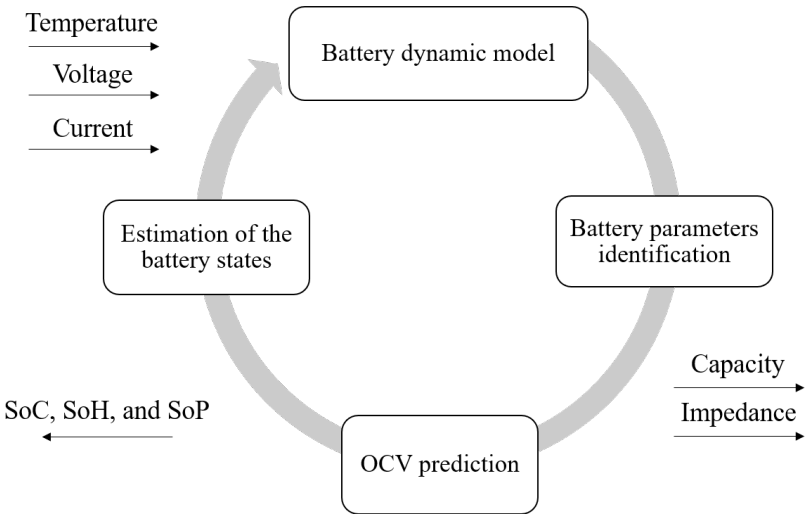


Figure 2.5 Basic functions of the battery monitoring module.

The battery states monitor is necessary to ensure an effective and robust EMS. The most favourite states include the SoC, SoH and SoP and are strongly dynamic with the varying operating conditions. The methods for battery states monitoring are required with time-variability of the battery characteristics such as the capacity and impedance of the battery. As shown in Figure 2.6, it is important to build a dynamic battery model to reflect the electrochemical changes during charging/discharging process. According to the input information of voltage, current and temperature, the algorithms used in the dynamic model must be able to adaptively estimate the variations of parameters such as the internal resistance and Ah capacity in real-time. Based on the dynamic battery model, a prediction of the battery OCV is subsequently obtained and applied to either a look-up table or the predefined empirical function to online estimate the SoC.

### 2.3.1 Review of battery models

The estimation of the battery states mainly includes the SoC, SoP and SoH. The SoC estimation could be considered as the parameter identification of the battery model.

According to the different options of battery models, the accuracy of the estimation is varying and impacted by the operating conditions such as temperature [97]. The significant challenge for an accurate SoC estimation is that the nonlinear characteristics of the battery are intensified by the changes of the current/voltage and the temperature. The amount of calculation/computation will increase and is difficult to be implemented on the controller if all the influencing factors are considered.

In order to reduce the cost of vehicle manufacturing, the establishment of the BMS needs to be verified by simulation and then obtain a practical validation through software-in-loop and hardware-in-loop (see Figure 2.4). The battery model could be built through three different approaches: mechanism modelling, experimental modelling and hybrid-methods modelling [98]. The mechanism modelling uses the theory of physical formulae and chemical reaction principles to establish the mathematical model. In experimental modelling, the controlled object is regarded as a "black box" and the battery model is built by recording the change rule of the characteristic parameters of the object through multiple groups of experiments. The hybrid modelling combines the mechanism modelling and experimental modelling.

The battery is a highly complex nonlinear electrochemical energy storage device. As the working process of the battery is dynamic, it is difficult to precisely describe the interactions occurring inside the battery by a specific formula (mechanism modelling works alone). Fully adopting experimentally generated data modelling requires large amount of testing data. The complexity and the calculation time of experimental data processed by algorithms increase with the extensive experimental data. Therefore,

hybrid modelling is more commonly used to select a reasonable formula and identify the pending parameters.

According to the different demands of the application scenarios, the selections of various battery models significantly affect the estimation accuracy for the monitoring module in BMS. The model with more accuracy has more complex operation and the expectation of hardware is higher. The mechanism modelling mainly includes the electrochemical model, empirical model, data driven model and equivalent circuit model (ECM) [99]. Table 2.6 lists general classifications of the battery models and compared the advantages/disadvantages.

As reported by recent works on the battery monitoring and models, the ECM does not require a comprehensive analysis of the electrochemical reaction inside the battery [100]. ECM uses an appropriate circuit to describe the external characteristics of the battery such as the DC internal resistance, polarization resistance and the OCV. The polarization of the battery usually means the potential deviates from the equilibrium potential when a current is passing through the battery.

There are three types of polarization: electrochemical polarization, concentration polarization and the Ohmic polarization [101]. The concentration polarization is caused by the consumption of the reactants and the surface of the electrode is not replenished. Some by-products produced in electrochemical reactions accumulate on the electrode surface and cannot be evacuated in time. The Ohmic polarization is caused by the contact resistance between various components such as the electrolyte, electrode material, and diaphragm resistance.

Table 2.6 The classifications of battery models.

| **Classifications of battery models** | | **Pros** | **Cons** |
|---|---|---|---|
| Empirical model | Shepherd model<br>Unnewehr universal model<br>Nernst model<br>Enhanced self-correcting (ESC) model<br>Zero-state hysteresis model | Simple expression and computational efficiency | Limited capability of describing the terminal voltage |
| ECM | Rint model<br>RC model<br>Thevenin model<br>PNGV model<br>GNL model | Easily understood and widely used in SoC estimation | Complex parameter identification process |
| Electrochemical model | Pseudo 2D model<br>Single particle model | High accuracy of voltage calculation | Require prior knowledge of the battery and time consuming |
| Data driven model | Neural Networks model<br>Radial Basis Function Neutral Networks<br>Support Vector Machine (SVM) model<br>Extreme Learning Machine (ELM) model | High accuracy of voltage calculation and no requirements on the prior knowledge of the battery | Laborious training dataset collection process |

The three types of polarization listed above are the obstructions to the electrochemical reaction of the battery. The internal resistance of the battery is the sum of the Ohmic resistance, electrochemical polarization resistance and the concentration polarization resistance, which are considered when the battery model is built by the method of ECM. Figure 2.6 provides a general process of building the battery model using the method of hybrid modelling. The following section will provide a brief review on several common ECM for battery models reported by Xiong *et al*. [102].

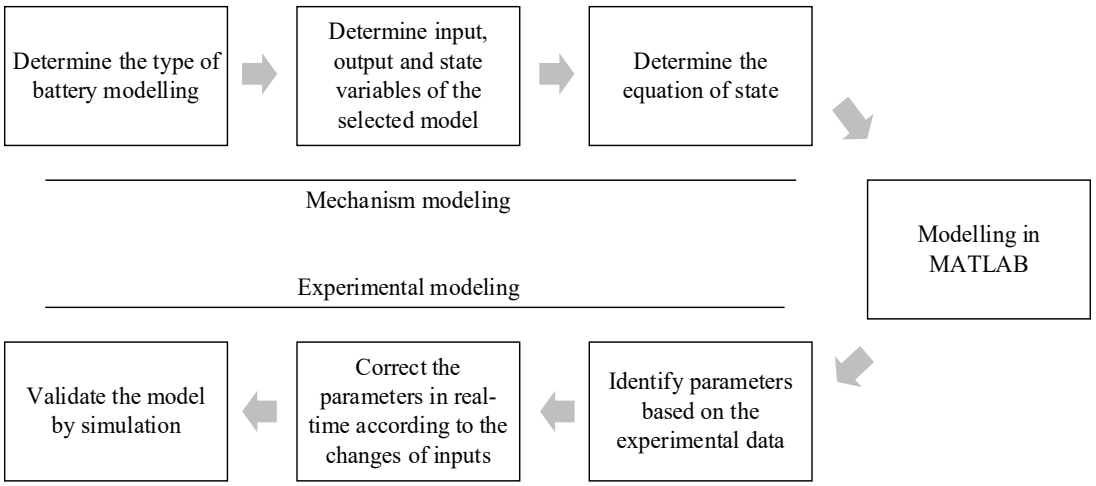


Figure 2.6 General process of hybrid modelling method for battery model establishment.

**The Rint model**

The Rint model, also called the internal resistance model, is the simplest ECM. As shown in Figure 2.7, the OCV of the battery is defined by an ideal voltage source. $R_0$ (internal resistance of the battery) and $U_{oc}$ (open circuit voltage of the battery) are functions of SoC and temperature. $I_L$ is the load current of the battery - positive $I_L$ means the battery is discharging and negative $I_L$ means charging. The advantage of Rint model is that the measurement of parameters is simple, the modelling simulation is easier to implement and has versatility. However, the accuracy of the Rint model is lower compared to other ECMs. Rint model is unable to reflect the dynamic performance of the battery under different charging/discharging conditions.

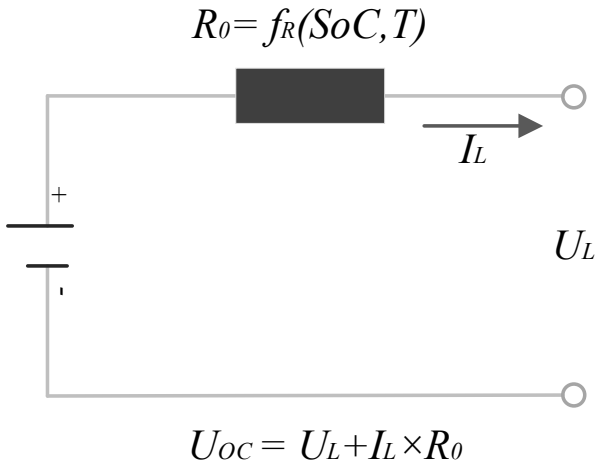


Figure 2.7 The Rint model for battery ECM.

**The RC model**

The ECM of RC model is shown in Figure 2.8 and includes three resistors and two capacitors. A large capacitor $C_b$ is used to describe the capacity of the battery, $C_c$ is a smaller capacitor to reflect the surface effect of the battery. The relationship between $U_b$ and $U_c$ could be obtained using Kirchhoff's current law. $R_t$ is the terminal resistance, $R_e$ is termination resistance, and $R_c$ is the capacitive resistance.

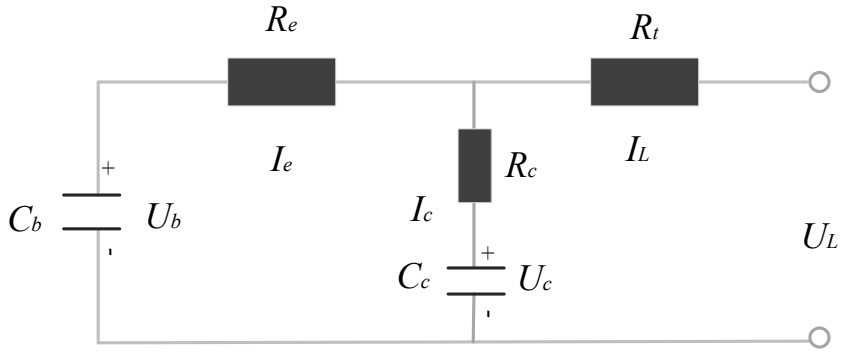


Figure 2.8 The RC model for battery ECM.

**The Thevenin model**

The Thevenin model is shown Figure 2.9 and is based on the internal resistance model. Thevenin model has one or more RC circuits connected in series and an ideal voltage source to express the OCV of the battery. The addition of multiple sets of RC networks will affect the accuracy of the battery model. With increasing number of RC networks involved, the amount of computation will increase too. The serial RC networks have forward-looking function which will predict the response to the load at specific SoC. The accuracy of Thevenin model is higher than the Rint model.

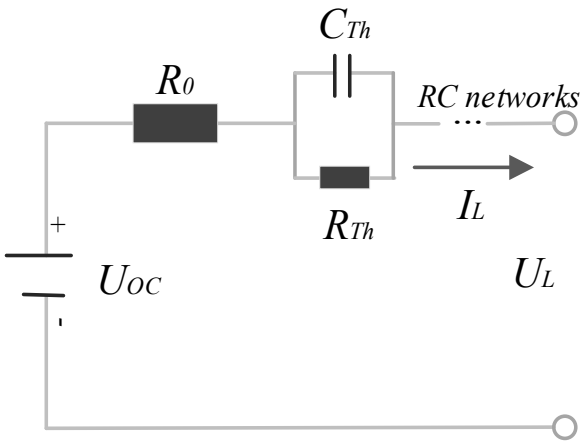


$$U_{OC} = R_0 \times I_L + U_L + U_{Th}$$

$$U_{Th} = {}^{1}/_{C_{Th}} (I_{Th} dt) = R_{Th} \times (I_L - I_{Th})$$

Figure 2.9 The Thevenin model for battery ECM.

**The PNGV model**

The Partnership for a New Generation of Vehicles (PNGV) model is proposed in PNGV battery test manual [103]. As shown is figure 2.10, the PNGV model is connected with a capacitor ($C_b$) in series based on the Thevenin model. *Uoc* is the OCV of the battery while $R_0$ is the Ohmic internal resistance, $R_p$ is the polarization

resistance, $C_p$ is the polarization capacitor, $I_L$ is the load current and $U_L$ is the load voltage. Compared to the Thevenin model, the PNGV model introduces capacitor $C_b$ to describe the effect of the load current variation over time on OCV when the battery is charging/discharging. In other words, the Thevenin model is only used to express the response when battery has a certain SoC value – this means an instantaneous static response. However, the PNGV model is able to characterize the dynamic response of the battery.

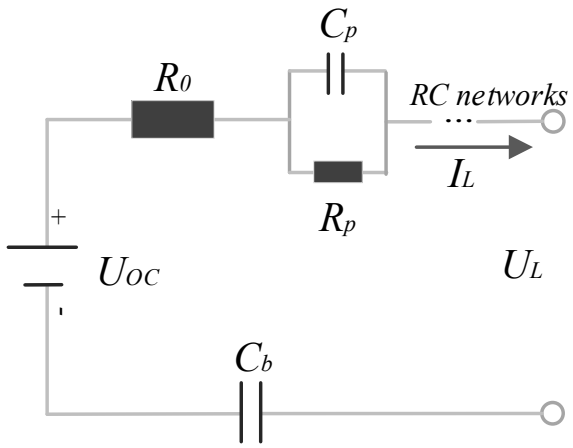


$$U_{OC} = U_L + {}^{1}/_{C_b}\left(\int I_L dt\right) + R_p I_p + R_0 I_L$$

Figure 2.10 The PNGV model for battery ECM.

**The GNL model**

The General Non-linear (GNL) model is developed from the Rint, Thevenin and PNGV models. As shown in figure 2.11, $C_p$ and $R_p$ constitute a RC network of electrochemical polarization. While the concentration polarization is expressed in another RC network with $C_c$ and $R_c$, $R_e$ indicates the self-discharge or over-charge internal resistance and $R_0$ represents the equivalent internal resistance. The additions

of circuit components in the GNL model gives a clearer physical meaning. The modelling simulation based on GNL model can precisely track the dynamic change of the battery voltage. The monitoring algorithms applied on the GNL model provide a higher accuracy for the battery SoC estimation, but the model has more difficult hardware implementation.

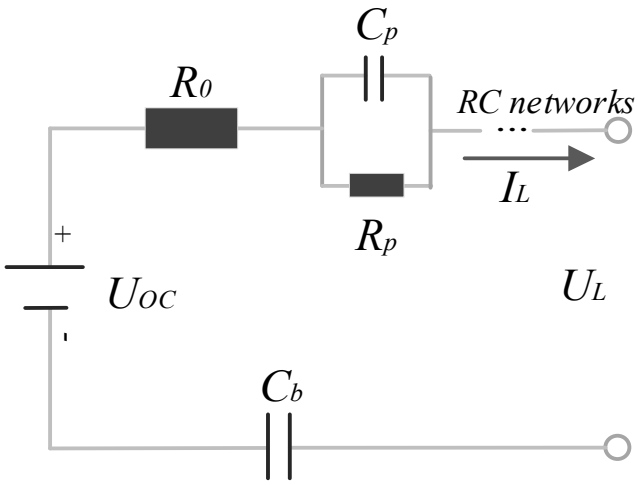


Figure 2.11 The GNL model for battery ECM.

### 2.3.2 SoC estimation algorithms

The battery SoC is used to describe the remaining charge of the battery in use, which is a significant parameter for vehicular battery usage. For the BEVs, an accurate SoC estimation could provide customers with charging demand alarms in time and prevent the battery packs from being over charged/discharged. A precise SoC for a single cell significantly benefits to the battery equalization. For the HEVs, SoC as a critical parameter participates in the dynamic coordination and energy management of the multiple power sources. Precise SoC estimation will optimize the fuel consumption and emissions from HEV effectively and improves the driving performance and ride comfort for users.

The manufacturers and designers of different BMS are maintaining their own definition of SoC and hence the estimation accuracy of algorithms used for SoC estimation is varying. It is significant to give a precise definition of SoC before estimation. Currently, a generally accepted definition of SoC is based on the angle of charge. For example, U.S. Advanced Battery Consortium (USA BC) gives a definition of SoC in the battery test manual as the ratio of residual charge to rated capacity under the same condition at a certain discharge rate [104]. On the other hand, Kia Motors from Korea defined the SoC from the perspective of energy, which is listed as follows [105]:

$$SoC = \frac{Remaining\ available\ energy}{Total\ available\ energy}.$$

In practical applications, the SoC of the battery is affected by charge/discharge rate, temperature, self-discharge, and aging, *etc.*. The BMS needs to adjust the definition of SoC. The EV Plus gives a definition of SoC as follows [106]:

$$SoC = \frac{Remaining\ capacity}{Rated\ capacity - Capacity\ attenuation\ factor},$$

$$Remaining\ capacity = Rated\ capacity - Net\ discharge - Self discharge - Temperature\ compensation\ capcity.$$

The different SoC definitions listed above are taking the single battery cell as the research object. There are always battery packs used in practical; therefore, it is a challenge to evenly define the SoC of battery pack. To ensure the safety of the battery, the SoC of the battery evaluated with the worst performance is often used as the SoC of whole battery pack.

The estimation of SoC is an important issue in EVs. Many researchers have discussed different methods for SoC estimation [107]. They include an estimation of SoC fully based on the discharge experiments, a method of load voltage (terminal voltage), OCV-based method, impedance-based method, the coulomb counting-based method (Ah method), the estimator with Kalman Filter- based methods, the estimator based on neural network, *etc.*. Different estimation methods could be combined with various battery models and the obtained accuracy of the SoC estimator could also be different. A summary of common methods for SoC estimation is shown in Table 2.7.

Table 2.7 The classification of battery SoC estimation methods.

| **SoC estimation methods** | **Static estimation oriented** | **Dynamic estimation oriented** | **Features** |
|---|---|---|---|
| Model-based Estimator | OCV-based estimation; Ah-based estimation. | Adaptive observer; Optimized recursive algorithms; Kalman Filter-based algorithms. | Static model has simple principle and obtain a clear relationship between OCV and SoC; Implementation has strong flexibility combined with dynamic algorithms; Dynamic algorithms could track the changes of voltage in real-time. |
| Data Driven Estimator | Impedance-based estimation. | Book-keeping methods /Look-up-tables; Machine learning techniques. | The estimation process needs to look up the Map composed of a great number of historical data; implementation requires a large-storage controller; Estimation accuracy is strongly relying on the historical data. |

The estimation methods can be used either alone or in combination with each other. The OCV-based method and Ah-based method are reported as the direct techniques

and are easily implementable approaches for SoC estimation. However, the OCV-based estimator suffers from the sensor noise and the initialization-induced offsets, while the Ah-based estimator requires a very long period of no-load connection to build an accurate measurement for the OCV of the battery [108]. Therefore, the static oriented methods are often combined with the adaptive algorithms in an indirect way to dynamically track the change of SoC.

The static oriented estimation in the classification of data driven estimator mainly rely on the groups number of experimental data of battery performance tests. The impedance-based method is built according to the relationship of impedance and SoC, which is often used for SoC estimation in lead-acid, NiMH and NiCd battery [109]. In terms of the lithium-ion battery, the impedance is strongly affected by the external environmental factors such as temperature. The impedance parameters alone are unable to provide an accurate SoC. When there is enough experimental data to establish accurate Maps/look-up tables for the battery and EM, it can be applied to the dynamic scenarios. In terms of the dynamic estimation, when the operating condition of the EV becomes complex, the requirement of experimental data quantity and accuracy of the impedance-based estimator is higher.

For different types of batteries, it is possible to achieve high accuracy SoC estimation with all above the method(s) either working alone or in combination. For example, the estimation method based on Kalman Filter has reported that the estimation error is less than 2% applied to the lead-acid battery and lithium manganate battery, while the estimation error of combining the methods of terminal voltage curve recognition and

Hamming Neural Networks is ~5% [110]. However, the same operating conditions applied to the $LiFePO_4$ had a lower estimation accuracy [111]. The main reason is that the convergence speed of the iterative algorithms is affected by the flatness of the middle section in SoC-OCV curve of $LiFePO_4$ battery. The battery modelling method, the design of the SoC estimator, and the experiment of battery performance test will be discussed in more detail in Chapter 5.

## 2.4 Concluding Remarks

This chapter presented various technical applications of EVs and state-of-art of EMS and monitoring technologies in HEVs. It was shown that, due to the technical limits on the energy/power density of the battery, the HEVs/PHEVs promise appreciable driving performance and less emission. Also, it was discussed that an efficient EMS for HEVs is a significant challenge while the SoC estimation is the key technology for the system running of the EMS and BMS in EVs. Therefore, a comprehensive review on the control strategies and algorithms for EMS and the estimation methods for the SoC monitoring has been provided in this chapter. The premeditated EMS based on rule-based control strategies, the causal EMS based on adaptive algorithms and the blended EMS combining the rule-based control and the dynamic algorithms has been proposed. Similarly, various SoC estimation methods were categorized into model-based and data-driven approaches including the static and dynamic groups. The essence of the estimator is to identify the parameters of the battery and track the changes. Therefore, the uses of different battery models affected accuracy of estimators. Different battery models used for SoC estimation were described. This

chapter summarized the advantages and disadvantages of four kinds of battery models. The ECM as the most popular battery model for SoC estimator reported four types of equivalent circuits. According to their characteristics, the different combinations with the estimating algorithms were implemented to confront the constrains of various computational and storable capacity in hardware.

# Chapter 3 Rule-based Control Strategy Design for Premeditated Energy Management System

This chapter is based on the work from the following publication in which the author of this thesis is the principal author: Ding, N., Lie, T., and Prasad, K. (2017), "The Design of Control Strategy for Blended Series-Parallel Power-Split PHEV–a Simulation Study", *International Journal of Transportation Systems*, *2*, 21-24.

The EMS will decide the long-term development and popularization of HEVs. For the PHEVs, an efficient EMS will fully utilize the advantages of the rechargeable batteries. However, the computational and storage capacity of the hardware where EMS is implemented has to be taken into account. Currently, the great challenge of EMS technology is how to realize an efficient electrical and mechanical resources scheduling and ensure a good driving experience under limited hardware conditions. The premeditated EMS relies on one/groups of rule(s)-based (fuzzy) control strategies and is an acclaimed option for the researchers because of the lucid principle and less computational load. Most of the proposed techniques of the premeditated EMS based on rules is designed according to the antecedent knowledge and experience from the engineers and normally has a poor emission performance when meeting the dynamic requirements. In this chapter, a rule-based control strategy for series-parallel PHEV is designed and simulated in MATLAB. The simulation calls the vehicle model based on real data in Advanced Vehicle SimulatOR (ADVISOR) to increase the credibility of the rule-based control strategy. The input is used of the real traffic data, while the output is the emission of the main harmful components and the fuel economy. The

proposed rule-based control strategy is finally verified by a comparison to the simulation based on same input vehicle model without the designed control strategy.

## 3.1 Introduction

As discussed in section 2.2 of Chapter 2, an efficient scheduling of multiple power sources is a significant issue for HEV/PHEV research. Due to the series-parallel configuration, the different working modes in series-parallel HEVs include:

1）Series mode - the ICE is connected to the generator in series to charge the battery.

2）Parallel mode - the ICE and EM are working in parallel to provide the propulsion at the same time.

3）Series-parallel mode - the ICE in series with the generator charges the battery and simultaneously works with the EM to drive the vehicle.

The fuel economy can be improved by switching different working modes - which means the control of the multiple working modes becomes more complex. Therefore, a suitable control strategy in EMS/BMS plays an important role in the following aspects:

- Increase the electric range mileage to obtain better dynamic performance.
- Decrease the emission to achieve the purpose of environmental protection.
- Improve the safety by providing a safe and efficient working environment for battery.

- Increase the efficiency to save the energy by switching to the most appropriate working mode under different road conditions.

Various rule-based control strategy for HEVs/PHEVs have been presented in literature, each having its own advantages and disadvantages [112, 113]. The main functions will be different according to the different logic design of the rule (s). The general design process of the premeditated EMS uses a rule-based control strategy in four steps:

Step1. System specification: using the specific theory, such as the theory of Hybrid Dynamic System (HDS) and building the mathematical relationships to describe and define the dynamic characteristics of discrete events and continuous variables in the hybrid system.

Step2. Obtain offline power distribution: defining the model of each subcomponent under a steady state. Then, seeking an optimal power distribution under different working conditions for each component by using specific method such as the Sequential Quadratic Programming (SQP).

Step3. Establish the online control strategies based on the rules using fuzzy logic: based on the offline solutions (optimal power distribution) obtained from last step, using dynamic algorithms to build the online rules of switching to different working modes. Alternatively, a fuzzy control system of power distribution can be established according to the fuzzy logic rules.

Step4. Optimize the control system: using the optimization algorithm (e.g. GA) to optimize the parameters set in the switching rule of working modes and the fuzzy control rules of power distribution obtained in Step 3, then, having an optimal EMS.

As discussed in Chapter 2 (see section 2.2.1), the rule-based control strategy uses the deterministic logic threshold or the fuzzy rules control. Most of the rules in the premeditated EMS are designed to ensure the components running in a highly efficient working area under various working conditions. For example, Cao and Ali built two modes according to different power demands - series mode in low load condition and parallel mode in high load condition [114]. However, the realistic conditions are more complicated and the threshold of power demand working alone cannot ensure the ICE working in an efficient area. Therefore, the rule-based control strategy proposed in [115] is built on a Markov model that was obtained from the statistics of several urban cycle conditions. Another example of rule-based control strategy demonstrated in [116] is applied in the Hydraulic Hybrid Vehicle (HHV). The hydraulic accumulator (ACC) used in HHV has the characteristics of high-power density, which benefits the dynamic performance such as the vehicle starting up, accelerating and climbing. The rules used for controlling the ACC and ICE are modes switching obtained through the actual experimental results from the vehicle testing engineer. There are four modes designed – ACC drive the vehicle alone in mode 1; in mode 2 the ICE provides propulsion and pressurizes the ACC; mode 3 is regenerative braking for energy recovery and mode 4 is the conventional friction deceleration braking mode. For uncertain road conditions and driving behaviours, the rule-based control strategy is considered as static reference of evaluation benchmark and normally works in conjunction with dynamic algorithms.

The rule-based control strategy optimized by dynamic programming (DP) is used in [117], which set the cost of engine fuel and battery energy as the objective function, starting/stopping working points of the ICE as the control variable and battery SoC as the state variable. [118] proposed a rule-based control strategy that switch the different modes according to set fixed working points on the maximum power curve of the ICE. Meanwhile, the fixed working points were optimized by DP, which has an objective function of battery consumption to improve the battery life at the expense of fuel economy.

Most of the research presented in literature on different premeditated EMS using rule-based control strategy are verified through simulation. This has been perceived as a motivation to design a rule-based control strategy for PHEV. To this end, this chapter initially focuses on analysing the power splitting of the power provided from battery and ICE when confronting power demand under various working conditions. Thereafter, the control logics of switching different modes are decided by threshold values of the battery SoC and engine torque. The proposed rule-based control strategy is then validated through the simulation using vehicle model and the inputs of driving cycles from real database. Finally, a comparison of the simulation results on the control of traditional working modes and the designed rule-based strategy is conducted. The results presented in this chapter were successfully published in a journal [84].

## 3.2 Design of the Rule-based Control Strategy

This rule-based control strategy design is setting the thresholds to switch working modes of the PHEV. The different modes design is to achieve the purpose of reducing the emission and the energy loss, then improve the fuel economy and the efficiency of

the power sources usage. The difference in working modes lies in the different transmission pathways between the electrical and mechanical energies. The working modes are defined according to the power splitting configurations of the PHEV. The following section illustrates the logic design of the novel working modes for the rule-based control strategy.

### 3.2.1 The power splitting configuration and the blended modes in PHEV

As described in Figure 2.3, three different connection modes are included in HEV based on the connection between the battery and ICE - series connection, parallel connection and series-parallel connection. Based on these three different connections, the traditional working modes in HEV include - the Electric Vehicle (EV) mode that only the battery provides the propulsion; the Charge Depletion (CD) mode where battery and ICE work in a parallel configuration with electricity as the main power; the Charge Sustaining (CS) mode in which the ICE provides a considerable propulsion despite being the main provider. Figure 3.1 illustrates the electrical and mechanical energy transfer in PHEVs.

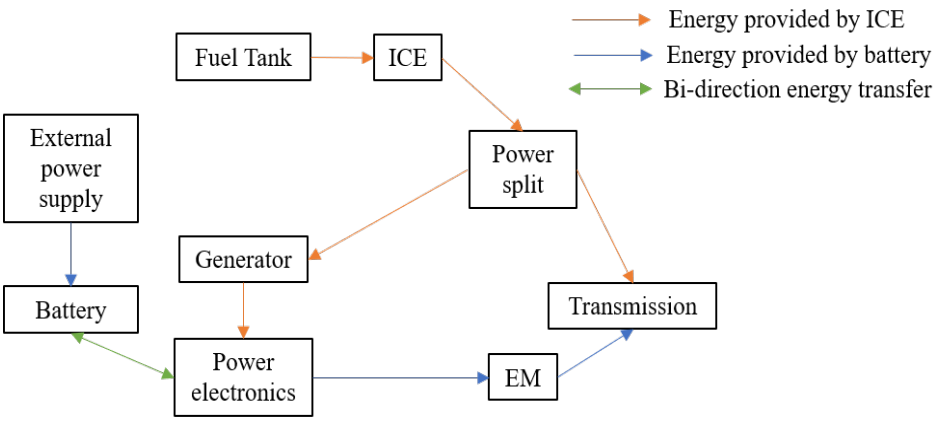


Figure 3.1 Energy transfer in PHEV.

When the vehicle is in a traffic condition that has low power demand and the battery has sufficient charge, the EV mode is forced to achieve “zero” emission. The CD mode is used when the electricity provided by battery cannot meet the power demand and the ICE is started to compensate for the lack of power. ICE works in the CD mode as compensation but when in CS mode, acts as the main power provider to drive the vehicle and charge the battery at the same time. The emission is gradually increased from “zero emission” in EV mode to CD and CS modes. The switching of different modes depends on the power demand, electric power provided by the battery and the power compensated from ICE. To decrease the emission, the design of the rule-based control strategy targets on avoiding the CS mode as much as possible. Based on this design logic, the following section (3.2.2) illustrates a novel rule-based control strategy.

### 3.2.2 The rule-based control design

For the series-parallel power split PHEV, a complex system cannot be avoided. Since the grid-able battery has been introduced, the thresholds of the parameters for working modes setting differ from other types of EVs. According to the analysis of the various charge levels in battery meeting different power demands, the rule-based control strategy proposed in this chapter is designed to increase the fuel economy and then decrease the emission. Figure 3.2 illustrates the design of SoC control strategy while the parameters used are listed in Table 3.1.

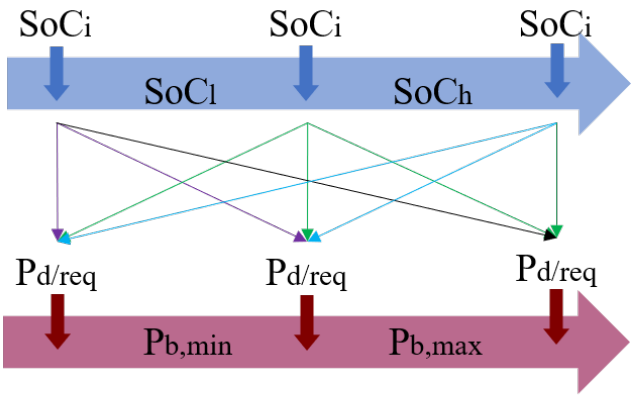


| | |
|---|---|
| → | **EV mode:** Battery fully provides power for the vehicle; ICE is not working. |
| → | **CD mode:** Battery fully provides power; ICE only provides the left to achieve the power demand. |
| → | **CSe2b mode:** Battery partially provides power; ICE working as the main power and charging the battery until achieves the point of $SoC_l$ |
| → | **CS mode:** Battey is not working; ICE provides main power for vehicle preferentially, then charging the battery till it is reaching the $SoC_l$. |

Figure 3.2 Design logic of the rule-based control strategy.

Table 3.1 Parameters of rule-based control strategy logic design

| **Parameters for design logic** | **Abbreviation** |
|---|---|
| Power demand/require | $P_{d/req}$ |
| High and low point SoC | $SoC_h$, $SoC_l$ |
| Maximum and minimum rated power of battery | $P_{b,max}$, $P_{b,min}$ |
| Instantaneous SoC | $SoC_i$ |

The design concepts for the strategy set the SoC as the priority and then consider the relationship between the power requirements and the maximum power of the battery. Compared to the working modes in traditional rule-based control strategy, the novelty of this design logic is introducing the $CS_{e2b}$ mode. In addition to setting the threshold value of $SoC_l$ and $SoC_h$, $0.5SoC_l$ has been added as the boundary of the $CS_{e2b}$ mode. The significant purpose of adding $CS_{e2b}$ mode is to last the time of pure electric propulsion and charging depletion as long as possible. It increases the percentage of EV and CD mode in the total logic control.

## 3.3 Simulation Validation

To verify the design logic, a comparison simulation based on the vehicle model and the road working conditions built from real data is presented in this section. The initial simulation model is based on the ADVISOR in MATLAB/Simulink operating environment. The control strategy proposed above will be set in MATLAB/Simulink with Simdriveline models which will invoke the same structural parameters from models of ADVISOR operating in the initial simulation. The initial control strategy will be compared to the designed rule-based control in the same vehicle model and under same input working conditions.

### 3.3.1 The parameters set in vehicle model

For the initial simulation model, it adopts the vehicle model of the first-generation Toyota Prius in ADVISOR. In terms of the rule-based control strategy, threshold values of the parameters will be set in power-split controller in Simulink Scape Driveline to achieve the design logic. Table 3.2 lists the significant parameters set in

the vehicle model. The critical values of $SoC_h$ and $SoC_l$ are set to 0.80 and 0.30, respectively.

Table 3.2 Parameters of vehicle model setting in simulation

| **Critical components of vehicle model** | **Parameters setting** |
|---|---|
| Engine | Size: 1.5L, Straight- 4\|I4 DOHC 16 valve.<br>Power: 43kW(58hp) at 4000rpm. |
| Electric motor | Power: 288V 30kW; 31kW (40hp) at 940-2000.<br>Torque: 305 N·m (225 lbf·ft) at 4000rpm. |
| Energy storage | NiMH battery with maximum 40kW power |
| Transmission | Planetary gear continuously varible transmission model |
| Wheel/Axle | Constant coefficient of rolling resistance model |
| Accessory | Constant power accessory load models |
| Override mass | 1368 kg |

### 3.3.2 The simulation and discussion

The parameters of initial conditions included several characteristics that can be adjusted from model blocks. For example, the value of the coefficient of air resistance is 0.3, wheel radius is 0.287 m, wind award area is 1.746 $m^2$ and the initial $SoC_0$ is 0.75. The input drive cycle uses one extended driving cycle of the Extra Urban Driving Cycle from a database of Economic Commission for Europe (CYC_ECE_EUDC) shown in Figure 3.3. The detailed information of one driving cycle input listed in Table 3.3. Figure 3.4 illustrates the SoC and emissions curves of the simulation results under one specific driving cycle of extended CYC_ECE_EUDC.

Table 3.3 Critical information of one CYC_ECE_EUDC driving cycle

| **Critical information of one drive cycle** | | **Vales** |
|---|---|---|
| Average speed | | 19.95 km/h |
| Distance | | 39.92 km |
| average | accelerate | 1.78 km/s$^2$ |
| | decelerate | -2.59 km/s$^2$ |
| Maximum speed | | 74.56 km/h |
| Maximum | accelerate | 3.46 km/s$^2$ |
| | decelerate | -4.56km/s$^2$ |
| Time | | 122.5 minutes |

The SoC estimation in this vehicle model uses the Ah method. Figure 3.4 (a) shows that the SoC of the battery decreases during the first 90 minutes of the driving cycle. That means the electric power is involved in propulsion for three quarters of the trip. From figure 3.3, it is clear that high-speed driving is not required in the first eighty minutes - remaining electricity in battery is affordable, battery is discharged.

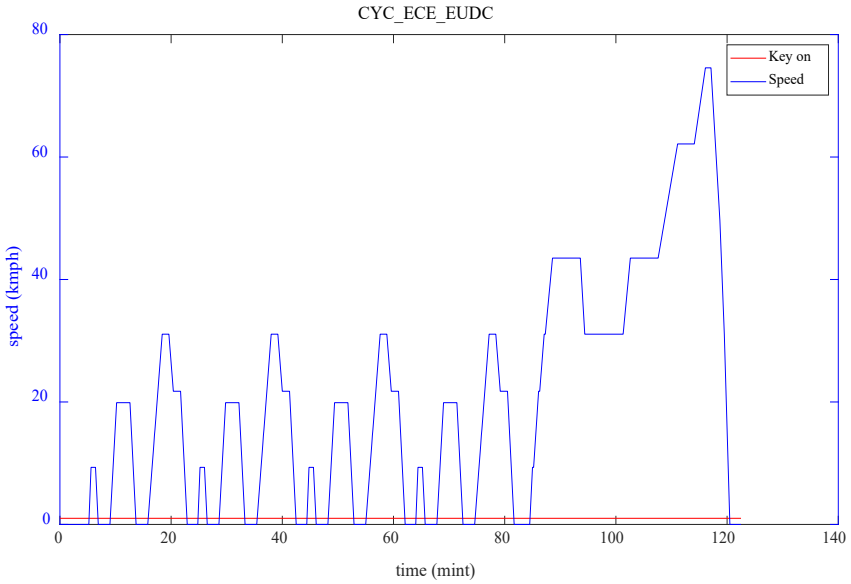


Figure 3.3 The speed input of extended CYC_ECE_EUDC.

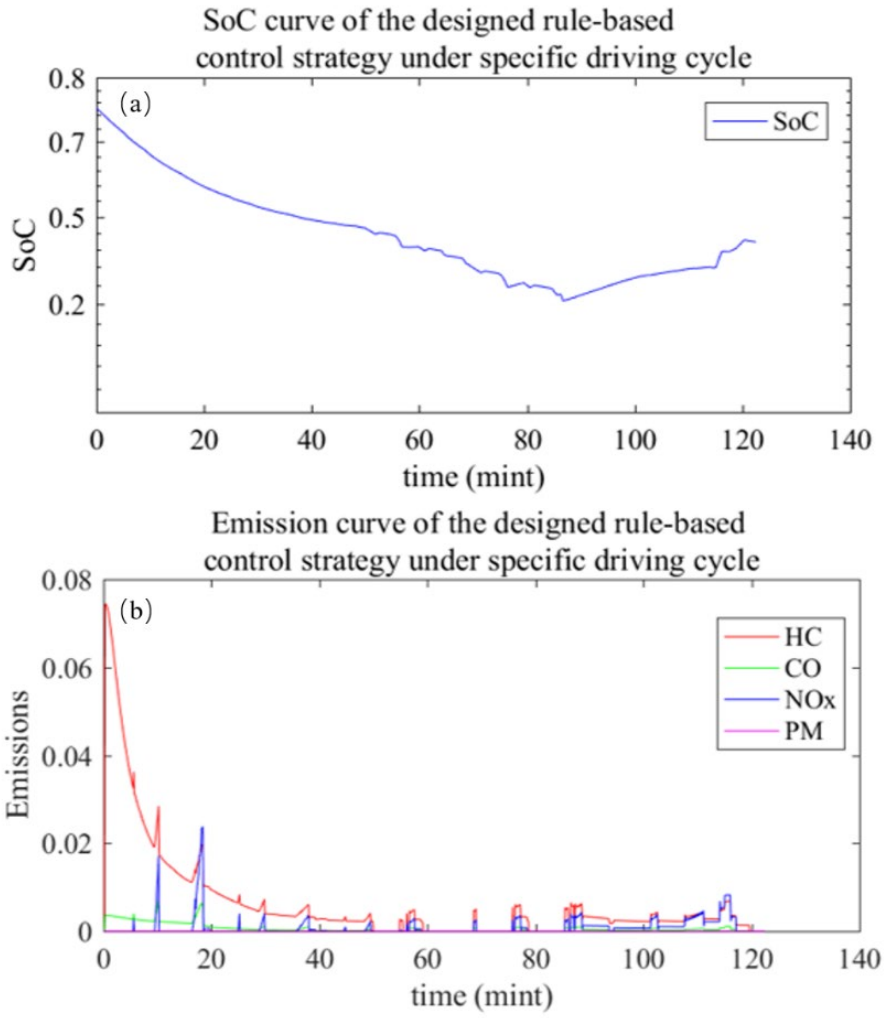


Figure 3.4 Simulation results of the emissions and SoC curve of thge designed rule-based control strategy.

The battery begins to charge at around the 90$^{th}$ minute around when the power demand is increasing with the speed up, as shown in Fig 3.4 (a). A similar charging and discharging trend could also be seen in Figure 3.5. In addition, Figures 3.6 and 3.7 illustrate the efficiency of motor and the difference between the achieved speed and the required speed, respectively. Figure 3.7 shows that the difference between the required speed and the achieved speed is in the $10^{-12}$ range, which seems negligible.

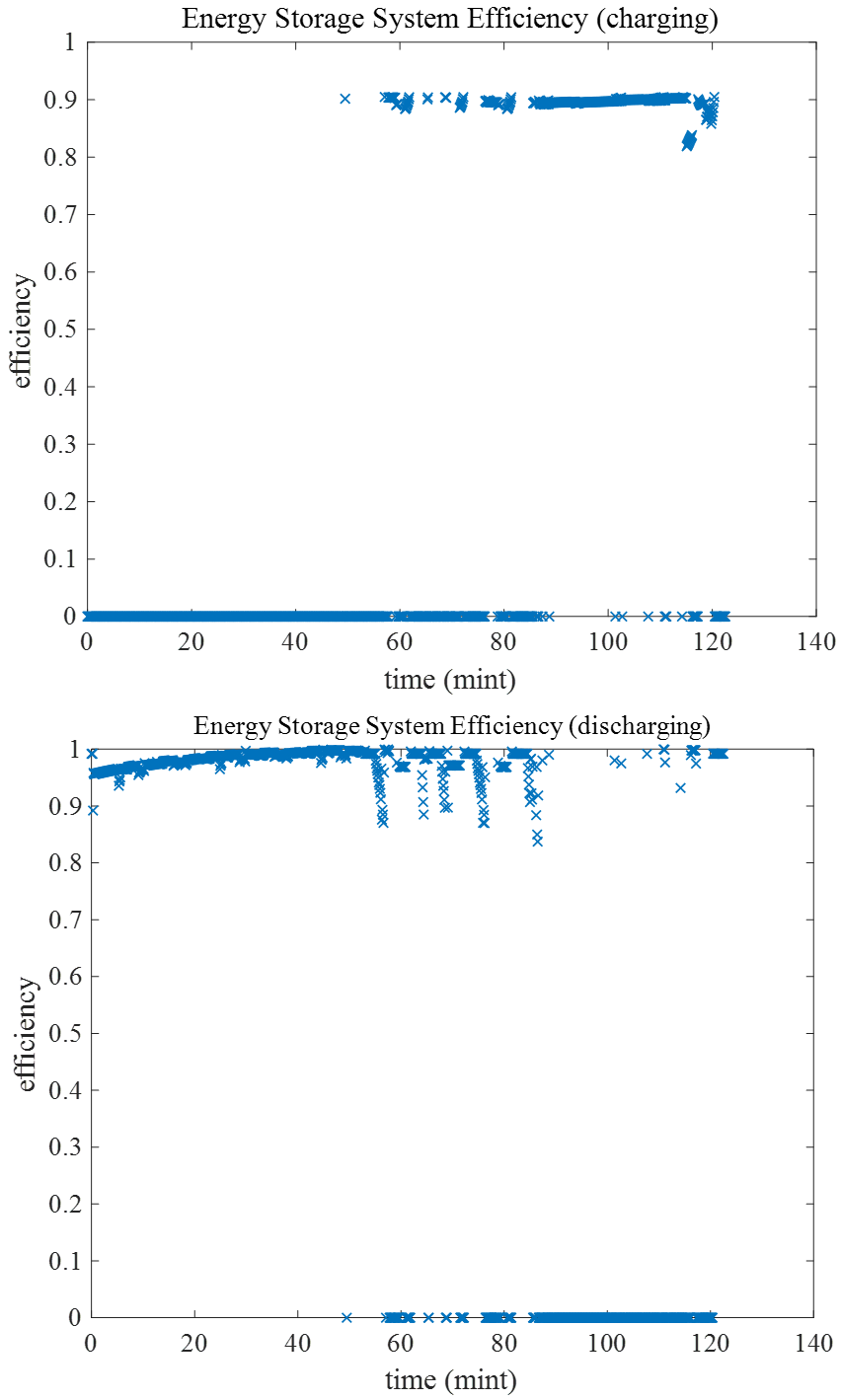


Figure 3.5 The simulation results of charging/discharging efficiency of the battery in specific driving cycle.

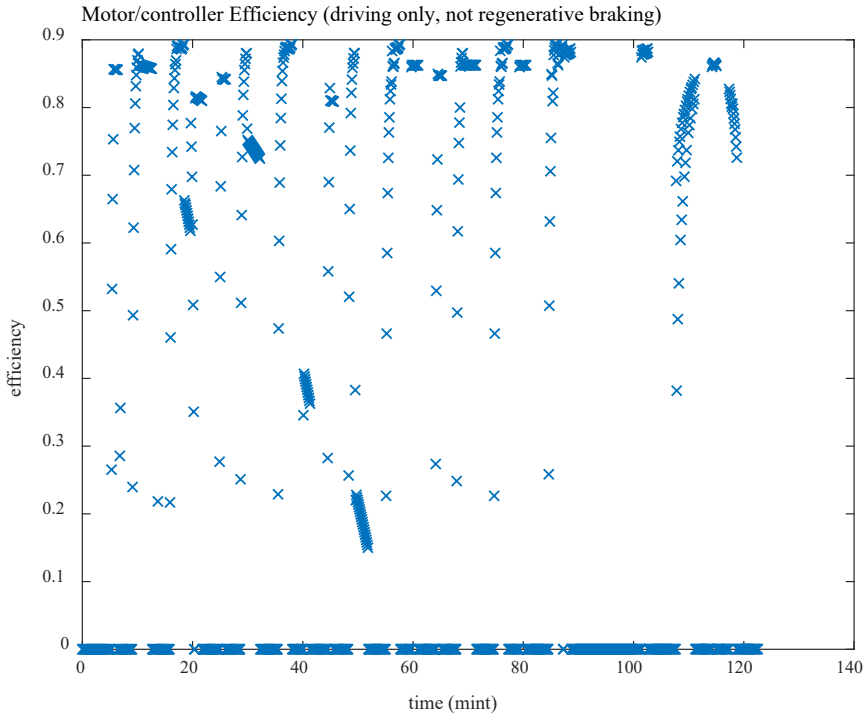


Figure 3.6 The simulation results of motor/controller efficiency in specific driving cycle.

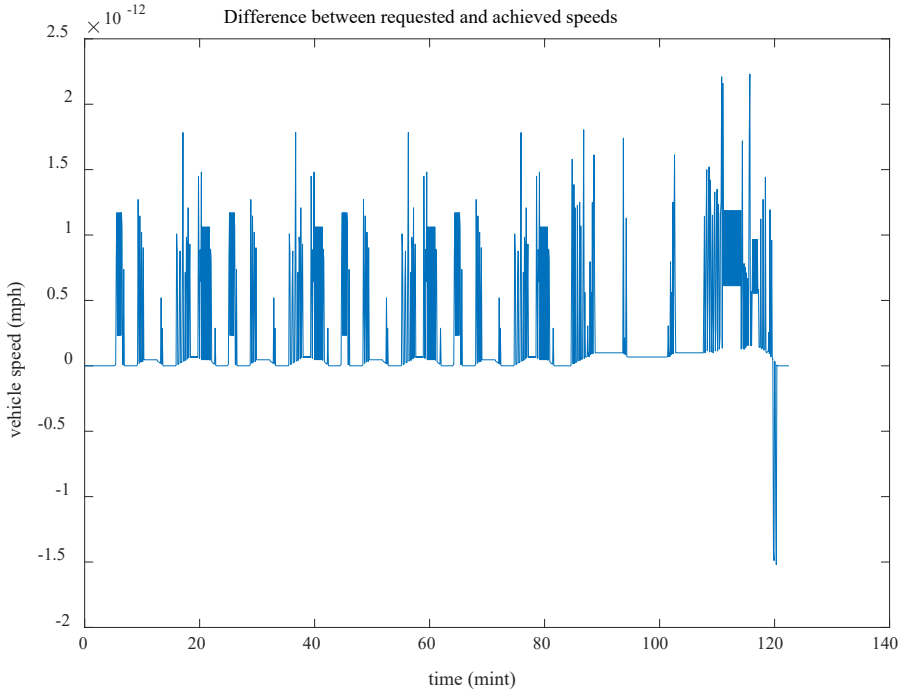


Figure 3.7 The simulation results of difference between achieved and required speed in specific driving cycle.

A comparison of the specific output values of different emission characteristics from simulation results of the traditional control strategy that are inherent in the vehicle model in ADVISOR and the designed rule-based control strategy is listed in Table 3.4. The emission of CO considerably reduced by 25.9% and the NOx emission reduced by 6.8%. There is, however, an increase in HC emission by 4.7%. The simulation results show that fuel economy (miles per gallon, mpg) increased from 45.4 to 57.9 under the designed rule-based control strategy. In terms of logic design, the engine works as the main power provider only in $CS_{e2b}$ mode. In CD or CS mode, the engine works as a parallel or auxiliary part to provide little propulsion. Thus, the vehicle performance has improved considerably through the designed rule-based control strategy.

Table 3.4 Comparison of simulation results between the designed rule-based control strategy and the inherent control strategy in ADVISOR model

| **Emission (g/km)** | **Designed rule-based control strategy** | **Inherent control strategy in Prius model** | **Comparison (%)** |
|---|---|---|---|
| CO | 0.898 | 1.213 | Decreased 25.9 |
| HC | 1.297 | 1.239 | Increased 4.7 |
| $NO_x$ | 0.161 | 0.173 | Decreased 6.7 |

## 3.4 Concluding Remarks

In chapter 2, it was discussed that the EMS plays an imperative role in the multi-energy power sources system, thus, determining the various working status of the components to avoid undesirable energy loss. This issue with most controlling and scheduling techniques proposed in literature is that it is hard to obtain an equilibrium between the efficient and sophisticated control strategies. It involves large number of calculations

and subsequent implementation costs. As a result, in this chapter, at first, the different working modes in HEV were analysed. The proposed technique included the relationships between the control logic and the working modes of the battery and the engine. A novel design of introducing the $CS_{e2b}$ mode was proposed to increase the proportion of electrical propulsion of the vehicle. The performance of the designed rule-based control strategy was verified by the simulation of Toyota Prius vehicle model and extended driving cycle (CYC_ECE_EUDC) based on real data in MATLAB. Compared to the conventional working states and inherent control strategy in ADVISOR, the simulation results of the designed rule-based control strategy successfully achieved reduction of CO and HC emissions while achieving an increase in fuel economy. These two are quite significant achievements of the work presented in this chapter.

# Chapter 4 Genetic Algorithm Optimization on the Rule-based Control Strategy for Premeditated Energy Management System

In Chapters 2 and 3, it was shown that the premeditated EMS used the method of rule-based control strategy for HEVs and can be difficult to satisfy the dynamic and complex driving conditions. The rule-based control strategy works as the reference for determining different working states of the components, which shows a poor efficiency when acting alone [119]. As a result, a hybrid EMS combined rule-based control strategy and dynamic optimization method is researched and described in this Chapter.

Various adaptive approaches applied for optimization are reported – they include the fuzzy logic control, dynamic programming, model predictive control, intelligent algorithms, *etc*. [120]. The Genetic Algorithm is one of the most widely used and well-developed heuristic evolutionary algorithms. Traditional optimization algorithms iteratively seek with a single initial value, which is easy to stray away from local optimal solution. The GA starts searching from sets of strings and a large coverage is conducive to global optimization. At the same time, the GA simultaneously processes multiple individuals in populations and reduces the risk of straying away from local optimal solution. The prerequisite knowledge of the search space or other supporting information is not required in GA. GA achieves parallelization with other algorithms on the hardware and has less calculational burden.

The GA optimization is verified by the simulative and comparative study in this chapter. The logic of the designed rule-based control strategy demonstrated in Chapter 3 is built in MATLAB_Stateflow while parameters to achieve the logic control are

converted into corresponding mechanical parameters in the vehicle model. Thereafter, bi-directional and dynamic simulation is conducted to obtain the optimal threshold values according to the fitness function based on reducing the emission and fuel consumption. The simulation results of the GA optimization compared to the designed rule-based control strategy working alone shows excellent performance in terms of emissions and fuel economy while meeting constraints set according to the power requirements  The results from this work have been submitted to a journal for publication and is currently under review.

## 4.1 Introduction

As discussed in Chapter 3, the designed rule-based control strategy is not ideal when encountering dynamic and complex driving cycles [81]. The adaptive algorithms applied in the EMS to optimize the rule-based control strategy for HEVs will improve the efficiency of the EMS when meeting different driving behaviours and environment. The algorithms for EMS have been in development since 1992 [83, 121]. These algorithms are used in different scenarios ranging from offline to online applications and from local to global optimizations.

Taking the memory constraint and the computational capacity into account, some of the algorithms with high efficiency have been used in some well-established energy control models [121]. As described in Chapter 2, control methods of the EMS have been classified into premeditated EMS and the causal EMS. The premeditated EMS uses a precalculated control policy and considers the values of inputs and real-life driving conditions to produce an expected control. The premeditated EMS with the rule-based control strategy is commonly used to generate a simplified and offline

control and does not face any computational complexity. On the other hand, casual EMS uses algorithms with dynamic characteristics to produce the control in real-time/online during real-world driving scenarios. A blended EMS combines both the premeditated EMS and the casual EMS. A premeditated decision and an instantaneous control are complementary to obtain a global and online optimization in blended EMS. The detailed optimization method applied in EMS design for the PHEV is shown in Figure 4.1. It could be divided into two pathways - rule-based control strategy and control/scheduling.

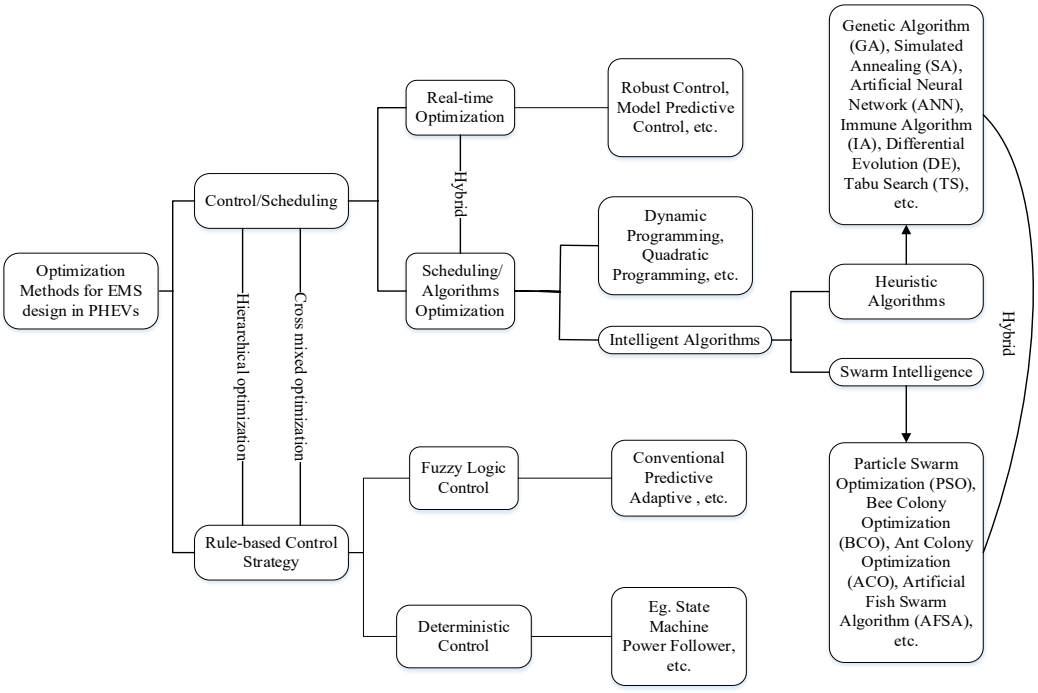


Figure 4.1 The main optimization methods utilized in vehicle EMS.

A logical relationship between the rule-based control strategy and the optimization objectives using genetic algorithm (GA) will be presented in following sections. The rule-based control strategy designs demonstrated in Chapter 3 have shown promising simulation results in terms of CO, HC and NOx emissions and better fuel economy. A

mathematical model of the hybrid rule-based control strategy and the optimization objectives using GA will be developed in this chapter. Simulation studies will be conducted using the EMS based on the proposed hybrid design to show the effectiveness in reducing emission and increasing FE. The findings of this Chapter have been submitted for a journal publication which is currently under review.

## 4.2 The Hybrid EMS Design

In Chapter 3, the objectives for rule-based control strategy design included improving the fuel economy while decreasing the emissions. They are also used as the optimization objectives in this Chapter. To solve the optimization problem in the EMS design, a mathematical model to quantitatively define the states and parameters of the system needs to be developed. Once the working states in the PHEV are defined, a mathematical model can be built and analysed with different optimization approaches to achieve an optimal parameter configuration for the EMS.

### 4.2.1 The preparation of the designed rule-based control strategy

The rule-based control strategy design is based on the theoretical analysis and an engineering intuition. The different working states in PHEV are defined with critical values. The setting of the threshold values such as the low ($SoC_l$) and high points ($SoC_h$) of the SoC in the battery will decide one of the 12 working states of the battery, engine and the EM. Figure 4.2 shows the designed rule-based control strategy with different logic states.

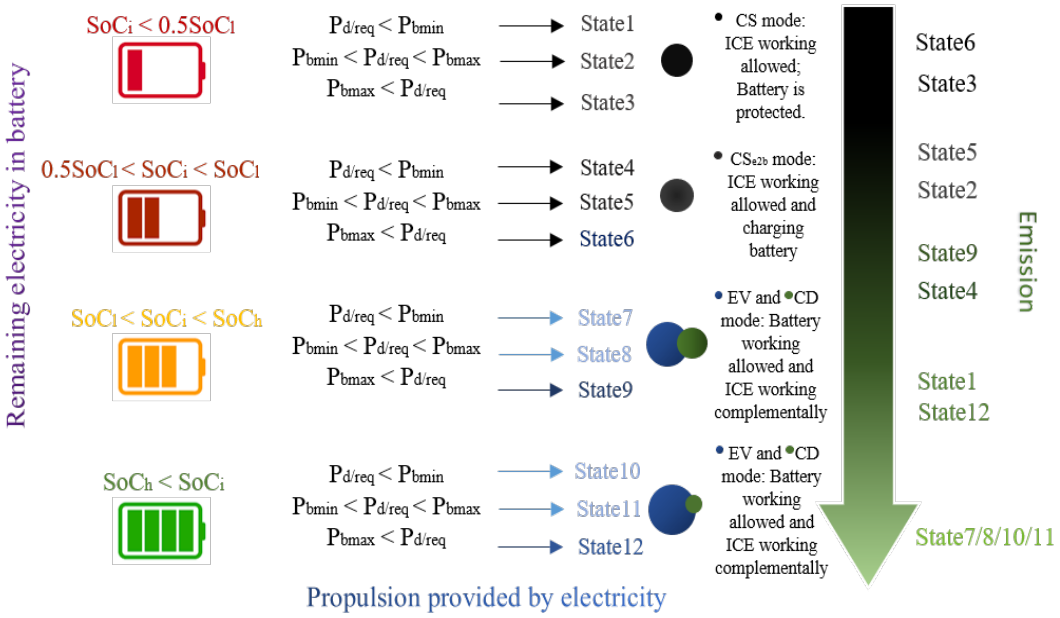


Figure 4.2 The logical states design of rule-based control strategy.

The main creative design of the rule-based control strategy is redefining the working states according to different power demand or requirements ($P_{d/req}$) and instantaneous value of the state of charge ($SoC_i$). Compared to the traditional control strategy, the designed rule-based control strategy reduces the range of the CS mode and sets up a new mode, CS Engine to Battery ($CS_{e2b}$) mode. The $CS_{e2b}$ mode allows the engine to charge the battery when the value of $SoC_i$ is lower than $SoC_l$ but not far away (higher than 50% of $SoC_l$). The engine will now charge the battery as soon as possible. When the $SoC_i$ becomes more than $SoC_l$, the working state will jump to EV and CD modes. Working in EV and CD modes will mean lower emission, which is a crucial design requirement for the EMS.

The $SoC_i$ and the $P_{d/req}$ will create 12 different states as shown in Figure 4.2. The value of $SoC_i$ shows an increasing trend from state 1 to state 12. The details of the engine and battery outputs in states 1 to 12 are itemized in Table 1 and shown in Figure 4.3.

States 1 to 3 refer to the battery output being zero. The series-parallel PHEV is powered by engine only and the battery is in a completely discharged state. The output of the engine will depend on the power demand to go faster/slower. When the amount of the charge in the battery is lower than the $SoC_l$ but higher than $0.5SoC_l$, the series-parallel PHEV will be in $CS_{e2b}$ mode. In the $CS_{e2b}$ mode (states 4 to 6), the engine charges the battery first to a level above $SoC_l$. Only after this is achieved, the battery provides power for propulsion. It should be mentioned that when power demand in state 6 is high, ICE is the major power provider and the battery will provide the necessary additional low power that is required. Under the conditions that the battery is charged by the ICE, the output value of the battery listed in Table 4.1 is zero, not negative, because the battery and ICE are two separate energy sources. The entire energy system (battery and ICE) cannot be recognized as a closed loop.

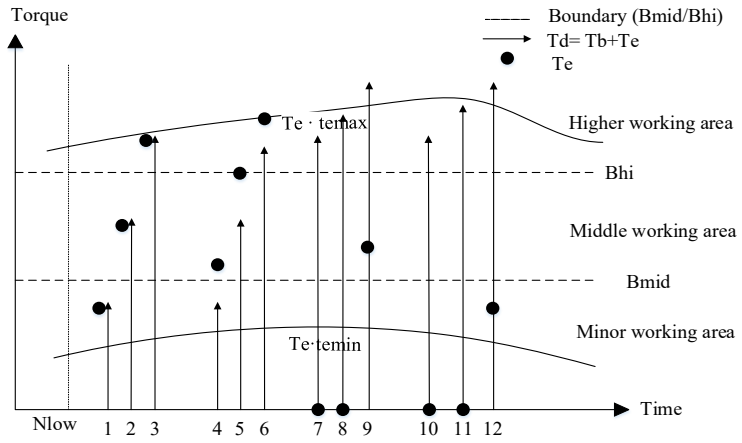


Figure 4.3The practical torque distribution of engine and battery in the rule-based control strategy

In states 7, 8, 10 and 11, once the $SoC_i$ is higher than $SoC_l$ and the power demand ($P_{d/req}$) is lower than the maximum power of the battery ($P_{bmax}$), the engine output will become zero. Table 4.1 shows that states 7, 8, 10, and 11 maintain the same output of

the engine and battery, which seems as if they could be merged. However, the output of the battery will also depend on the $P_{d/req}$, which is at different levels in states 7, 8, 10 and 11. In states 9 and 12, the battery will be set as the main power and is working in the maximum power ($P_{bmax}$) range. Meanwhile, the ICE as an auxiliary component in states 9 and 12, will work in a minimum (area shown in Figure 4.3 and small-medium range (middle working minor working area shown in Figure 4.3), respectively, depending on the instantaneous charge and power demand. Figure 4.2 shows the states 1 to 12 according to the degree of electric power participating in propulsion. The states are also ranked based on the emission in each state (green means pollution free).

Table 4.1 The power output in logic states of the rule-based control strategy

| **Condition** | **State** | **Engine** | **Battery** |
|---|---|---|---|
| $SoC_i < 0.5SoC_l$ | 1 | Output = $P_{d/req}$ | Output = 0 |
| | 2 | | |
| | 3 | Output = $P_{emax}$ | |
| $0.5SoC_l < SoC_i < SoC_l$ | 4 | Output = $P_{e2b} + P_{d/req}$ | Output = 0 |
| | 5 | | |
| | 6 | | |
| $SoC_l < SoC_i < SoC_h$ | 7 | Output = 0 | Output = $P_{d/req}$ |
| | 8 | | |
| | 9 | Output = $P_{d/req} - P_{bmax}$ | Output = $P_{bmax}$ |
| $SoC_h < SoC_i$ | 10 | Output = 0 | Output = $P_{d/req}$ |
| | 11 | | |
| | 12 | Output = $P_{d/req} - P_{bmax}$ | Output = $P_{bmax}$ |

### 4.2.2 The optimization model of the Genetic Algorithm (GA)

The GA is defined as a random search algorithm based on natural selection and genetic mechanism [122]. The optimal solution obtained by GA will not be affected by the limitations of the area and the conditions. One of the significant advantages of the GA is the strong robustness, especially when addressing a complicated and sophisticated optimization problem [122]. The GA is widely used in various fields such as complex function optimization, picture processing, machine learning, *etc.* [123].

The common process of the GA optimization is shown in Figure 4.4. It encodes the solutions from the solution space of the optimization problem to produce the initial generation of the population. According to the principle of the survival of the fittest, a new generation with better performance will be individually obtained from the previous generation. After the selection, the selected solutions will be crossed over and mutated to create a new generation. This process will be iteratively operated until a group of the solutions that show the optimum adaptive performance for the system are obtained [124].

Based on the rule-based control design strategy and the GA, the hybrid EMS of the series-parallel PHEV will be designed to reduce the Fuel Consumption (FC) and emission. The hybrid EMS design will be verified through simulation. The simulation requires an accurate mathematical model. The significant part of the mathematical module building is a correct logical relationship between the rule-based control design strategy and the GA.

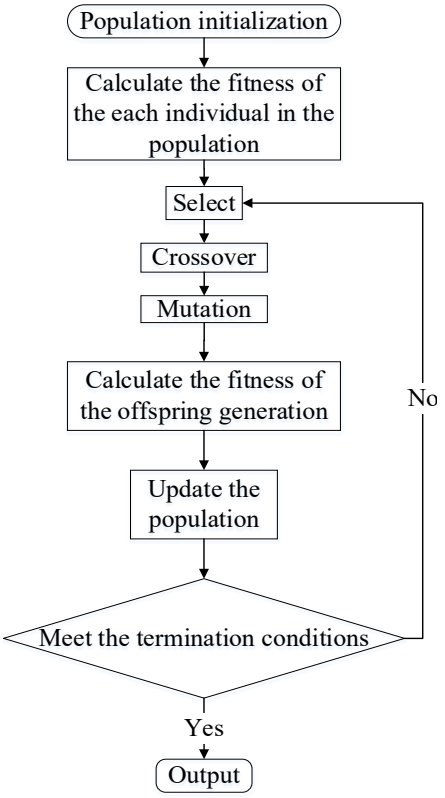


Figure 4.4 The flowchart of the GA optimization

The optimization results of the GA are sensitive to the basic set parameters such as the encoding method, the genetic operators and the iterative update model [125]. The encoding methods refer to the group of solutions. The genetic operators include the crossover operator and the mutation operator; the iterative update model depends on the fitness function, the initial generation, the population size and the termination conditions [126]. The assignment of the parameters strongly depends on the different states in the rule-based control design strategy. Therefore, the model setting of the hybrid EMS design will start from establishing the mathematical model.

## 4.3 The Hybrid Mathematical Model Building

The EMS design in this Chapter combines the rule-based control strategy and GA. The approach of GA optimization includes the constrained conditions such as the acceleration requirements, climbing ability, maximum velocity and others. The optimization objectives include the emission reduction and FE growth.

In order to obtain the most effective controlling parameters of the EMS such as the $SoC_l$, the process of using the GA searches for the optimum value for each parameter in the finite solution space. Searching the solution of the controlling parameters is based on the calculation of the fitness function [127]. The general mathematical model is expressed in equation (4-1) as follows:

$$\text{Nonlinear Programming (NLP)} \begin{cases} \min F(x) \\ s.t.\ g_j(x) \geq 0 \qquad j = 1, 2, \dots, m \end{cases}' \tag{4-1},$$

where the *F(x)* is the fitness function and $g_j(x)$ are the different constraints that refer to the performance of the vehicle.

### 4.3.1 The fitness functions

The fitness function for the GA operation is defined in Equation (4-2). The specific expressions for FC and the emission are further shown in Equation (4-3) for *F(x)*.

$$\text{Fitness function}: F(x) = \begin{cases} Fuel\ consumption: Fuel\ (x) \\ Emission: CO(x), HC(x), NO_x(x) \end{cases} \tag{4-2}$$

$$F(x) = \frac{\omega_1}{F_{Fuel-goal}} \int Fuel\,(t)dt + \frac{\omega_2}{F_{CO-goal}} \int CO\,(t)dt + \frac{\omega_3}{F_{HC-goal}} \int HC(t)dt + \frac{\omega_4}{F_{NO_x-goal}} \int NO_x(t)dt \quad (4\text{-}3),$$

where, $\omega_1$ to $\omega_4$ are the different weighting factors, $F_{Fuel\text{-}goal}$, $F_{CO\text{-}goal}$, $F_{HC\text{-}goal}$ and $F_{NOx\text{-}goal}$ are the desired values of the sub-targets. The expectation value of each sub-target are decided by the requirements of the road emission policies [128]. $\int Fuel\,(t)dt$ is the cumulative value of the instantaneous FC. It should be noted that the FC is expressed as litres/100km. Similarly, $\int CO\,(t)dt$ , $\int HC\,(t)dt$ and $\int NO_x(t)dt$ are the cumulative values of the instantaneous emissions of CO, HC, and $NO_x$, respectively. The constraint conditions referring to the vehicle performance are listed in Table 4.2.

Table 4.2 The constraints condition for vehicle performance

| **Constraints Condition** | **Requirements** | **Expression** |
|---|---|---|
| The maximum velocity ($V_{max}$) | ≥ 160 km/h | $g_1 = V_{max} \geq 160$ km/h |
| The acceleration time from 0 to 100 km/h ($T_{0\sim100km/h}$) | ≤ 12s | $g_2 = T_{0\sim100km/h} \leq 12$s |
| The acceleration time from 40 to 100 km/h ($T_{40\sim100km/h}$) | ≤ 8s | $g_3 = T_{40\sim100km/h} \leq 8$s |
| The climbing gradient within 10s at 20 km/h ($G_{20in10s}$) | ≥ 30◦ | $g_4 = G_{20in10s} \geq 30\%$ |
| The difference in velocity between the actual speed and the required speed in the cycle condition ($\Delta V$) | ≤ 0.2 km/h | $g_5 = \Delta V \leq 0.2$ km/h |
| The difference between the initial and terminal value of SoC in a cycle condition ($\Delta SoC$) | ≤ 0.5% | $g_6 = \Delta SoC \leq 0.5\%$ |

There are several mathematical methods to merge the constraint condition to the fitness function [129, 130]. The penalty function is one of the most widespread mathematical methods for the constraint condition. The use of the penalty function is highly practical and reliable. The penalty function establishes a specific constructor function based on the constraint condition. According to the individual degree of the deviation from constraints, the penalty function will decrease the value of the fitness and adds to the objective function. The optimization problem with the constraint conditions in the GA process will be converted to the final fitness function. Therefore, the fitness function with the constraint conditions discussed above can be converted to the final evaluation function that is described in Equation (4-4) as follows:

$$E\ (x) = \begin{cases} min\, F(x), & g_j(x) \geq 0\ \forall j = 1, \quad 2, \dots, m \\ F_{worst}(x) + \ \alpha \sum_{j}^{m} \left\{ max\ \left(0, g_j(x)\right) \right\}^2, & g_j(x) < 0 \end{cases} \tag{4-4},$$

where m is the number of the constraints and $\alpha$ is the penalty factor in the penalty function, $g_j(x)$ is the constraint condition, and $F_{worst}(x)$ is the objective function of the worst solution in the population.

### 4.3.2 The set of solutions of the GA

A significant process in GA is defining the dimension of the solutions according to the rule-based control design strategy. The calculation of fitness value in GA is based on the vehicle model in the simulation environment. Therefore, the set of solutions include not only the controlling parameters but also the related mechanical parameters, for example, the torque demand ($T_d$), the torque from the engine ($T_e$) and the battery

or EM ($T_b$). $T_d$ also refers to the total output torque from the coupler. Based on the rule-based control design strategy (see Figure 4.2 and Table 4.1), the mechanical states of the EM and the ICE from states 1 to 12 are shown in Figure 4.3. In the figure, the X-axis is time and the Y-axis is torque. There are three fundamental lines that are particular to the characteristic curve of ICE: the lines of the $T_e \cdot t_{emax}$ and $T_e \cdot t_{emin}$ in the figure show the maximum and minimum output powers of the ICE, respectively and $t_{emax}$ and $t_{emin}$ are the maximum and minimum torque envelope coefficients, respectively. This is taken from the database in ADVISOR [131]. $N_{low}$ is the start-stop line for the engine. In the area to the left of $N_{low}$, the engine is off while it is on in the area to the right of $N_{low}$. Based on the logical states of the rule-based control design strategy, the dotted straight lines in the figure separate the three working areas – minor, middle and higher working areas. In states 1, 2 and 3, the total torque $T_d$ is entirely due to ICE - the battery is not supplying any power. In states 4, 5 and 6, the torque from the engine charges the battery with priority and provides the propulsion at the same time. The ICE stops in states 7, 8, 10 and 11 where the value of $T_e$ is zero. The $T_b$ is the dominating torque in states 9 and 12 - while $T_e$ is not zero in these states, it is small compared to $T_b$. Based on the conditions illustrated in Figure 4.3, the group of solutions in GA process include 8 parameters of the vehicle model. The eight-dimensional solution as a group in the GA process is shown in Table 4.3.

Table 4.3 the group of the solutions for GA optimization based on rule-based control strategy

| The group of solution | Parameter representative | Parameter properties |
|---|---|---|
| $x_1$ | $SoC_l$ | Logical controlling |
| $x_2$ | $SoC_h$ | |
| $x_3$ | $C_{tchg}$ | |
| $x_4$ | $B_{mid}$ | |
| $x_5$ | $B_{hi}$ | |
| $x_6$ | $N_{low}$ | Mechanical |
| $x_7$ | $t_{emax}$ | |
| $x_8$ | $t_{emin}$ | |

The parameter $N_{low}$ will decide the state to start the engine. $B_{mid}$ is the boundary at which the engine jumps from minor working area into the middle working area. $B_{hi}$ is the boundary at which the engine jumps from middle working area to high working area. In the rule-based control strategy, $B_{mid}$ and $B_{hi}$ have specific values, *i.e.*, 0.25 and 0.7, respectively. But in GA, these two values will be varying and will be optimized. $t_{emax}$ and $t_{emin}$ are the maximum and minimum torque envelope coefficients, respectively. $SoC_h$ and $SoC_l$ of the battery are the other two significant controlling parameters relating to the battery. The coefficient of the charging torque ($C_{tchg}$) will decide the amount of torque difference between the engine and EM. The $C_{tchg}$ decides the threshold of high and low charge from the engine to the battery.

### 4.3.3 The initial population setting of the GA

The size of population (*NP*) is a parameter that significantly impacts the optimum results. The values of *NP* can vary from ten to hundreds of thousands depending on specific problems [132]. Usually, the value of *NP* is set 10 times the dimension of the

set of solutions [132]. It should be pointed out that there is no direct evidence that the *NP* relates to the dimension. Using the principle of '10 times the dimension' to set the *NP* value has been shown not applicable to a large population, for example, if the dimension is more than 100 [132]. The computing complexity will linearly increase with the convergence time in a large population with high dimension. A small *NP* seems more appropriate in small-scale optimization problems [132].

Meanwhile, reduced *NP* appears in large-scale optimization problems because of the advantage of forming the subset population [133]. For example, serval researchers have set *NP* as $2^d$, where $d$ refers to the dimension [134]. For very large-scale optimization problems, a larger *NP* with a high-dimension solution will significantly increase the calculation complexity and operation cycle [135]. In terms of energy optimization in PHEV, the general scale of dimension is no more than 20 and the range of *NP* will be in a range from 50 to 200 [136].

### 4.3.4 The parameters of operators in the GA

In order to obtain an optimum solution, the best offspring solution will be selected to bring the qualified gene to the next generation. Through the selection of suitable gene, optimum solution is achieved through an iterative process.

The comma selection is one of the most common methods used in GA [137]. It randomly takes $\mu$ solutions from the parent population based on the fitness value. The selected solution meeting the termination condition is roughly considered as the best solution [138]. However, the comma selection lacks precision - the main reason is the possibility of missing the better solution due to the randomness [138]. Compared to

the comma selection, the plus selection enhances the diversity of the gene. The plus selection forms the new generation that includes part of $\mu$ offspring solutions in random selection and the $\lambda$ parent solutions [139].

The process of the comma selection and plus selection depends on the randomness. The roulette wheel selection is better than both in terms of the fitness proportional selection. The probability of being selected by the roulette wheel depends on the individual fitness value of each solution [139]. The mathematical expression of the selection probability ($P_s$) in a roulette wheel is shown in Equation (4-5). The $P_s$ is the ratio of fitness value of individual solution ($F(x_i)$) to the sum of the fitness values of the whole generation that includes $n$ sets of solutions [140]. The different selection method should be appropriately adopted according to the specific scenarios.

$$P_S = \frac{\mathrm{F}(x_i)}{\sum_{i=1}^{n} F(x_i)} \tag{4-5}$$

The crossover operator is commonly in the form of probability ($P_c$) or a dynamic function of variables [141]. One of the common crossover operations is the N-node crossover. Two groups of solutions (chromosomes) are divided into $N$ nodes. The offspring will then be generated by randomly exchanging the corresponding partition of these two groups of solutions [142].

Another commonly used crossover method is the arithmetic crossover operation [141]. The arithmetic crossover is known as the intermedia crossover, which calculates the arithmetic mean value of two sets of solutions as the generated offspring [141]. The $P_c$

is a constant ratio in the uniform crossover, which will control the frequency of crossover operation [123]. The common range of $P_c$ is from 0.25 to1. A large $P_c$ enhances the ability to develop the new searching area but can easily reduce the performance of the solution. A low $P_c$ leads to slow GA searching speed [141].

The mutation operation is the auxiliary searching process in GA. The main purpose of mutation is maintaining the diversity of the population [143]. The form of mutation operator is similar to the crossover, which could be a constant probability ($P_m$) or a dynamic function of variables [144]. The Gaussian mutation as the representative dynamic operator has been extensively reported [145]. The Gaussian mutation is based on the Gaussian distribution. The offspring ($X'$) generated through the Gaussian mutation as shown in Equation (4-6).

$$X' = X_i + \gamma \cdot N(\tau, \sigma^2) \tag{4-6}$$

where the $X_i$ is the group of solutions after the crossover operation and $\gamma$ is the mutation rate. It multiplies the normal distribution with a mathematical expectation of $\tau$ and variance of $\sigma^2$. The term $\gamma \cdot N(\tau, \sigma^2)$ results in an increased local area searching. It improves the convergence of the algorithm but could affect the global evolution [90].

The flip mutation based on the randomness is frequently utilized in the binary coding method [90]. In flip mutation, each of the bit will be reversed with the probability of $\gamma = \frac{1}{L}$, where $L$ is the length of the string [146]. Another main approach of mutation is the random mutation with a specific probability ($P_m$). The common range of the $P_m$

is from 0.001 to 0.1. Generally, the risk of losing the significant characteristics (gene) is prevented from the low $P_m$. A high $P_m$ convert the GA to the random search [136, 147].

## 4.4 The Simulation Studies

The essence of GA is a probabilistic searching algorithm depending on the iterative fitness value [129]. For the proposed hybrid optimization in this research, the rule-based control design strategy targets on the steady EMS. The dynamic searching is achieved through the GA optimization simulation. As described in Sections 4.3.3 and 4.3.4, the initial *NP* setting is 100; the roulette wheel is used in selection process; the *N-node* approach is used in the crossover and the Gaussian mutation is adopted.

### 4.4.1 The simulation preparation of the GA optimization

The process of the hybrid optimization with simulation is shown in Figure 4.5. According to the mathematical model shown in Equations (4-1) to (4-6), the GA operation in MATLAB mainly includes the eight parameters expressed in Equation (4-7) as follows:

$$\text{GA}= (C, E, P_0, NP, \Phi, T, \Psi, T) \tag{4-7}$$

where $C$ is the encoding method, $E$ is the evaluation approach, $P_0$ is the initial population, $NP$ is the size of the population, $T$ is the termination condition, $\Phi$, $T$ and $\Psi$ are the selection, crossover and mutation operators, respectively. The lower and upper limits of the group of solutions from $x_1$ to $x_8$ are listed in Table 4.4.

Table 4.4 The value range of each solution

| The group of solution | Parameter representative | Lower limit | Upper limit |
|---|---|---|---|
| $x_1$ | $SoC_l$ | 0.1 | 0.5 |
| $x_2$ | $SoC_h$ | 0.5 | 0.9 |
| $x_3$ | $C_{tchg}$ | 0 | 1 |
| $x_4$ | $B_{mid}$ | 0 | 0.6 |
| $x_5$ | $B_{hi}$ | 0.4 | 0.8 |
| $x_6$ | $N_{low}$ | 10 | 30 |
| $x_7$ | $t_{emax}$ | 0.3 | 0.8 |
| $x_8$ | $t_{emin}$ | 0.7 | 0.91 |

The first step (see in Figure 4.5) is logically mapping the rule-based control design strategy to the group of solutions in GA. It decides the group of parameters/threshold values that will be optimized in the vehicle model.

Since each solution operated in the vehicle model is a real number, appropriate encoding and decoding methods are required in the process of GA optimization. Therefore, the group of solutions is firstly encoded through binary code in step 2 (see Figure 4.5). The length of the bit string ($L_{total}$) depends on the accuracy of the actual numerical values of each solution. The length of the string for the group of solutions ($X$) is a sum of length of individual solution after encoding ($L_i$). The binary coding method for each solution is given by Equation (4-8) as shown below.

$$2^{L_i-1} < (b_i - a_i) \times 10^A \leq 2^{L_i} - 1 \tag{4-8}$$

where $b_i$ and $a_i$ refer to the upper and lower limits of each solution, respectively. $A$ is the accuracy of the solution, down to two decimal points in this section.

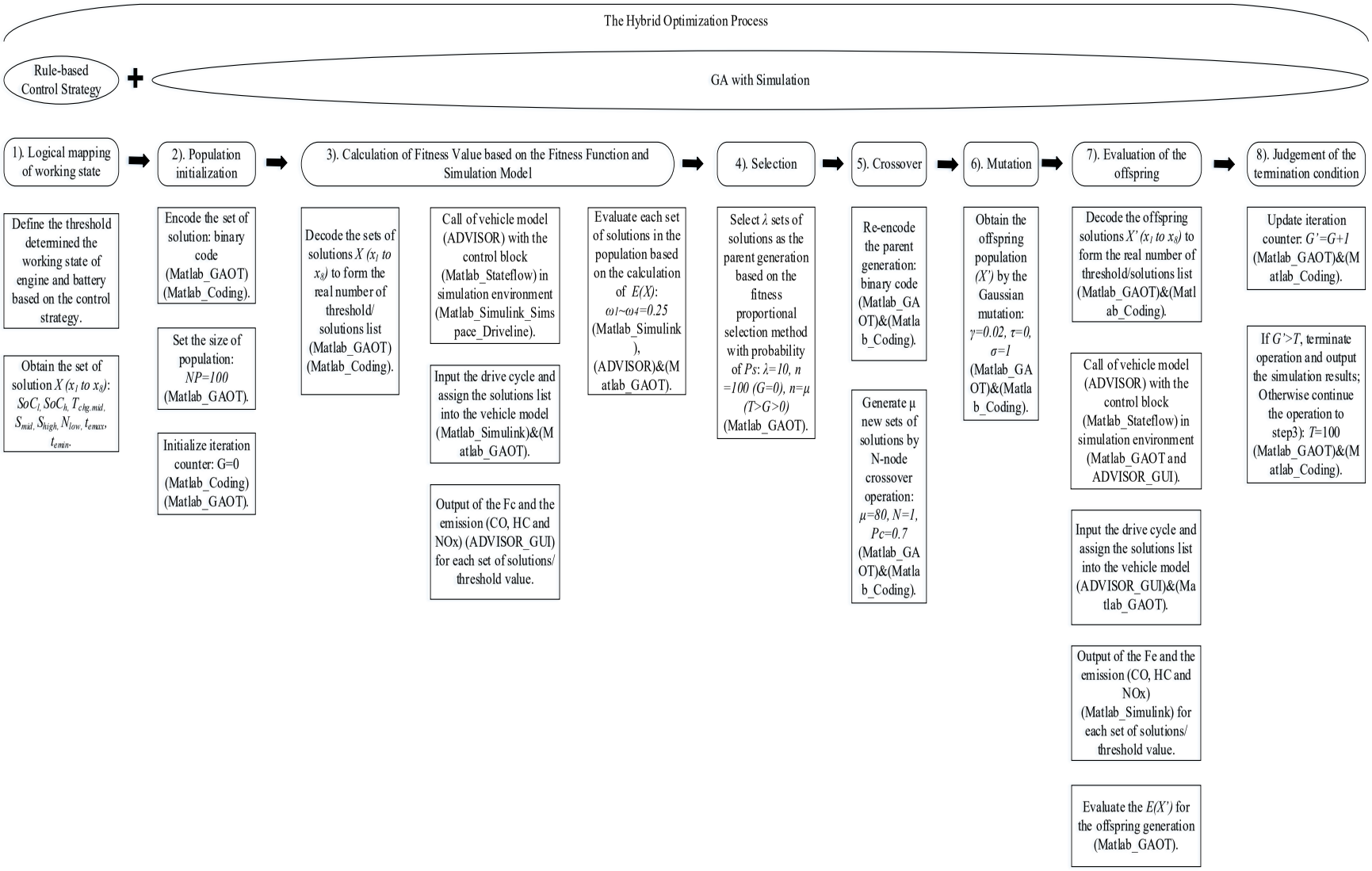


Figure 4.5 The hybrid optimization simulation process of rule-based control and the GA.

For example, $L_1 = 6$ when $b_1 = 0.9$ and $a_1 = 0.5$ for $x_1$. Therefore, the encoded string with $L_{total} = 47$ is obtained, where ($L_1$, $L_2$, $L_3$, $L_4$, $L_5$, $L_6$, $L_7$, $L_8$) = (6, 6, 7, 6, 6, 11, 6, 5).

Once the population is generated, the genotyped string will be encoded to form initial population ($P_0$). The value of $NP$ is 100 in this section. The generation counter ($G$) is initialized to 0 when it randomly generates 100 sets of solutions. The calculation process is conducted in the MATLAB_GAOT based on the vehicle model and input working conditions.

The third step (see Figure 4.5) evaluates the solution through the fitness function. The expression of fitness function directly or indirectly refers to the variable in the general utilization of GA. $X$ ($x_1$, $x_2$, $\cdots$, $x_8$) is the set of variables in the fitness function shown in Equation (4-3). However, right hand side of Equation (4-3) is the sum of the integrals of emissions and fuel consumption over time. Compared to the common fitness function, the specific difference in this scenario is the fitness evaluation. The different solutions from $x_1$ to $x_8$ will be set in vehicle model. Then, the working conditions are input to the vehicle model to obtain the corresponding results of emission and fuel consumption.

The solutions will be decoded in the form of binary string into a real value that could be set in the vehicle model. The vehicle model (PRIUS_JPN_defaults_in 2013) is called from the ADVISOR [131]. The different working states in rule-based control design strategy are achieved in the control block in MATLAB_stateflow. The penalty function with constraints $g_1$ to $g_6$ will be calculated by calling the interface of the

adv_no_gui in ADVISOR. The optimization target sub-values, $F_{Fule\text{-}goal}$, $F_{CO\text{-}goal}$, $F_{CH\text{-}goal}$ and $F_{NOx\text{-}goal}$, are set in MATLAB_GAOT to evaluate the fitness function $E(X)$. Table 4.5 lists the values set for each target sub-values based on the Europe emission standard [128]. Since the optimization weights are assumed to be the same for each optimization goal in this Chapter, the weighting factors $\omega_1$ to $\omega_4$ in Equation (4-3) are all set equal to 0.25 (1/4).

Table 4.5 the target sub-value set for the fitness function in GA [128]

| **Europe emission standard** | $F_{Fule\text{-}goal}$ **(L/100 km)** | $F_{CO\text{-}goal}$ **(g/km)** | $F_{CH\text{-}goal}$ **(g/km)** | $F_{NOx\text{-}goal}$ **(g/km)** |
|---|---|---|---|---|
| EURO VI (Sep. 2014) passenger vehicle | 6 | 1.00 | 0.10 | 0.08 |

Step 4 (see in Figure 4.5) is the selection operation. In this research, 10 sets of solutions ($\lambda$ = 10) are selected as the parent to be breeding. The fitness proportional selection method in Equation (4-5) is adopted. The $P_s$ uses $n = NP = 100$ when selecting the solutions from the first or initial generation ($G$ = 0) and $n = \mu = 80$ after the first generation until termination.

The process of the crossover occurs after obtaining the selected offspring. Since the selection is based on the fitness evaluation in the form of a real number, the first operation in step 5 (see Figure 4.5) is re-encoding the parent generation. The N-node crossover operation is utilized in this research. One node ($N$ = 1) randomly divides the string into two segments. The segments will correspondingly crossover with the probability of 0.7 ($P_c$ = 0.7).

The mutation to maintain the diversity of the solution space will be occur in step 6 (see in Figure 4.5). The fitness proportional selection method was used to find a better solution in step 5 (see Figure 4.5). The Gaussian mutation was found to improve the capability of local search. The Gaussian mutation will hardly affect the convergence of calculation for a small-scale scenario. Equation (4-6) uses the standard normal distribution, in which $\tau = 0$, $\sigma = 1$. The mutation probability approximately takes $\gamma = 0.02$ since the value of $P_m$ is 1/47 ($1/L$) when the accuracy is to two decimal places.

According to the normal GA process shown in Figure 4.2, the offspring generation ($X'$) produced in step 6 will be similarly re-evaluated in step 7 (see Figure 4.5). The operation is achieved by decoding the offspring generation, calling the vehicle model and running the same work cycle. After the evaluation of the offspring generation $E(X')$, the iteration counter will be updated by $G' = G+1$. The GA process in step 8 (see Figure 4.5) will be capped at 100 if the solution is not yet achieved.

### 4.4.2 The simulation model

The simulation results of the hybrid optimization design are compared to the single function of the rule-based control strategy [84]. Therefore, the vehicle model called from ADVISOR is the same as the one in simulation of the rule-based control design strategy in Chapter 3. The detailed information of the vehicle model was listed in Table 3.2. The logic of the designed rule-based control strategy is achieved through MATLAB Simulink_stateflow. The whole vehicle model block and the rule-based control design strategy in Stateflow block built using the Simulink environment is shown in Figure 4.6.

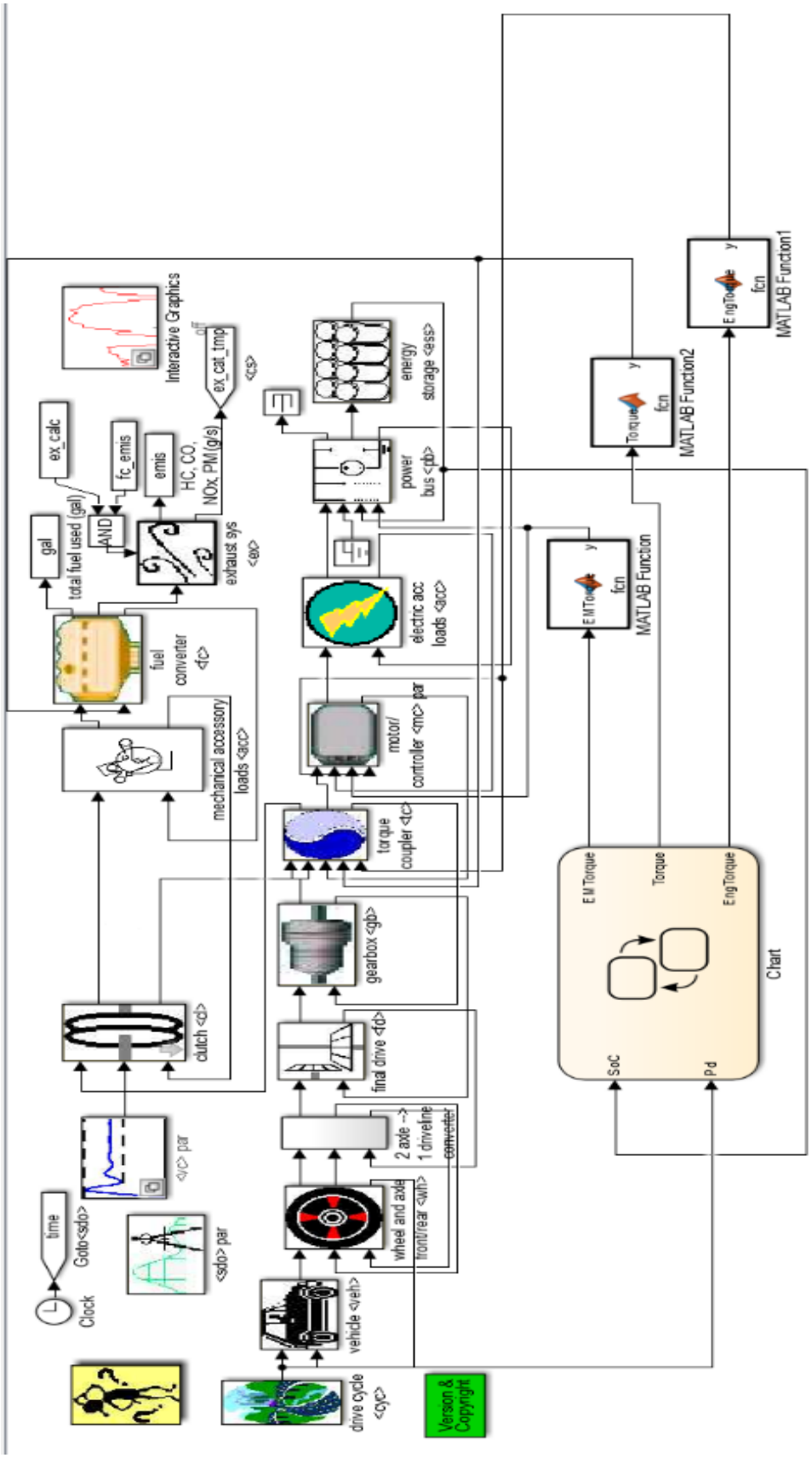


Figure 4.6 The vehicle model with the rule-based control strategy for simulation

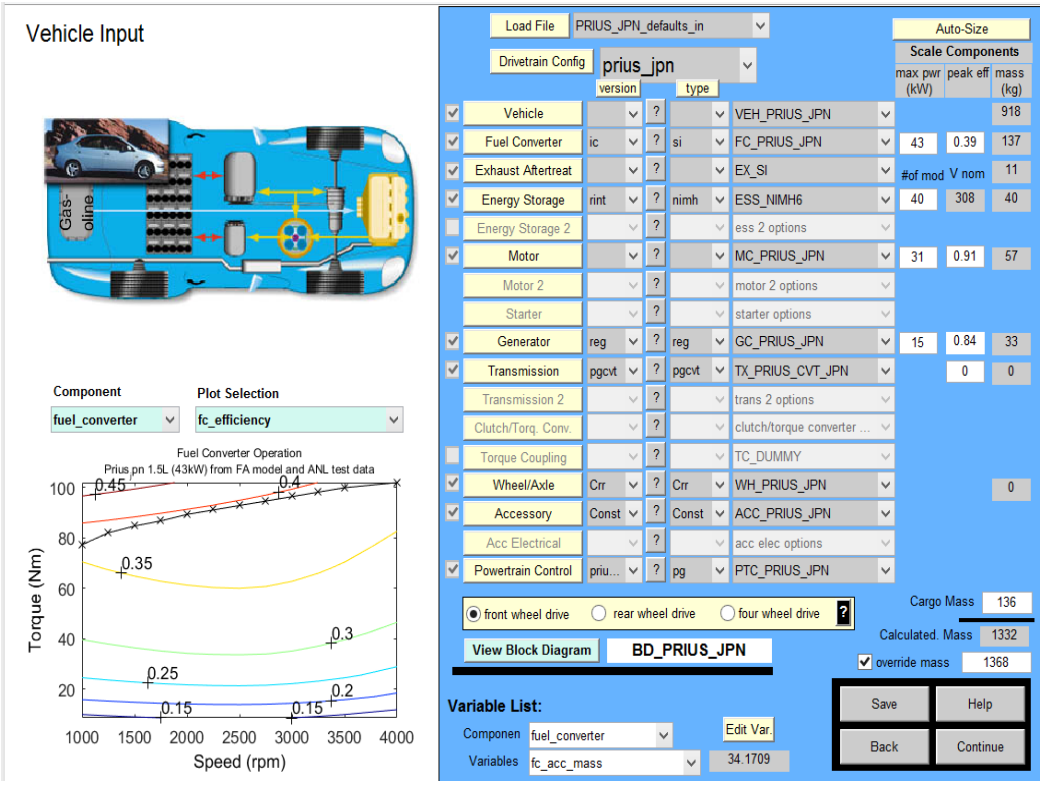


Figure 4.7 The vehicle model called from ADVISOR for simulation.

The GA process was operated in the MATLAB_GAOT and the ADVISOR_GUI based on the simulation process described in Figure 4.7. The GA is achieved by scripting the functions from MATLAB_GAOT. There are five docking ports. They include two inputs from the drive cycle ($P_d$) and energy storage ($SoC$), respectively. Three outputs to Simulink are the EMTorque to EM, Torque to ICE and EngTorque to the generator. In terms of the state jump and conditional transfers of the individual block, the enumeration variables (Engmode, Genmode and EMmode) are built by an enumerated-type function. The value transfer in different states is realized through the truth table in MATLAB_stateflow (see Figure 4.8).

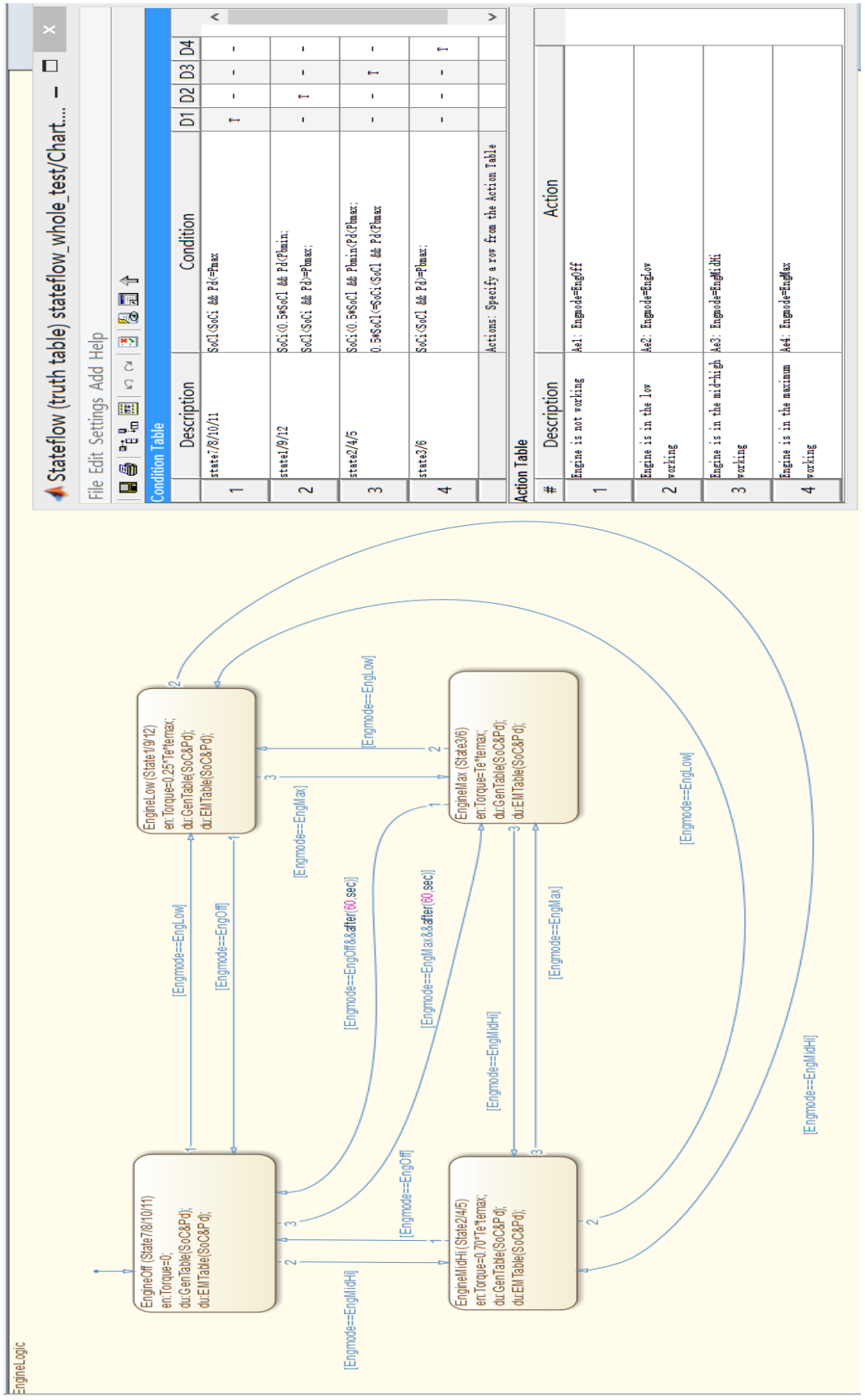
Stateflow (truth table) stateflow_whole_test/Chart....
File Edit Settings Add Help
Condition Table
Condition
Description
D1
D2
D3
D4
1
state7/8/10/11
SoC1<SoC1 && Pd<Pmax
T
-
-
-
2
state1/9/12
SoC1<0.5*SoC1 && Pd<Pmin;
SoC1<SoC1 && Pd>=Pmax;
-
T
-
-
3
state2/4/5
SoC1<0.5*SoC1 && Pmin<Pd<Pmax;
0.5*SoC1<=SoC1<SoC1 && Pd<Pmax
-
-
T
-
4
state3/6
SoC1<SoC1 && Pd>=Pmax;
-
-
-
T
Actions: Specify a row from the Action Table
Action Table
#
Description
Action
1
Engine is not working
Ae1: Engmode=EngOff
2
Engine is in the low working
Ae2: Engmode=EngLow
3
Engine is in the mid-high working
Ae3: Engmode=EngMidHi
4
Engine is in the maximum working
Ae4: Engmode=EngMax
EngineLogic
EngineOff (State7/8/10/11)
en:Torque=0;
dur:GenTable(SoC&Pd);
dur:EMTable(SoC&Pd);
EngineLow (State1/9/12)
en:Torque=0.25*Te*temax;
dur:GenTable(SoC&Pd);
dur:EMTable(SoC&Pd);
EngineMidHi (State2/4/5)
en:Torque=0.70*Te*temax;
dur:GenTable(SoC&Pd);
dur:EMTable(SoC&Pd);
EngineMax (State3/6)
en:Torque=Te*temax;
dur:GenTable(SoC&Pd);
dur:EMTable(SoC&Pd);
[Engmode==EngLow]
[Engmode==EngOff]
[Engmode==EngMax]
[Engmode==EngLow]
[Engmode==EngOff&&after(60,sec)]
[Engmode==EngMax&&after(60,sec)]
[Engmode==EngMidHi]
[Engmode==EngMax]
[Engmode==EngMidHi]
[Engmode==EngLow]
[Engmode==EngMidHi]

(a)

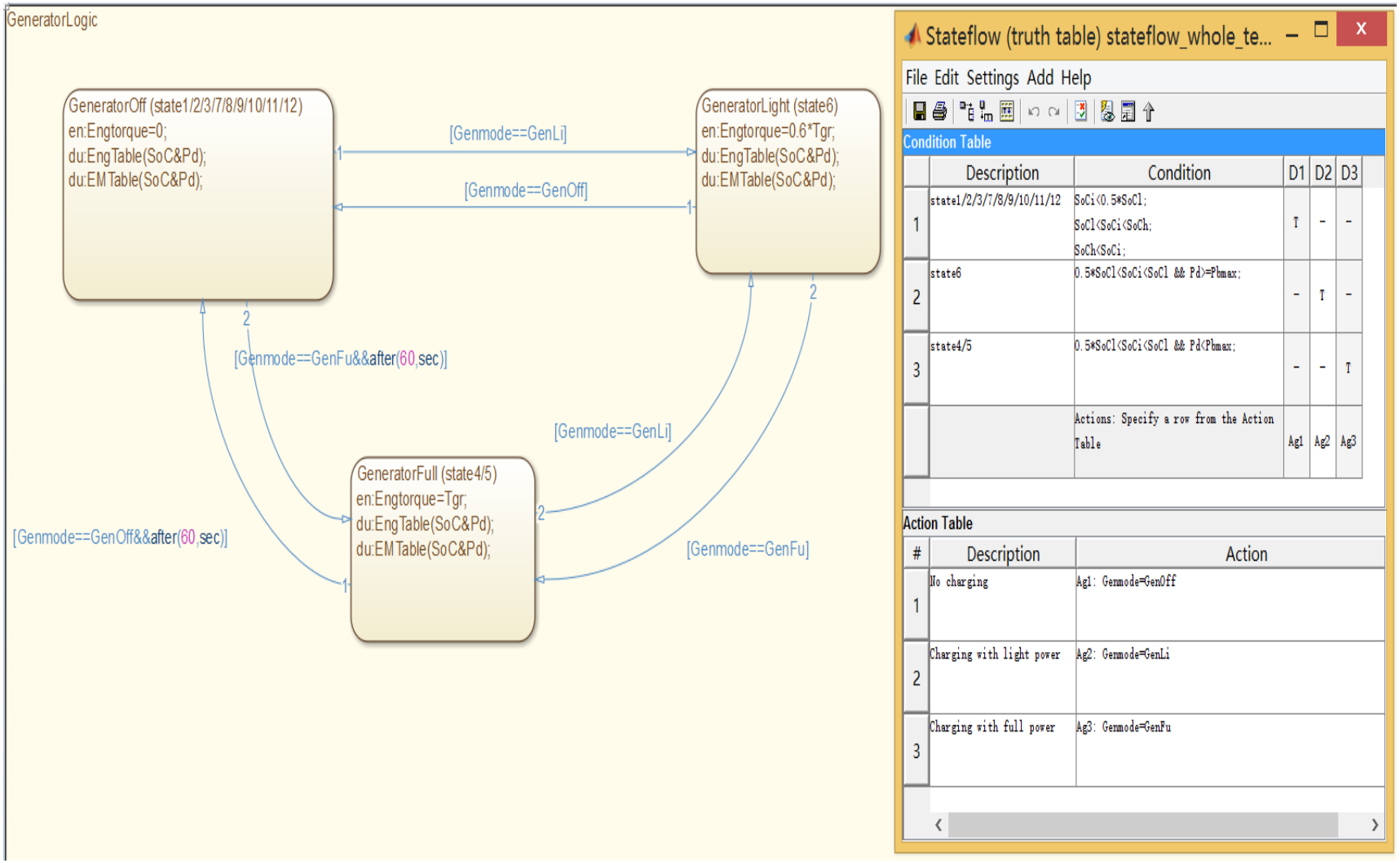


| | Description | Condition | D1 | D2 | D3 |
|---|---|---|---|---|---|
| 1 | state1/2/3/7/8/9/10/11/12 | SoCi<0.5*SoCl;<br>SoCl<SoCi<SoCh;<br>SoCh<SoCi; | T | - | - |
| 2 | state6 | 0.5*SoCl<SoCi<SoCl && Pd>=Pbmax; | - | T | - |
| 3 | state4/5 | 0.5*SoCl<SoCi<SoCl && Pd<Pbmax; | - | - | T |
| | | Actions: Specify a row from the Action Table | Ag1 | Ag2 | Ag3 |

| # | Description | Action |
|---|---|---|
| 1 | No charging | Ag1: Genmode=GenOff |
| 2 | Charging with light power | Ag2: Genmode=GenLi |
| 3 | Charging with full power | Ag3: Genmode=GenFu |

(b)

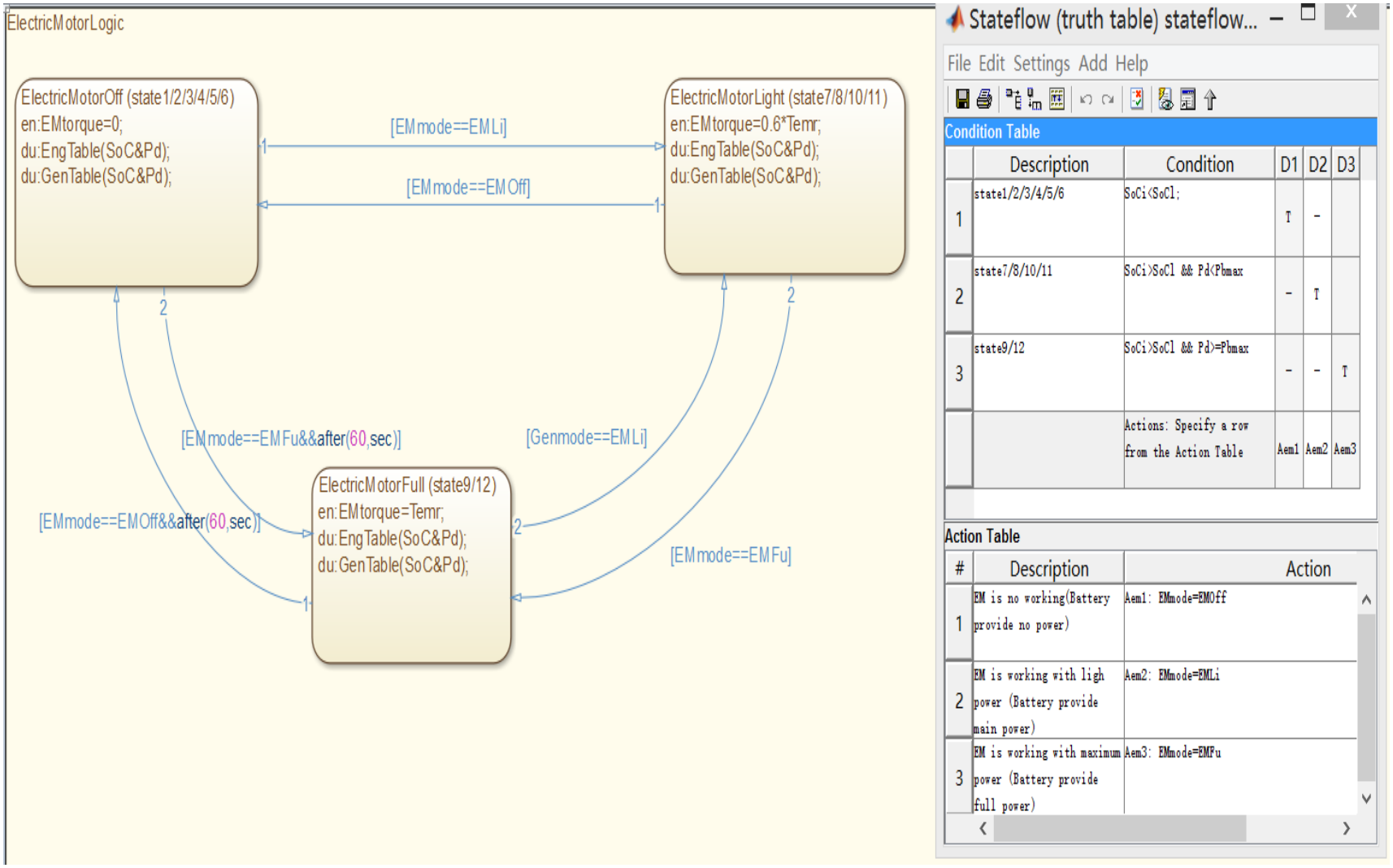


Figure 4.8 The rule-based control design strategy achieved in Matlab_Stateflow: (a) the rule-based control logic of the engine, (b) the control logic of the generator and (c) the control logic of the EM

Figures 4.8 (a), (b) and (c) show the internal state jumps and the corresponding truth table in the blocks of the ICE, generator and EM, respectively. The values of mechanical parameters and the initial values of logical controlling parameters are listed in Table 6. The parameter marked with an asterisk (*) is the one that will be optimized in the GA process. To clearly compare the hybrid optimization design to the rule-based control design strategy, input of working condition will adopt the same Extended CYC_ECE_EUDC, as shown in Figure3.3 in Chapter 3.

### 4.4.3 The simulation results

Based on the simulation process described in Section 4.4.2, the simulation results are plotted in a MATLAB environment. The curve of the GA objectives values is shown in Figure 4.9. The objectives of each section are plotted in a three-dimensional diagram in Figure 4.10, which is the HC, CO and $NO_x$ emission based on the charging factor and number of iterations. The detailed data of each optimal objectives and the parameters extracted from the simulation are listed in Table 4.6.

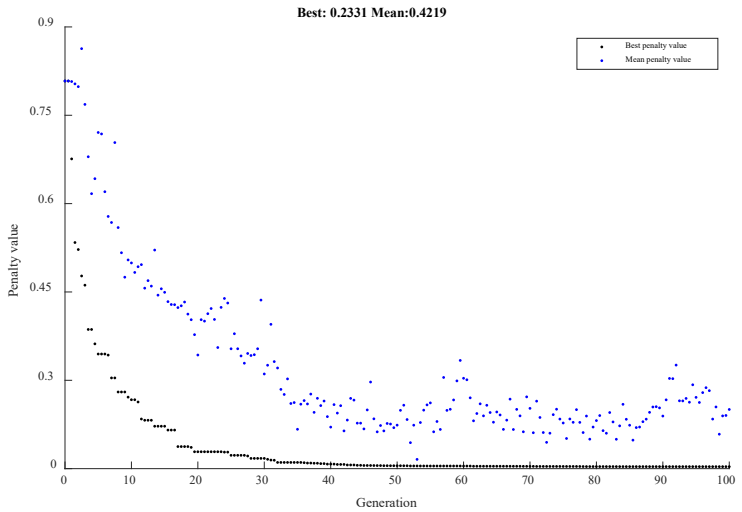


Figure 4.9 The GA optimization results based on the fitness value and iterations.

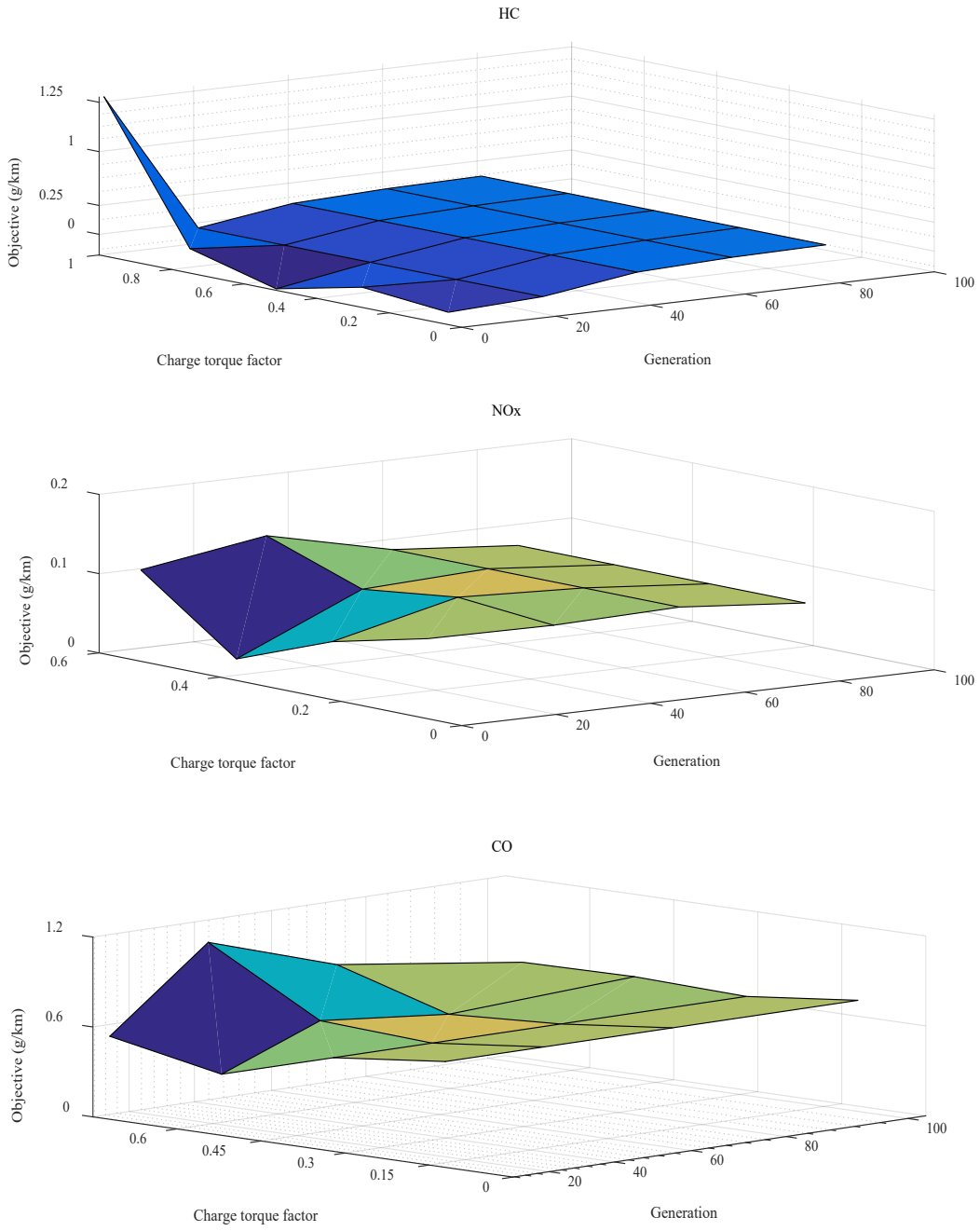


Figure 4.10 The objective optimization of HC, CO and NOx emission based on the charging factor and iterations.

Table 4.6 The GA iterative optimization results of each solution in the critical generation

| Iterations | $SoC_l$ | $SoC_h$ | $C_{tchg}$ | $B_{mid}$ | $B_{hi}$ | $N_{low}$ | $t_{emax}$ | $t_{emin}$ | CO (g/km) | HC (g/km) | NOx (g/km) | FE (MPG) |
|---|---|---|---|---|---|---|---|---|---|---|---|---|
| 10 | 0.35 | 0.82 | 0.42 | 0.29 | 0.66 | 15.17 | 0.78 | 0.43 | 1.12 | 0.20 | 0.08 | 60.1 |
| 20 | 0.32 | 0.85 | 0.53 | 0.33 | 0.71 | 15.06 | 0.76 | 0.47 | 0.89 | 0.11 | 0.08 | 62.6 |
| 30 | 0.36 | 0.83 | 0.53 | 0.34 | 0.65 | 15.72 | 0.73 | 0.39 | 0.98 | 0.08 | 0.07 | 61.7 |
| 40 | 0.33 | 0.83 | 0.56 | 0.26 | 0.69 | 15.10 | 0.73 | 0.41 | 0.88 | 0.08 | 0.07 | 66.3 |
| 50 | 0.37 | 0.79 | 0.46 | 0.28 | 0.64 | 14.82 | 0.72 | 0.38 | 0.96 | 0.10 | 0.11 | 59.6 |
| 60 | 0.40 | 0.82 | 0.50 | 0.29 | 0.66 | 15.17 | 0.78 | 0.40 | 1.12 | 0.10 | 0.06 | 64.1 |
| 70 | 0.35 | 0.85 | 0.51 | 0.33 | 0.71 | 15.06 | 0.76 | 0.37 | 0.93 | 0.09 | 0.07 | 60.6 |
| 80 | 0.34 | 0.80 | 0.49 | 0.34 | 0.62 | 16.00 | 0.69 | 0.41 | 0.99 | 0.08 | 0.07 | 60.8 |
| 90 | 0.35 | 0.84 | 0.50 | 0.30 | 0.63 | 15.39 | 0.71 | 0.39 | 0.99 | 0.11 | 0.09 | 59.9 |

### 4.4.4 The analysis

According to the simulation results of the GA optimization shown in Figure 4.9, there is no significant fluctuation after the 30$^{th}$ generation, while the curve of GA optimization shows a convergence around the 35$^{th}$ generation.

Figure 4.10 clearly shows that the emission of the HC has local linear decline. There is a notable decrease in HC emission around 20 iterations. It achieved the minimum emission when the value of $C_{tchg}$ was around 0.53. The optimization of the CO emission similarly shows a local linear decrease. For the emission optimization of the $NO_x$, a minimum value is obtained when the $C_{tchg}$ is around 0.5 in the 60$^{th}$ generation.

According to the information listed in Table 4.6, a significant decrease in the optimization objective of HC occurred from the third to the 20th generation, from 0.2 to 0.11. Compared to other values of parameters, the difference of $t_{emax}$ and $t_{emin}$ between the 20th generation (0.76 and 0.47) and the convergent results in 80th generation (0.69 and 0.41) are smallest. The parameters $t_{emax}$ and $t_{emin}$ appear to have maximum influence on the HC emission. Meanwhile, the lowest point of 0.06 around the 60th generation for the $NO_x$ emission seems to relate to the logical parameters of the battery (*SoC* and $C_{tchg}$). The trends and the fluctuations of the CO emission implied corresponding changes with the logical parameters of $B_{mid}$ and $B_{hi}$ between 10th and 30th generations. However, the results at the 20th and 30th generation show that the optimization objective of the CO emission increased from number (0.89) to (0.98). Table 4.7 shows the comparison of the simulation results.

Table 4.7 Comparison of the simulation results

| **Objectives** | | **Before Optimization** | **Rule-based strategy** | **Hybrid** | |
|---|---|---|---|---|---|
| | | | | **Optimal Target** | **GA Optimization** |
| Emissions (g/km) | HC | 1.24 | 1.30 | 0.1 | 0.08 |
| | CO | 1.21 | 0.90 | 1 | 0.88 |
| | $NO_x$ | 0.17 | 0.16 | 0.08 | 0.07 |
| Fuel Economy (MPG) | FE | 45.4 | 57.9 | 47.1 | 66.3 |
| Objective Evaluation | E | | 0.71 | min*F(x)* | Mean: 0.42<br>Best: 0.23 |

Compared to other reported results using GA related algorithms [117, 148], the simulation results show a significant improvement in both FE and emission. The

majority of the hybrid EMS design based on rule-based control strategy and GA adopts the hierarchical optimization [149]. Compared to the hybrid approach in this case, the multi-level optimization requires a more accurate model. Much of the available literature sets the vehicle performance as one of the objectives such as the velocity ratio to optimize [150, 151]. Compared to the results obtained using both algorithms and other types of methods such as the optimization based on orthogonal experimental design and Non-dominant sort GA (NSGA-II) [136], the proposed hybrid optimization in this Chapter shows an improvement in the CO emission and FE. However, the constraints condition in [136] seems to be more strict. For example, the time set to achieve an acceleration from 0 to 100 km/h was 10 seconds in [136], while 12 seconds is required in this research as well as some other work. The computation time for the model used in our work is around 120 minutes using a desktop running with an Intel (R) Core i7-6700 CPU and 32 GB memory. While no such specific numbers are available, it is generally reported that the computational time increases with the model complexity [152].

## 4.5 Concluding Remarks

This Chapter reports results using an EMS based on hybrid rule-based control design strategy and GA to reduce the emission and improve the FE. A mathematical model is developed to connect the rule-based control design strategy and the GA. The simulation results from this mathematical model show improvements in FE, HC and NOx emissions. In terms of the GA process, the sub-targets set in the fitness function were successfully achieved around the 30th generation. Compared to the single function of the rule-based control design strategy, the hybrid method obtains a

dramatic decrease in the emission of HC from 1.3 to 0.08 g/km (93% reduction). At the same time, the emission of $NO_x$ decreased from 0.16 to 0.08 g/km (50% reduction), while CO emission marginally decreased from 0.90 to 0.88 g/km (2% reduction). The FE increased from 57.9 to 66.3 MPG.

# Chapter 5 A Real-Time State of Charge Estimation Using an Improved Extended Kalman Filter Algorithm Based on a Composite Lithium-Based Battery Model

This chapter is based on the work from the following publication in which the author of this thesis is the principal author: Ding, N., Prasad, K., Lie, T. T., and Cui, J. (2019)," State of Charge Estimation of a Composite Lithium-Based Battery Model Based on an Improved Extended Kalman Filter Algorithm," *Inventions*, *4*(4), 66.

In Chapters 3 and 4, it was discussed that the significance of EMS to improve the efficiency of the energy dispatching in PHEVs. The SoC is one of the most critical basis of implementation of the EMS, which requires high estimation accuracy. The battery is the soul component of the vehicles driven by electricity. The electrochemical reactions make it difficult to accurately and intuitively describe the battery SoC. Chapter 2 also discussed that the SoC estimation of the battery can be seen as the dynamic identification of the internal parameters. The internal parameters of the battery significantly depend on the different adoptions of the battery models. Consequently, in this Chapter, an analysis on the various battery models is performed, in order to build an appropriate battery model for parameters identification. Thereafter, groups of experiments are carried out on the lithium-based battery. The experimental data is processed by the method of Recursive Least Squares (RLS) to achieve the offline parameters identification. Based on the adopted battery model and the offline parameters identification, a model of an improved extended Kalman Filter (EKF) algorithm is proposed to achieve the real-time parameters identification for dynamic SoC estimation. The simulation results show that the designed improved EKF can have

higher estimation accuracy, which significantly contribute to the SoC estimation for the monitoring module in EMS/BMS.

## 5.1 Introduction

In previous Chapters, it has been mentioned many times that the difficulties of the manufacturing technology and the assembly implementation of the battery restrain the development of EVs. The battery as the main power source directly affects vehicle performance. The BMS is a significant issue to the battery utilization in the vehicle. The main functions of BMS include improvement of the effectiveness of the battery utilization, prevention of over-charging and over-discharging, prolonging the battery life and monitoring of the battery status. The high effectiveness of the BMS/EMS in EVs will mainly depend on accurate information exchange between the modules. As discussed in section 2.3, the basic function of the monitor module in BMS is to capture and monitor the status of the battery and includes the SoC, SoP, and SoH [153]. The SoC of the battery is a crucial element to decide the battery operating condition. In terms of practical applications, the SoC is also the key factor to ensure the implementation of each module function in the BMS/EMS [154].

As described in section 2.1.2, the use of different types of batteries in EVs started from the lead-acid battery and quickly progressed to nickel-metal hydride (NiMH) battery and eventually to lithium-ion and ternary lithium battery [155]. The working trend of the cell and battery pack in EVs is a dynamic and non-linear change, specifically in the lithium-based battery applications [156]. In section 2.3, it has been discussed that the value of SoC is not directly measurable. The SoC is affected by serval factors such

as the battery terminal voltage, current and temperature. Moreover, measurements of voltage, current, etc. often occur with inevitable noises that lead to errors.

The main objective for SoC estimation is to design an appropriate method with considerable accuracy and simplicity. Based on an overview of the SoC estimation algorithms in section 2.3.2, the detailed applications of different estimation methods are discussed firstly in this Chapter. Thereafter, it proposed a novel composite battery model based on the electrochemical models. Then, offline identification of parameters is done using experimental data. With these offline parameters, a battery model is subsequently built using MATLAB simulation. This model includes the effects of temperature, charge/discharge rate, direct current resistance, etc. Using this battery model, it consequently implemented the iEKF algorithm to estimate the SoC in MATLAB Simulink. The iEKF method combines the OCV, Ah and EKF methods: the OCV-SoC function in this work provide an initial value; Ah counting module online identifies the parameters of the battery model; the errors in the OCV and Ah estimation are corrected by the EKF algorithm. Under both static and dynamic operating conditions, it is shown that the iEKF algorithm applied on the novel composite battery model results in better accuracy of the SoC estimation than other EKF based methods.

### 5.1.1 The analysis of SoC estimators based on different methods

The commonly used estimation methods of SoC mainly are based on Open Circuit Voltage (OCV) measurement, the coulomb counting method (Ah method), the method of Electrochemical Impedance Spectroscopy (EIS), the method based on neural network, the Kalman Filter (KF) based methods, *etc.*[157]. The OCV-based estimation, Ah method and EIS could be described as direct measurement methods. Taking into

account the practicality, the advantage of direct measurement methods is its easy implementation and low cost. However, the values of OCV and the current are obtained through an open-loop estimator. The hysteresis phenomena and the sensor drift will lead to inevitable and cumulative errors, which will significantly impact the operation of the BMS and the use of battery itself [154]. The estimation approach of the neural network is a data-driven method. The main purpose of the data-driven method is to simulate the nonlinear and dynamic characteristics of the battery. This method requires large Random Access Memory (RAM) storage to train the system for the learning process of the neural network [158]. Other machine learning methods such as the fuzzy logic, support vector machine and genetic algorithm have been extensively researched for battery SoC estimation [159-162]. The machine learning method improves the intelligence of the system, but the results are difficult to interpret and hence is not convenient in real practice. The need for appropriate storage requirement appears in the look-up table method of the SoC estimation. The look-up table sourced from the relationship curve of SoC-OCV is inadvisable for online application. A regular recalibration is required to update the table information [163].

Another significant approach of SoC estimation is the model-based method, which is robust and is based on a close-loop-feedback system. The standard KF method is a well-known approach to estimate the internal state of a dynamic linear system [164]. To precisely describe the nonlinear working state of the battery, several KF relevant approaches have been used to obtain SoC estimation [165]. The extended KF (EKF) method mathematically transforms the standard (linear matrix) KF to fit a nonlinear system. Besides, several EKF-based methods, such as lazy EKF and robust EKF, are

proposed to estimate the SoC of the battery and in different scenarios for vehicle onboard battery and microgrid energy storage units [166, 167]. The Dual EKF (DEKF) adopted in [168, 169] to estimate the SoC of the battery and the parameter of the model shows faster convergence in shorter calculation time. The unscented KF (UKF) transforms the nonlinear models by linear interpolation. Sun et al. [170] discussed an adaptive UKF (AUKF) algorithm for SoC estimation which shows higher accuracy than the EKF-based estimator. The main issue of the UKF based methods is using the Unscented Transform to deal with the nonlinear transfer of the mean and covariance. Compared to the EKF, the UKF method approximates the probability density distribution of the nonlinear function instead of the nonlinear function approximation. Therefore, the UKF methods are more accurate [171-173]. However, the UKF-based estimator seems more applicable to the situation where the system is less nonlinear. The iterative update of the covariance in the UKF-based algorithm is prone to negative definite matrix in a highly nonlinear system. In addition to the methods related to KF, other model-based methods are reported in literature. For example, the Luenberger observer and sliding mode observer showed an accurate SoC estimation but is very complex [174].

## 5.2 The Battery Model

The State of Charge (SoC) is used to identify the remaining capacity status of the battery. The value of SoC cannot be directly measured but obtained by analyzing external characteristics. Different battery manufactures in the market have a different definition of the SoC. Equation (5-1) gives a numerical definition of SoC.

$$\mathrm{SoC} = \frac{C_Q}{C_I} \tag{5-1}$$

where the $C_Q$ is the remaining capacity, and the $C_I$ is the rated capacity when the battery is discharged with a constant current $I$.

The process of using the model-based method to estimate SoC could be considered as the dynamic identification for the parameters representing the characteristics of the battery. The choice of the models will determine the mathematical relationship of the different parameters. The equations of the state in the algorithms will also vary from the different model selections. Figure 5.1 shows a logical structure of the battery model build-up.

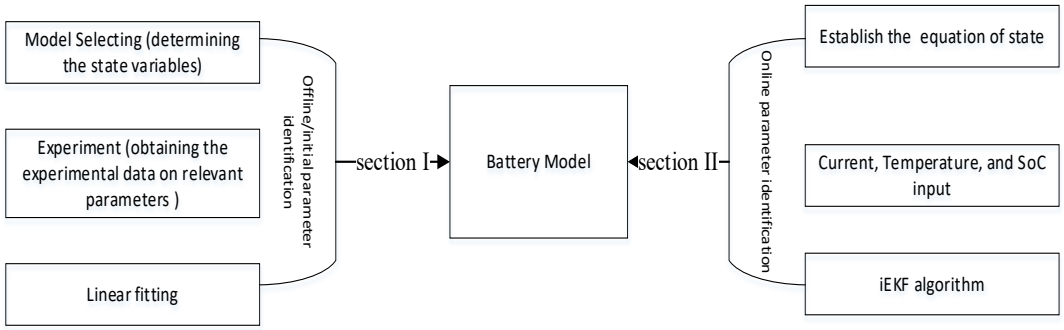


Figure 5.1 The logical structure of the battery model build-up

The modeling steps are described as follows:

1. Selecting the battery model (A novel composite electrochemical model).
2. Determining the different parameters to be identified based on the selected model.
3. Performing a series of characteristics tests on the battery.
4. Linear fitting of the experimental data (offline identification).
5. Building the model in MATLAB.

6. Obtaining the equation of state.

7. Developing the online estimation algorithm (iEKF).

8. Inputting the current, temperature and SoC (simulations in static and dynamic conditions).

As shown in Figure 5.1, the battery model is constructed in two sections: offline parameter identification in section I and online parameter identification in section II. Steps 1 to 6 are the preparation steps for the battery model establishment. They will seriously influence the accuracy of the online estimation based on the iEKF algorithm in step 7. The series of experiments in step 3 refers to four different battery tests (see Sections 5.3.1 and 5.3.4). The experiments reflect the external characteristics of the battery and relate to the factors affecting the SoC estimation. The main factors affecting the battery capacity are the charge/discharge rate, temperature, the charge/discharge cycle (battery aging) and self-discharge of the battery [175]. Taking these factors into account, SoC ($Q_{tI}$) definition is amended as [176, 177]:

$$Q_{tI} = \eta Q_{ti} = \eta \int_0^t I d\tau \tag{5-2}$$

where $t$ is the charge/discharge duration time, $Q_{ti}$ is the total quantity of electric charge/discharge during the period $t$, $I$ is the current over a time interval 0 to $t$ and $\eta$ is the efficiency coefficient which includes both the charge/discharge rate ($\eta_i$) and the temperature influence coefficient ($\eta_T$).

### 5.2.1 The composite battery model

For the composite battery model, the SoC is considered as a state variable x in the system, $x_k$ is the number of the state vector. The output $y_k$ is the voltage of the battery model. The composite model is built based on three different electrochemical models as follows [83, 178]:

Shepherd model:

$$y_k = E_0 - Ri_k - K_1/x_k \tag{5-3}$$

Unnewehr universal model:

$$y_k = E_0 - Ri_k - K_2 \cdot x_k \tag{5-4}$$

Nernst model:

$$y_k = E_0 - Ri_k + K_3 \cdot \ln(x_k) + K_4 \cdot \ln(1 - x_k) \tag{5-5}$$

where $E_0$ is the OCV when the battery is fully charged and $R$ is the internal resistance which will change with different charge/discharge status and SoC, $i_k$ is the instantaneous current at time $k$ (negative when the battery is charging and positive when discharging). $K_1$ to $K_4$ are the matching parameters to be identified through battery experiments. The state equation based on the composite battery model is described as follows:

$$x_{k+1} = x_k - (\eta_i \Delta t/\eta_T Q_n) \cdot i_k \tag{5-6}$$

While the output equation is

$$y_k = K_0 - Ri_k - K_1/x_k - K_2 \cdot x_k + K_3 \cdot \ln(x_k) + K_4 \cdot \ln(1 - x_k) \quad (5\text{-}7)$$

where $K_0$ is the OCV of the fully charged battery and has the same physical meaning as $E_0$. However, $E_0$ in Equations (5-3)–(5-5) is the actual measured value while $K_0$ is obtained by the identification based on OCV-SoC experimental data (see in Section 5.3.4). Equations (5-3)–(5-5) are combined in Equation (5-7). The electrochemical models of Equations (5-3)–(5-5) reflect the relationship between the terminal voltage and the SoC ($x_k$). $R$ is the internal resistance (Ohmic resistance) and changes with the charging/discharging state of the battery ($Ri_k$). $K_1/x_k$ from Equation (5-3) and $K_2 \cdot x_k$ from Equation (5-4) reflect the polarization resistances of the battery. $K_3 \cdot \ln x_k$ and $K_4 \cdot \ln(1 - x_k)$ from Equation (5-5) represent the influence of the internal temperature and material activity during the electrochemical reaction of the battery, respectively.

The SoC estimation is not directly considered in most of the research discussing the battery models. On the other hand, the accuracy of the battery model significantly affects the estimation of the SoC of the battery [179]. Justifying accurate battery models mainly depends on the dynamic tracking of the battery terminal voltage and the identification of parameters. Many bench tests are used to verify the accuracy of the battery models, such as HPPC test, pulsed charge/discharge cycles and dynamic stress test [180, 181]. At the same time, the experimental data used to verify the battery model is also applied to design the SoC estimators.

In terms of the electrochemical model, various chemical reactions are carefully considered. They include the reaction occurring at the anode and cathode of the battery

and the electrolyte ion transfer process. Equations (5-3)–(5-5) are simplified electrochemical models based on empirical modeling method and have the advantages of simple expression and computational efficiency. However, there are some drawbacks when using models in Equations (5-3)–(5-5) alone or their correction models such as the new Electrochemical Polarization (EP) model [173, 181]. Compared to the equivalent circuit models (ECMs) [182, 183], the composite model described in this work shows sufficient accuracy and short execution time. The composite battery model in this research uses the calculation results of Equation (5-7) to replace the direct measurement of OCV, which is known to be difficult [184] but still used in other electrochemical models and ECMs. The advantage of linear parameters in the proposed model reduces the difficulty of parameter identification. With less complexity, the proposed composite battery model minimizes the number of the parameters to be identified while fully considering the influencing factors by combing $K_1$ to $K_4$.

## 5.3 The Experiments and Offline Parameter Identification

The mathematical parameters ($\eta_i$, $\eta_T$, $R$, $K_0$, $K_1$, $K_2$, $K_3$, $K_4$) of the composite battery model shown in Equations (5-6) and (5-7) require a validation. The initial identification of the parameters is an offline and static estimation, obtained by polynomial curve fitting of the experimental data (see Figures 5.2–5.8). The charge/discharge rate factor $\eta_i$ was obtained by the charge and discharge test. Similarly, the temperature influence coefficient $\eta_T$ was obtained from temperature characteristic test. The other parameters ($R$, $K_0$, $K_1$, $K_2$, $K_3$, $K_4$) were obtained through a Hybrid Pulse Power Characterization (HPPC) test and OCV-SoC test [185]. All the

tests were conducted on a $LiFePO_4$ battery (single cell) with 206 Ah rated capacity and 3.2 V rated voltage.

### 5.3.1 Charge and discharge rate test

The main purpose of this test is determining the influence from different charging/discharging rates on the actual capacity of the battery. According to the definition of SoC shown in Equation (5-2), the difference between the rated capacity and the measured capacity is caused by the variable parameter of $\eta_i$. The determination of $\eta_i$ is based on the experimental data to establish a linear fit relationship. Five groups of different rates (0.2 C, 0.5 C, 1 C, 2 C and 3 C) with a constant current at room temperature (25 °C) were conducted in charging and discharging tests, respectively. There was a 1 h resting time before starting the discharging test after the charging test was completed.

Tables 5.1 and 5.2 show a specific data point of both capacity and energy retention for charging and discharging tests, respectively. The curves of the capacity retention rate for the charge and discharge rate tests for the $LiFePO_4$ battery are shown in Figures 5.2 and 5.3, respectively. From Figures 5.2 and 5.3, it is clear that the actual capacity of the battery will decrease as the charge/discharge rate increases.

Table 5.1 The capacity and energy retention rate with specific charge rate

| **Charge Rate Test** | **0.2 C** | **0.5 C** | **1.0 C** | **2.0 C** | **3.0 C** |
|---|---|---|---|---|---|
| Capacity/Ah | 211.45 | 208.95 | 206.88 | 204.07 | 194.76 |
| Capacity retention rate/% | 102.21 | 101.00 | 100.00 | 98.64 | 94.14 |
| Energy/Wh | 707.76 | 706.36 | 708.04 | 712.64 | 692.15 |
| Energy retention rate/% | 99.96 | 99.76 | 100.00 | 100.65 | 97.76 |

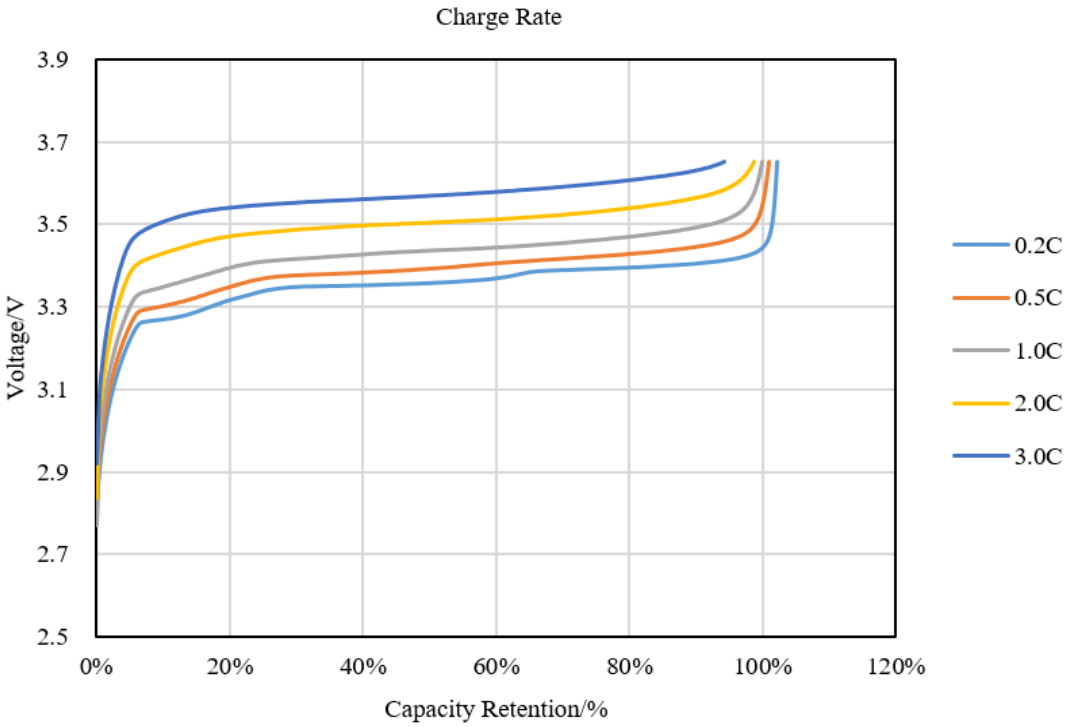


Figure 5.2 Capacity retention curves at different charge rates

Table 5.2 The capacity and energy retention rate with specific discharge rate

| **Charge Rate Test** | **0.2 C** | **0.5 C** | **1.0 C** | **2.0 C** | **3.0 C** |
|---|---|---|---|---|---|
| Capacity/Ah | 214.31 | 212.94 | 211.84 | 211.28 | 211.08 |
| Capacity retention rate/% | 101.16 | 100.52 | 100.00 | 99.74 | 99.64 |
| Energy/Wh | 687.83 | 672.22 | 657.33 | 641.41 | 628.45 |
| Energy retention rate/% | 104.64 | 102.26 | 100.00 | 97.58 | 95.61 |

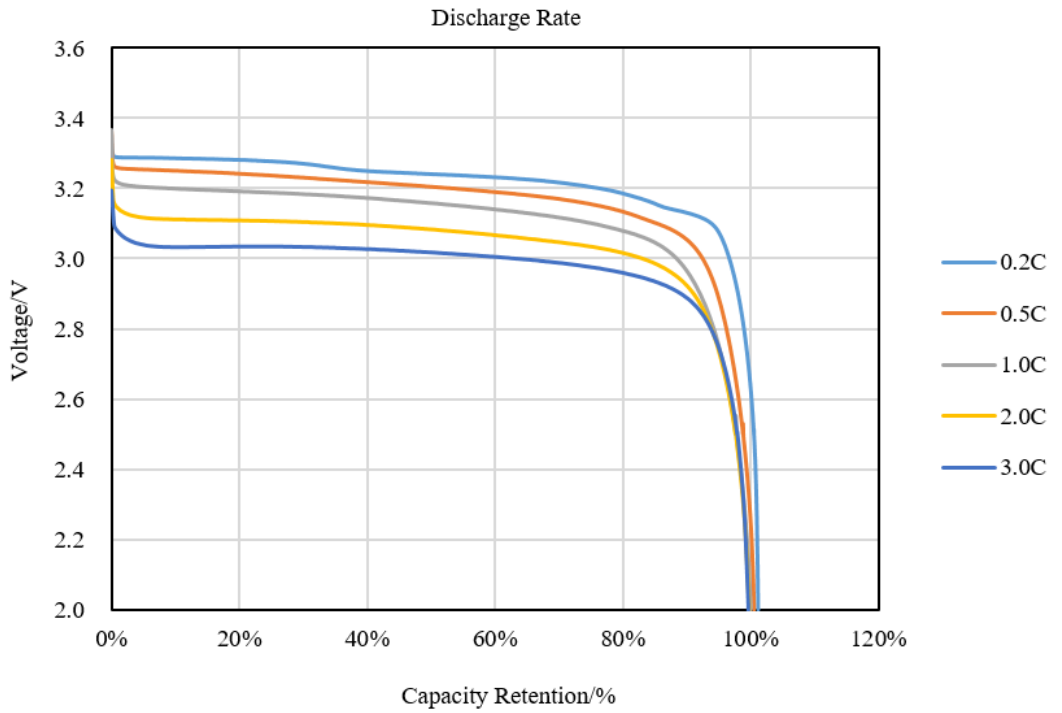


Figure 5.3 Capacity retention curves at different discharge rates

### 5.3.2 Temperature characteristics test

Similar to the charge/discharge rate, the battery shows nonlinear behavior with ambient temperature changes. The working temperature of the lithium-based battery pack in actual situations is not a constant. Therefore, a temperature coefficient ($\eta_T$) has to be introduced to represent the impact of temperature on the SoC estimation.

The test involved using the 1 C rate to discharge a fully charged battery under different (constant) temperature conditions ($-20$ ℃, $-10$ ℃, 0 ℃, 25 ℃ and 45 ℃). Table 5.3 shows a specific data point in both the capacity and energy retention rates at specific temperatures. The change curves of capacity retention rate for the $LiFePO_4$ battery at different temperature are shown in Figure 5.4.

Table 5.3 The capacity and energy retention rate with specific temperature condition

| Temperature Characteristic Test | −20 °C | −10 °C | 0 °C | 25 °C | 45 °C |
|---|---|---|---|---|---|
| Capacity/Ah | 194.18 | 201.14 | 205.49 | 211.27 | 211.35 |
| Capacity retention rate/% | 91.91 | 95.20 | 97.26 | 100.00 | 100.00 |
| Energy/Wh | 523.18 | 566.18 | 600.52 | 657.80 | 668.46 |
| Energy retention rate/% | 79.54 | 86.07 | 91.29 | 100.00 | 101.62 |

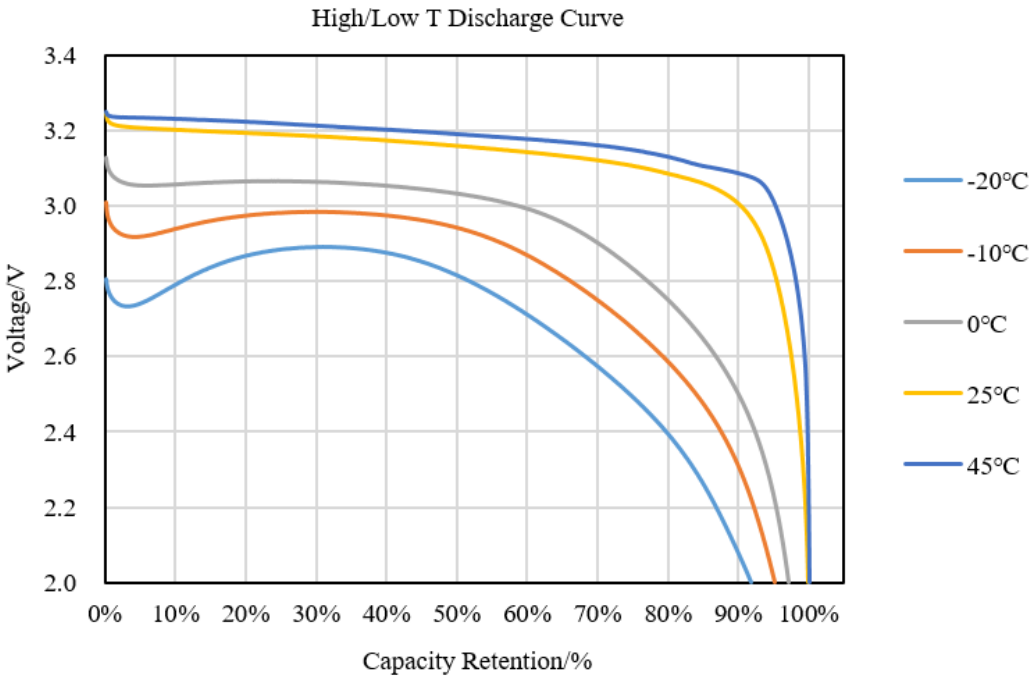


Figure 5.4 Capacity retention curves at a different temperatures

The increase in temperature reduces the overpotential, which will cause an increase in the activity of the chemicals inside the battery. Thus, the discharge capacity of the battery increases at (constant) higher temperature conditions. The experimental results

shown in Figure 5.4 are consistent with the theoretical analysis—the capacity of the $LiFePO_4$ battery decreases with the decreasing temperature [186].

### 5.3.3 Hybrid pulse power characterization (HPPC) test

The HPPC test is one of the most common approaches to offline parameter identification. It adopts the HPPC from Freedom CAR Battery Test Manual (published in 2003) to initially identify the parameters of direct current resistance (DCR) [185]. The DCR, which includes both Ohmic resistance and the polarization resistance, is dynamic. The HPPC test is used to obtain DCR parameters as a function of SoC from the voltage response values. The series of pulse experiments of HPPC is to reliably establish cell voltage response time constants during “discharge”, “rest” and “regen” regions. The standard process of HPPC test is described in Figure 5.5, where $C_1/1$ is 1C charge/discharge rate.

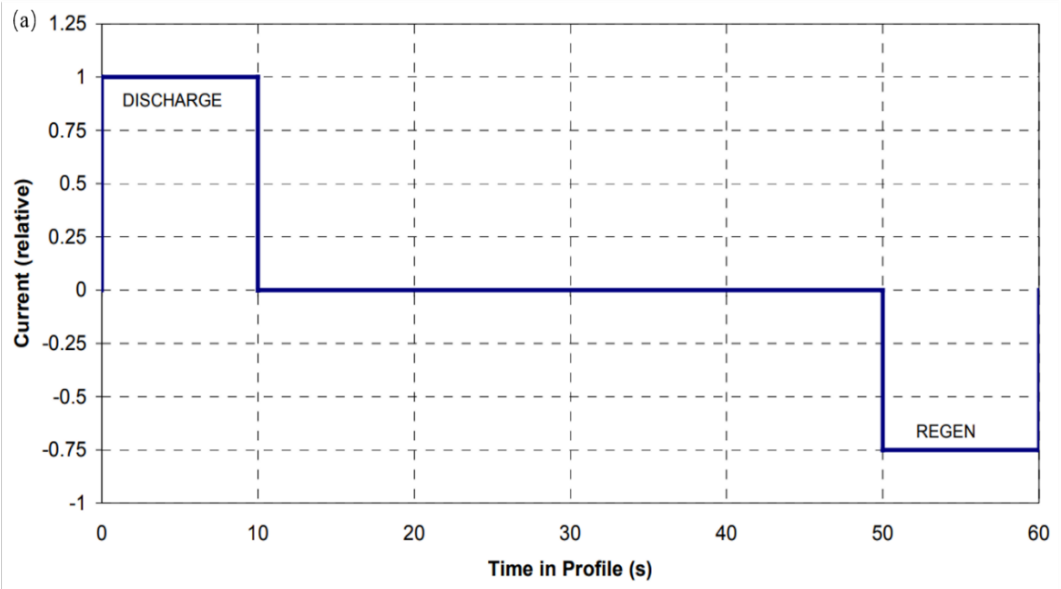

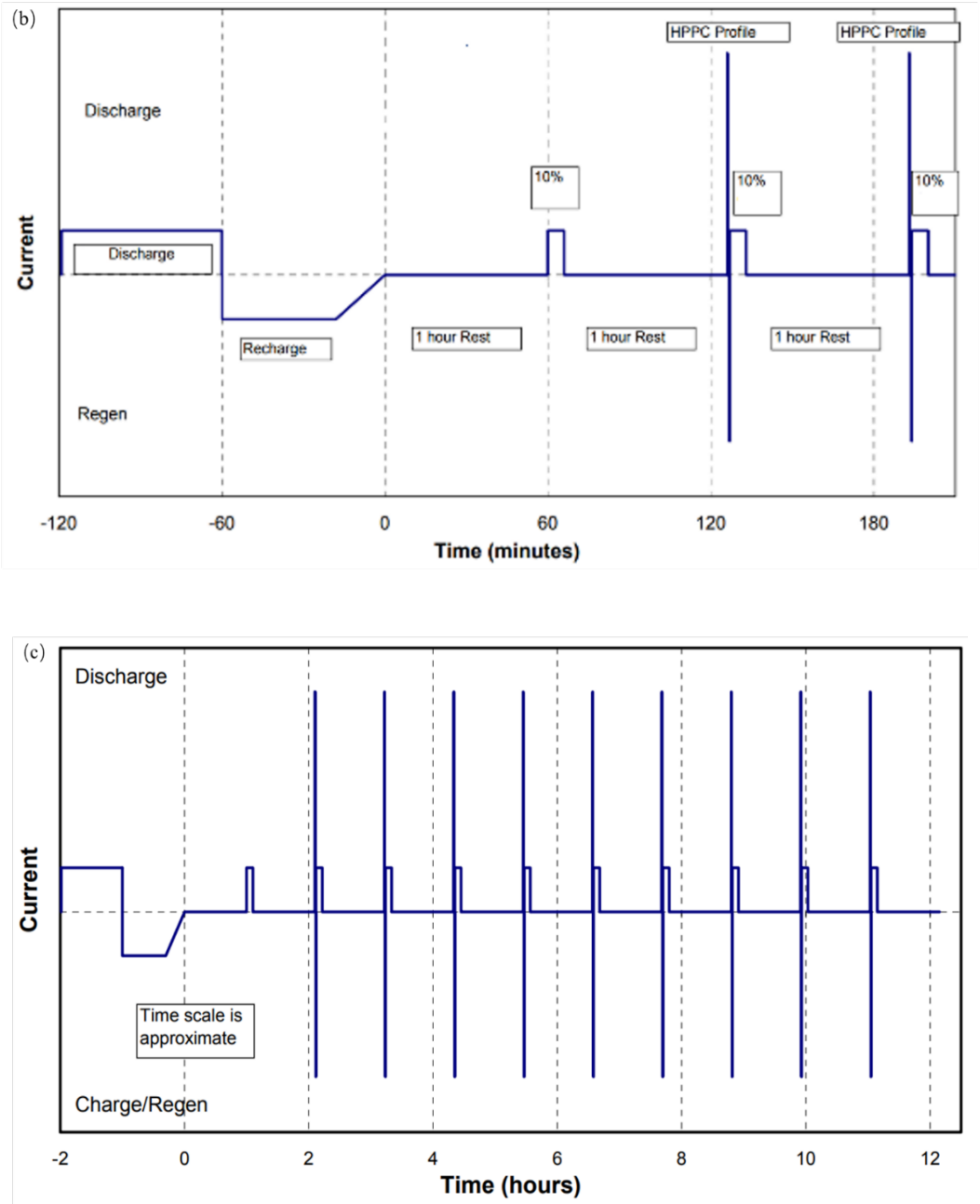


Figure 5.5 The HPPC test. (a) the HPPC test profile, (b) the start of HPPC test sequence, (c) the complete HPPC sequence

The HPPC test includes nine single repeated sequences (Figure 5.5 c). Each sequence is separated by 10% SoC or depth of discharge (DOD) with constant current discharge

segments from 90% to 10% (Figure 5.5 b). One HPPC profile includes 10 s discharge, 40 s rest and 10 s charge (Figure 5.5 a). There is one hour resting time between each sequence (Figure 5.5 b). It should be noted that the spikes shown in Figure 5.5 b,c are basically the HPPC profile of Figure 5.5 a. This test uses 4 C discharge and 3 C charge. The data collection interval of the HPPC test is 0.2 s. The HPPC experimental results are shown in Table 5.4 and include the voltage and the DCR. $V_{before}$ and $V_{after}$ are the measured voltage values before and after charging/discharge test, respectively. DCR values are rounded to two decimal places.

Table 5.4 The HPPC test charging/discharging power and DCR.

| **SoC** | **206Ah 4C Discharge/3C Charge** | | | | | |
|---|---|---|---|---|---|---|
| | **Discharge** | | | **Charge** | | |
| | **$V_{before}$ (mV)** | **$V_{after}$ (mV)** | **DCR (mΩ)** | **$V_{before}$ (mV)** | **$V_{after}$ (mV)** | **DCR (mΩ)** |
| 90% | 3328.30 | 2910.70 | 0.45 | 3277.20 | 3613.20 | 0.49 |
| 80% | 3327.40 | 2893.70 | 0.47 | 3267.20 | 3612.90 | 0.50 |
| 70% | 3327.40 | 2881.60 | 0.48 | 3258.90 | 3610.10 | 0.51 |
| 60% | 3296.70 | 2857.40 | 0.48 | 3244.90 | 3586.90 | 0.50 |
| 50% | 3289.00 | 2829.80 | 0.50 | 3230.40 | 3580.40 | 0.51 |
| 40% | 3288.00 | 2805.90 | 0.52 | 3217.30 | 3577.30 | 0.52 |
| 30% | 3284.30 | 2775.60 | 0.55 | 3201.50 | 3570.10 | 0.53 |
| 20% | 3254.50 | 2707.40 | 0.59 | 3169.90 | 3539.40 | 0.53 |
| 10% | 3209.60 | 2422.10 | 0.86 | 3110.40 | 3497.00 | 0.56 |

### 5.3.4 OCV-SoC test

The open-circuit voltage (OCV) test is significant and necessary for the estimation of $K_0$. The operating characteristics of the battery show that a proportional relationship exists between OCV and SoC. The OCV is roughly regarded as a linearized function of SoC in a simplified system [187]. For example, the OCV rises with the increase in SoC. The current SoC of the battery can be calculated through a model relationship between OCV and SoC. The experimental steps used to obtain an approximate OCV value are shown in Figure 5.6.

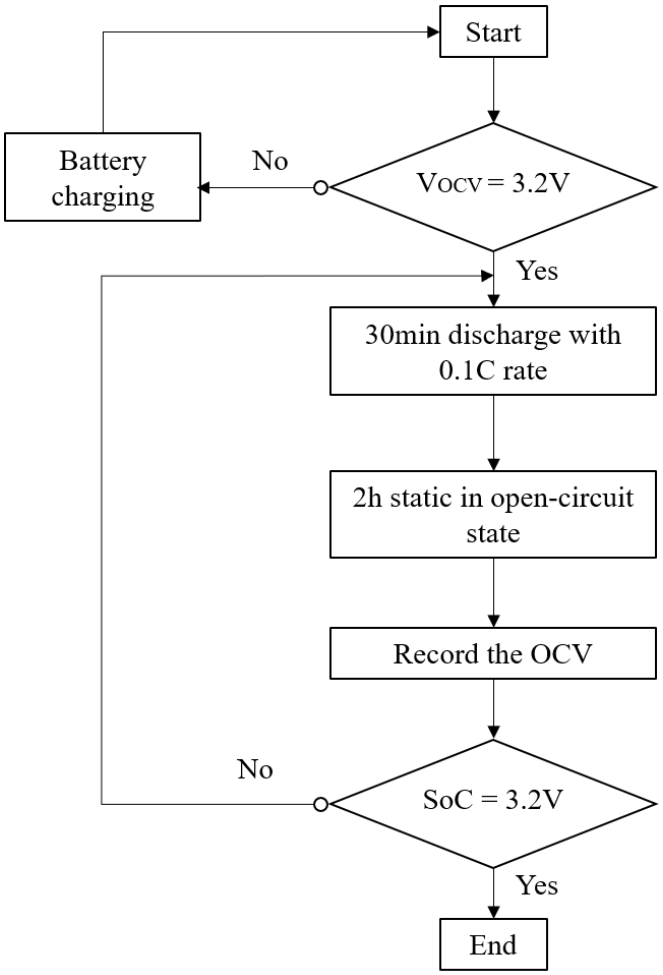


Figure 5.6 OCV-SoC test process

### 5.3.5 Offline parameter identification

The data shown in the various tests described in Sections 5.3.1 to 5.3.4 was obtained by real experimental bench based on $LiFePO_4$ battery (206 Ah, 3.2 V). A convincing offline parameters identification was required to achieve a reliable mathematical battery model for the simulation of KF. Eight parameters ($\eta_i$, $\eta_T$, $R$, $K_0$, $K_1$, $K_2$, $K_3$, $K_4$) were identified by the approach of linear fitting and recursive least squares (RLS) in MATLAB. The experimental data was input into MATLAB in the form of different sets of data points. In terms of $\eta_i$, relationship between the actual capacity and the charge/discharge rate were quantified by linear fitting functions in MATLAB. A second-order polynomial linear fitting equation for $\eta_i$ was obtained by the use of the polyfit function:

$$\text{Polyfit } (i, \eta_i, 2)$$

$$\eta_i = \frac{15873}{5.47i^2 - 156.8i + 16301} \tag{5-8}$$

where $i$ represents the charging-discharging current in A. Similarly, the polynomial curve of the temperature coefficient ($\eta_T$) was obtained by MATLAB polyfit function, as follows:

$$\text{Polyfit } (T, \eta_T, 1)$$

$$\eta_T = 0.55T + 76.83 \tag{5-9}$$

where $T$ is the actual temperature of the battery.

The rest of parameters ($K_0$, $R$, $K_1$, $K_2$, $K_3$, $K_4$) were obtained by the method of RLS. Figure 5.7 shows that the vales of parameters begin to converge after 1500 iterations. The values of the parameters were as follows: $R$ = 0.0048, $K_1$ = −0.000268, $K_2$ = 0.1495, $K_3$ = 0.111 and $K_4$ = −0.01955. The value of $K_0$ was 3.191 and is not shown in the figure. The accuracy in the estimation of parameters was high, of the order of ±0.3%. The mathematical model based on linear fitting from real experimental data is therefore reliable for SoC estimation using iEKF.

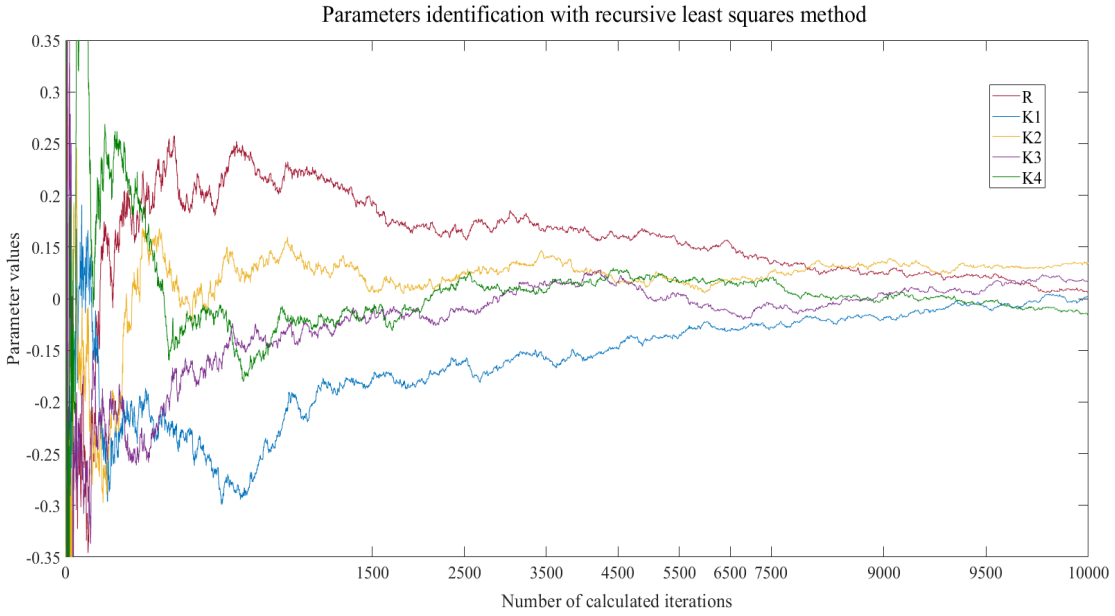


Figure 5.7 Parameters identification results in the composite model

## 5.4 The SoC Estimation on an Improved EKF Algorithm

The crucial objective of addressing the filtering problem is filtering any noise from the observed noisy signal. Taking specific situations into account such as signal processing, target tracking and control system, the solution for filtering problem can be generally transformed into a statistical estimation of the system status. Based on the

theory of time domain state space, the KF algorithm achieves an estimation of the state of the system by recursive iteration.

### 5.4.1 Analysis of the KF and EKF algorithm

The standard KF is mainly used in a linear dynamic system to estimate the unknown variable which cannot be directly measured. The optimal estimation is the core of the KF algorithm, which is based on the prediction estimation and algorithmic amendment. The processing objects of the KF algorithm include the real system and the system model [188]. The real system includes the measurable input $u_k$, the real output $y_k$ and the unmeasurable state $x_k$. The system model includes the same input $u_k$, the known state $x_k$ and the output $y_x$ based on the specific battery model. The optimal estimation is obtained through a comparison between the $y_k$ and $y_x$ to amend the prediction estimation. The state variable $x_k$ of the system model is closer to the real value of $y_k$. The state-space system model of the discrete-time standard KF is expressed as follows:

$$\begin{cases} state\ formula: x_{k+1} = A_k x_k + B_k u_k + w_k \\ output\ formula: y_k = C_k x_k + D_k u_k + v_k \end{cases} \tag{5-10}$$

where $k$ is the discrete time point, $x_k$, $u_k$ and $y_k$ are the state variables of the input and the output of the system, respectively. $w_k$ is the process noise variable which is used to describe the superimposed noise and error during state transition. $v_k$ is the measurement noise variable which is used to describe the generated noise and error when the input is measured. $A_k$, $B_k$, $C_k$ and $D_k$ are the equation matching coefficients reflecting the dynamic characteristics of the system. Figure 5.8 shows the state-space model of the discrete simple KF.

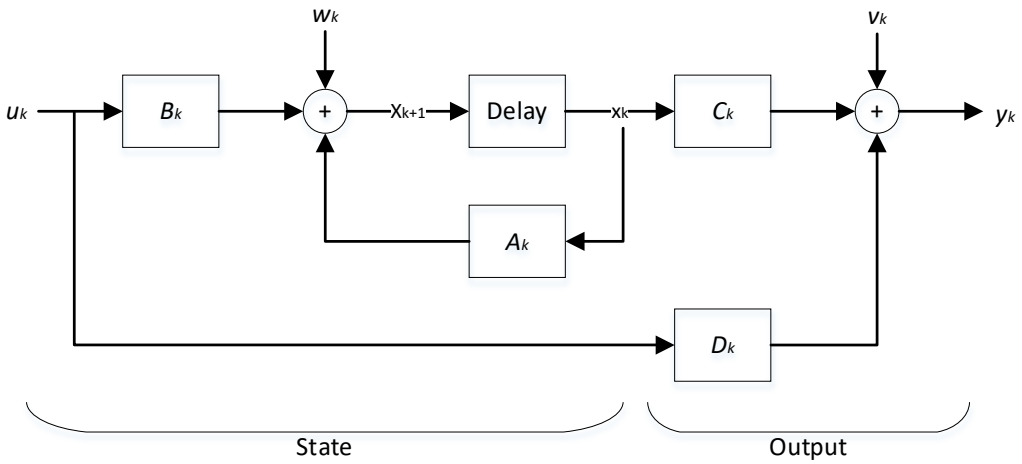


Figure 5.8 The state-space model of discrete simple KF

Two different estimates of the state variable $x_k$ and the mean square error of estimation $P_k$ are made at each sampling interval. For example, the first-time predictive estimate of $x_k^-$ is obtained by the iterative recursion using the state equations based on $x_{k-1}^+$. The predictive estimates of $x_k^-$ and $P_k^-$ are completed before the $y_k$ measurement. The calculation of the optimal estimates of $x_k^+$ and $P_k^+$ start after the measurement of $y_k$ is processed. To obtain the optimal estimation of $x_k^+$ and $P_k^+$, the predictive estimates of $x_k^-$ and $P_k^-$ will be amended after the calculation of $y_k$.

The processing steps of standard KF algorithm are as follows:

1. Initial value of $x_0^+$ and $P_0^+$:

$$x_0^+ = E[x_0] \tag{5-11}$$

$$P_0^+ = E[(x_0 - x_0^+)(x_0 - x_0^+)^T] \tag{5-12}$$

2. Predictive estimate of the $x_k^-$ and $P_k^-$:

$$x_k^- = A_{k-1}x_{k-1}^+ + B_{k-1}u_{k-1} \tag{5-13}$$

$$P_k^- = A_{k-1}P_{k-1}^+A_{k-1}^T + D_w \tag{5-14}$$

3. KF gain $L_k$ (weighting coefficient matrix)

$$L_k = P_k^- C_k^T (C_k P_k^- C_k^T + D_v)^{-1} \tag{5-15}$$

4. Optimal estimate of the $x_k^-$ and $P_k^-$:

$$x_k^+ = x_k^- + L_k(Y_k - y_k) \tag{5-16}$$

$$P_k^- = (1 - L_k C_k) P_k^- \tag{5-17}$$

where $D_w$ and $D_v$ in Equations (5-14) and (5-15) are the covariance of the process noise $w_k$ and the measurement noise $v_k$, respectively.

The standard KF algorithm shows the advanced estimation of the linear dynamic system. In terms of the nonlinear dynamic system such as the battery pack of EVs, the EKF algorithm linearly transforms the nonlinear system through an extended state-space model, then uses the iterative calculation of the standard EK algorithm to obtain the optimal estimation [189]. The state-space system model of the EKF is expressed as:

$$\begin{cases} state\ formula: x_{k+1} = f(x_k, u_k) + w_k \\ output\ formula: y_k = g(x_k, u_k) + v_k \end{cases} \tag{5-18}$$

where $f(x_k, u_k)$ and $g(x_k, u_k)$ are the state transfer function and the measurement function of the nonlinear system, respectively. The nonlinear discrete-time state-space model of the EKF algorithm is shown in Figure 5.9.

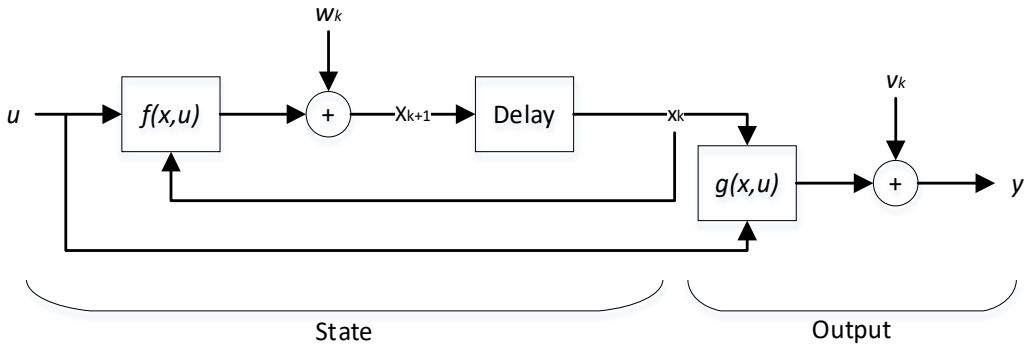


Figure 5.9 The state-space model of EKF

Compared to the standard KF algorithm, the state-space model of EKF algorithm is different. However, the algorithm implementation is similar to the standard KF, which mainly includes the initialization, the predictive estimate and the optimal estimate. The $A_{k-1}x_{k-1}^{+} + B_{k-1}u_{k-1}$ in predictive estimate of standard KF is replaced by $(x_k^-, u_k)$, while $g(x_k^-, u_k)$ substitutes $C_k x_k + D_k u_k$ in the optimal estimate. The calculation process of EKF is shown in Figure 5.10.

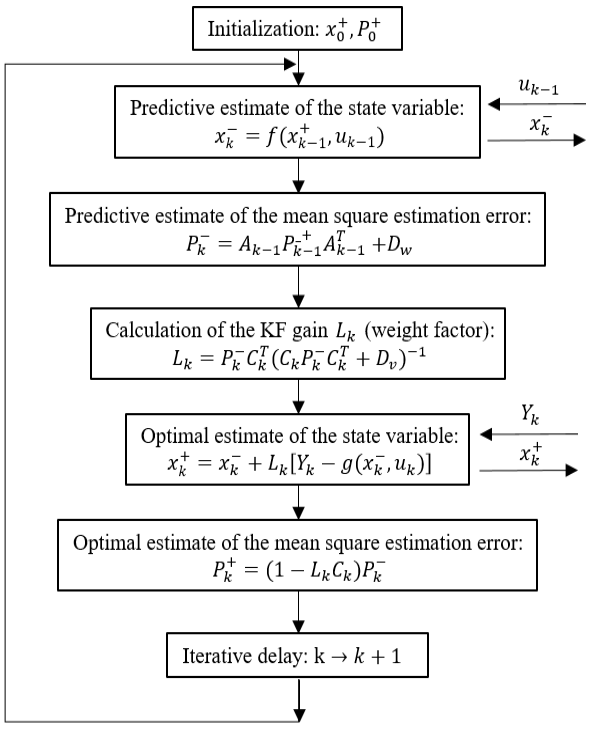


Figure 5.10 The calculation process of EKF

### 5.4.2 The SoC estimation model corrected by EKF based on composite model

The complexity of the SoC estimation increases because of the internal nonlinearization of the battery and the significant impact of external conditions. In addition, the working process of the battery for EVs involves large current changes and a single and regular approach hardly achieves an online accurate SoC estimation. Taking the estimate accuracy and the calculation cost into consideration, an iEKF algorithm is proposed. The iEKF algorithm combines the OCV method, Ah method and the EKF algorithm. Based on the actual experimental battery data and the initial/offline parameter extraction using MATLAB, the algorithm implementation of the iEKF is shown in Figure 5.11.

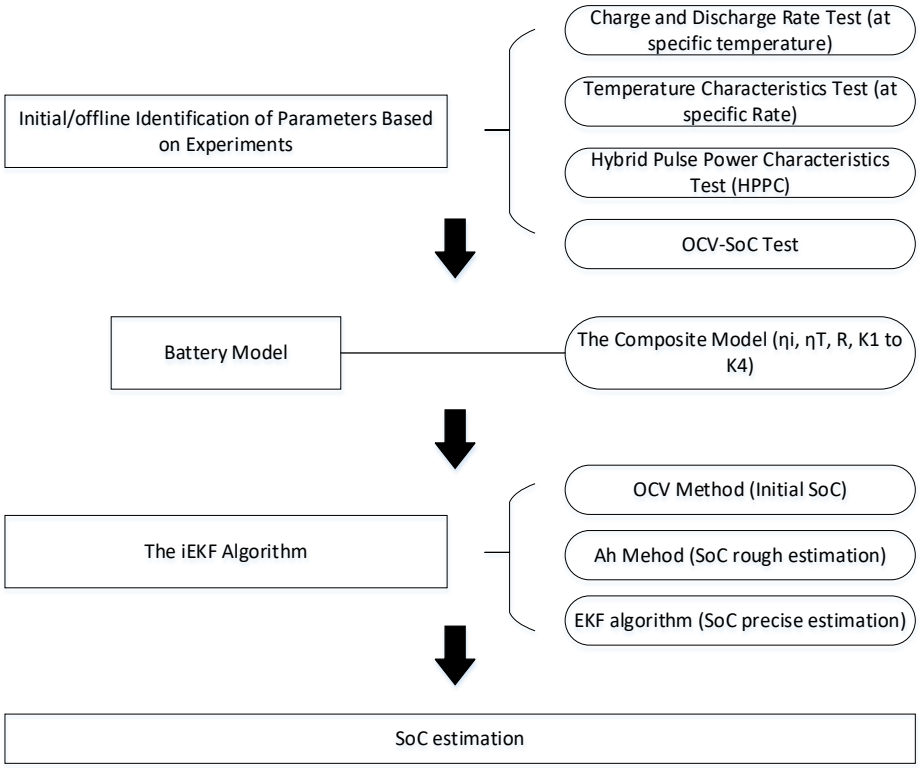


Figure 5.11 The iEKF algorithm implementation

The main function of OCV method is to provide a relatively accurate initial estimation of the SoC. OCV-SoC curve obtained from the OCV-SoC test (see Section 5.3.4) is used to provide an initialized SoC estimation for Ah method and EKF algorithm. A piecewise function is used for curve fitting the experimental data in OCV-SoC test. The mathematical expression of OCV-SoC relation is as follows ($x$ is the measured OCV):

$$\begin{cases} x > 3335, SoC = 1 \\ 3327 \le X \le 3335, SoC = 1 - \frac{8.4745x^2 - 56710x + 94872550}{14512} \\ 3297 < x < 3327, SoC = 1 - \frac{-0.26997x^2 + 1740x - 2798620}{14512} \\ 3283 \le x \le 3297, SoC = 1 - \frac{7.1273x^2 - 47222x + 78219350}{14512} \\ 3179 < x < 3283, SoC = 1 - \frac{-0.2017x^2 + 1256.2x - 1941900}{14512} \\ 2828 \le x \le 3179, SoC = 1 - \frac{-0.00735x^2 + 40.533x - 41359}{14512} \\ x < 2828, SoC = 0 \end{cases} \quad (5\text{-}19)$$

The Ah method quantifies the external influence factors which mainly refer to the charging/discharging rate and the temperature. The principle of Ah method is shown in equation (5-20).

$$SoC_{k+1} = SoC_k - \frac{1}{Q_n}\int_k^{k+1} \frac{\eta_i}{\eta_T} i dt \quad (5\text{-}20)$$

where $i$ is positive when discharging, but negative when charging. The coefficient of charging/discharging rate ($\eta_i$) and temperature ($\eta_T$) are obtained by Equations (5-8) and (5-9), respectively.

In terms of the implementation of EKF algorithm, the composite model described in Equations (5-3)–(5-5) is adopted. The state-space model of EKF algorithm based on the composite battery model uses Equation (5-6) as the state equation and the Equation

(5-7) as the output equation. The EKF is expected to show a strong algorithm correction ability [190, 191]. The problem of inaccurate initialized estimation of OCV method and the current accumulated error in Ah method will be addressed by using EKF.

The implementation of EKF algorithm is as follows:

1. Model establishment: Use Equations (5-6) and (5-7).

2. Determination of system parameters:

$$A_{k-1} = \frac{\partial f(x_{k-1},u_{k-1})}{\partial x_{k-1}}\Big|_{x_{k-1}=x_{k-1}^{+}} = 1 \tag{5-21}$$

$$C_k = \frac{\partial y_k}{\partial x_k}\Big|_{x_k=x_k^{-}} = K_1/(x_k^{-})^2 - K_2 + K_3/x_k^{-} - K_4/(1-x_k^{-}) \tag{5-22}$$

3. Initialization of the state variable and the covariance.

$$x_0^{+} = SoC_0, P_0^{+} = var(x_0) \tag{5-23}$$

4. Iterative calculation of the EKF.

$$\begin{gathered} x_k^{-} = x_{k-1}^{+} - \left(\frac{\eta_i \Delta t}{\eta_T Q_n}\right) i_{k-1} \\ y_k = K_0 - Ri_k - K_1/x_k^{-} - K_2 x_k^{-} + \\ K_3\, ln(x_k^{-}) + K_4\, ln(1-x_k^{-}) \\ P_k^{-} = A_{k-1} P_{k-1}^{+} A_{k-1}^{T} + D_w \\ L_k = \frac{P_k^{-} C_k^{T}}{C_k P_k^{-} C_k^{T} + D_v} \\ x_k^{+} = x_k^{-} + L_k(Y_k - y_k) \\ P_k^{+} = (1 - L_k C_k) P_k^{-} \\ k = 1,2,3 \ldots \end{gathered} \tag{5-24}$$

$A_{k-1}$ and $C_k$ are defined in Step 2 by using Equations (21), (22) and (25). The $SoC_0$ is calculated based on the remaining charge (after charging/discharging) in the previous state and the OCV in the current state. $P_0^{+}$, $D_w$ and $D_v$ relate to the performance of the

battery and the data collection system. In order to update the status of the system, the sampling frequency is set in the Simulink equal to 2.5 times the bandwidth of the sampled signal as per the “Nyquist-Shannon sampling” criterion.

## 5.5 The Simulation Validation of the Improved EKF Algorithm

### 5.5.1 The validation of the improved EKF algorithm

In order to verify the actual effect of the iEKF, the model described in Section 4 has been simulated in MATLAB/Simulink. The inputs of the model, current and temperature, are set by constant values (1 C, 2 °C) which refer to the static operation condition. The initial guess for SoC is set at 70% based on existing published work [180, 192, 193].

### 5.5.2 The simulation results

Figure 5.12 shows the comparison between standard SoC, the SoC estimated by Ah counting model and the SoC estimation results of iEKF method. The standard SoC was calculated values based on the charging/discharging experimental data. The fit between the standard SoC and the iEKF estimation gets better with increasing simulation time.

Figure 5.13 shows the error covariance of the composite SoC model with and without the iEKF under static operation condition. The error with the use of iEKF is very small reflecting the effectiveness of the improved EKF method. The error covariance with the iEKF under static operation condition was of the order of $10^{-7}$.

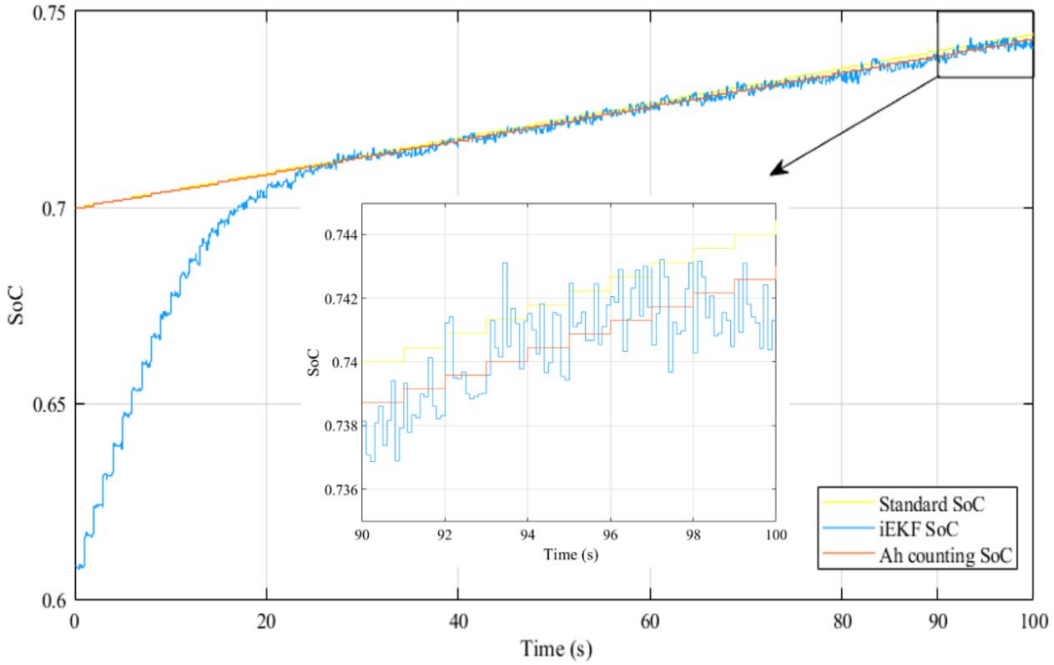


Figure 5.12 Comparison SOCs under static operation conditions

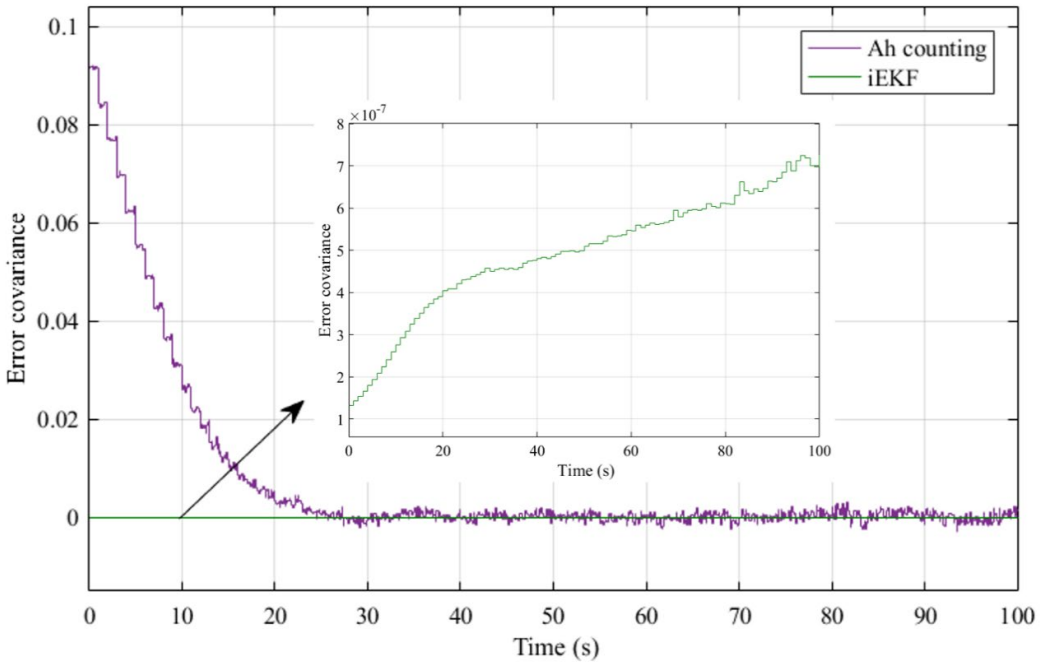


Figure 5.13 Comparison of error covariance between iEKF model and Ah counting model under static operation conditions

The MATLAB inputs of dynamic current efficiency and temperature are shown in Figure 5.14 a,b, respectively. Figures 5.15 compares the SoC estimation error under dynamic operation condition of the composite battery model with and without the iEKF. Figure 5.15 a gives the calculation results over a time of 1000 s while Figure 5.15 b shows local calculation results from 0 to 100 s. The estimation error using iEKF is insignificant (of the order of $10^{-6}$), thereby providing credibility to the iEKF method. The error covariance with the iEKF under static operation condition was of the order of $10^{-7}$. Table 5.5 gives the calculated estimation error based on the error curves shown in Figures 5.13 and 5.15 (a), (b).

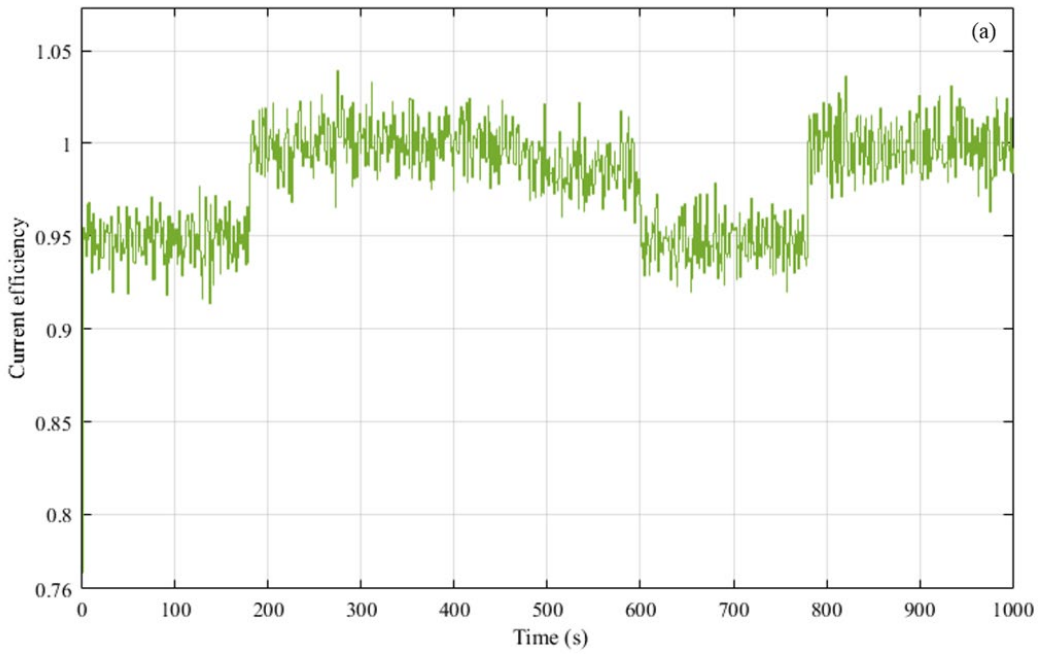

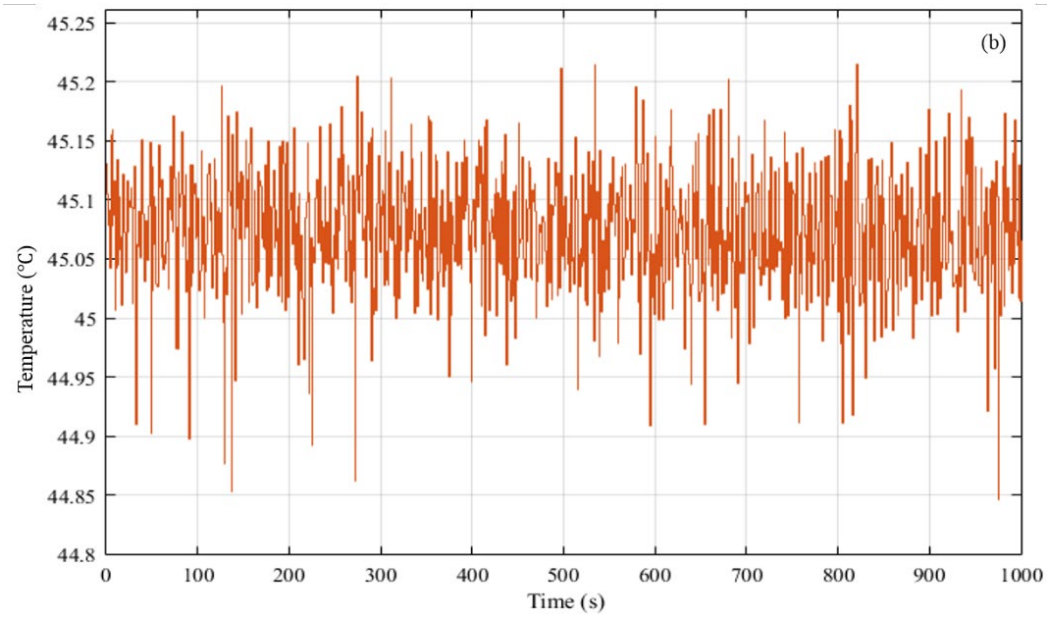


Figure 5.14 MATLAB inputs of (a) The input current efficiency and (b) The input temperature for the SOC estimation under dynamic operating conditions

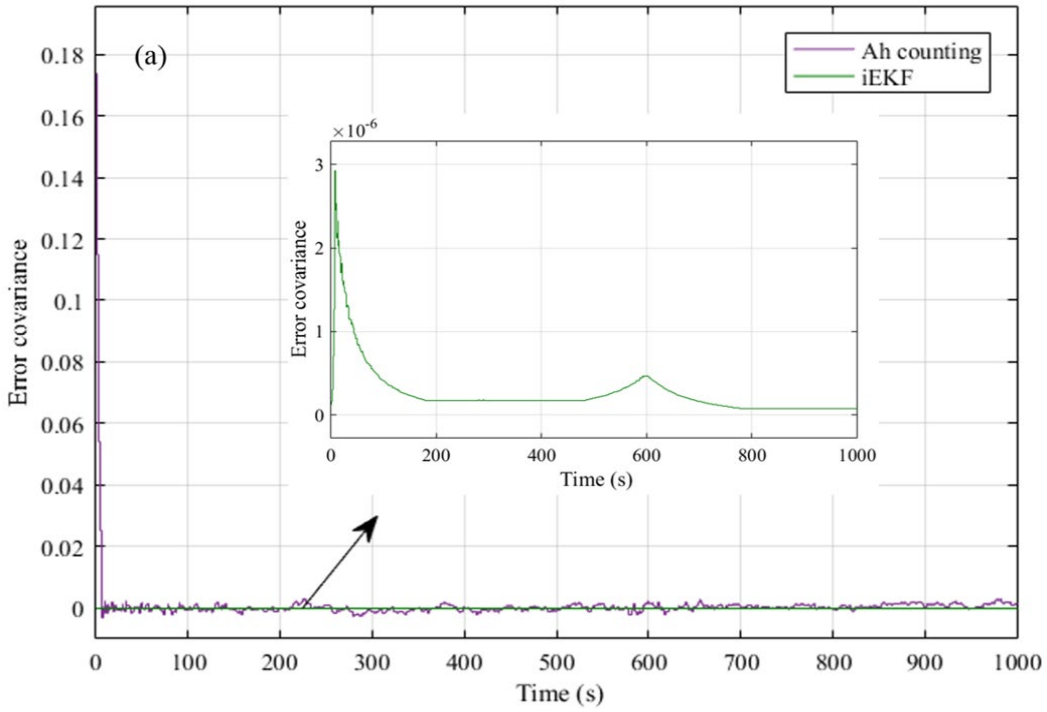

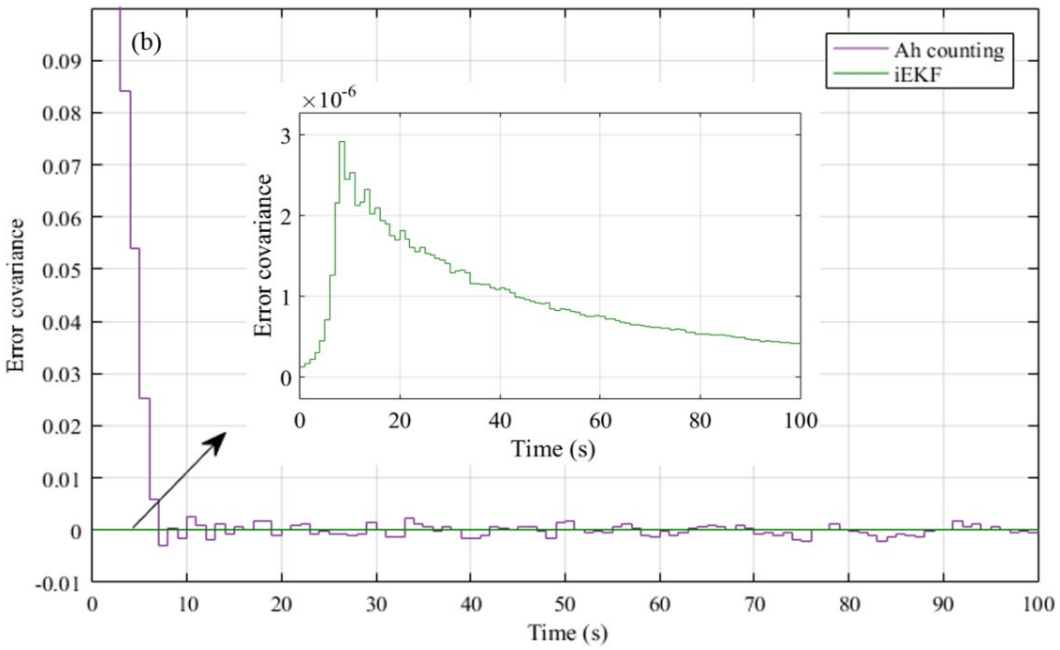


Figure 5.15 Comparison of error covariance between iEKF and Ah models under dynamic operating conditions: (a) over a time of 1000 s (b) from 0 to 100 s..

The inset in both the figures shows the magnified plot of the error covariance of the iEKF model only. Note the extremely small value of error covariance of the iEKF model.

Table 5.5 The SoC estimation error based on the iEKF method under static/dynamic condition

| Operation Condition | Maximum Error (%) | Average Error (%) | Relative Error (%) |
|---|---|---|---|
| Static | 2.39 | 1.43 | 1.20 |
| Dynamic | 6.76 | 3.94 | 2.15 |

As shown in Figure 5.12, the estimator based on iEKF shows high degree of agreement tracking the change in SoC. Comparing the curves of estimation error shown in Figures 5.13 and 5.15, the iEKF algorithm obtains better noise filtering performance. It should be pointed out that the dynamic operation condition shown in Figure 5.14 causes more

fluctuation in the estimation error curve than in static operation condition. From the comparison results shown in Table 5.5, the estimation errors increase under dynamic operation conditions. This means the estimation difficulty will become more challenging under dynamic operation conditions.

Since the estimator is sensitive to different operation conditions, the quality of the estimator cannot be fairly compared with different approaches. Several factors such as the battery model, the battery types and the experimental methods for the offline parameter identification affect the performance of the estimator. For example, the estimator based on EKF with the Thevenin model reported an absolute mean error of 4.42% under dynamic operation conditions [194]. Tested results of SoC estimation showed a relative error of 1.5% when using an estimator based on extended fractional KF with the fractional order PNGV model [195]. The SoC estimators based on different battery models using EKF and dual EKF methods have been compared in [191]. Plett [196] built the battery models based on a group of Pulsed-current test and adopted the UDDS dynamic test on LiPB battery, which shown estimation error of the battery models varying from 1% to 6.5%. The iEKF proposed in this research shows a relative error of 1.2% and 2.15% under static and dynamic conditions, respectively. The SoC estimation based on the improved-EKF model discussed in this Chapter shows good accuracy and the method itself has less complexity compared to other well-established methods such as the EKF based on the Thevenin or PNGV models.

It has also carried out simulations using the proposed iEKF model but with different initial SoCs of 20% and 50% and were able to achieve similar accuracy as that of the SOC value of 70%: relative error under static and dynamic operating condition with

initial SoC of 20% and 50% are less than 2%. The relative errors of the SOC estimation for the 20%, 50% and 70% initial guess are compared in Table 5.6. The results shown in Table 5.6 further strengthen the credibility of the designed iEKF model.

Table 5.6 The comparison of relative error (%) between SoC estimation based on the iEKF and Ah counting methods under static/dynamic condition

| Estimation error / Operation | Initinal SoC of 20% | | Initinal SoC of 50% | | Initinal SoC of 70% | |
|---|---|---|---|---|---|---|
| | Ah counting | iEKF | Ah counting | iEKF | Ah counting | iEKF |
| Static | 14.9 | 0.8 | 15.3 | 1.0 | 15.0 | 1.2 |
| Dynamic | 17.7 | 1.7 | 18.5 | 2.0 | 19.7 | 2.1 |

### 5.5.3 The Issues of Practical Implementation

In practical applications, several issues influenced the estimation accuracy and the engineering applicability of the estimator. It has concluded in five aspects to be considered in practical implementation.

1) The number of estimated parameters

Parameters are estimated through limited observations with error during the estimation process. The fewer the estimated parameters, the higher the accuracy of the estimation. To improve the robustness and the applicability of the estimator, a battery model with fewer parameters could be used. For example, RC ECM included five parameters shown in Chapter two, Figure 2.9.

2) Signal-noise ratio (SNR)

The SNR describes that signals are disturbed by the noise in electronic devices and system. The signals collected in the system are obtained through the

sensors, which has the noise, and error in this scenario. A larger SNR value means less interference from noise or error. In practical implementation, the value of signal might be near zero to make the SNR value smaller disregarded the noise, which will impact the accuracy of the parameter estimation. Moreover, a ‘dead zone’ might appear in the process of identifying parameters using adaptive algorithm. The ‘dead zone’ can be captured by calculating the relationship between the model residual value and the estimation error of sensors, as shown in equation (5-25).

$$|\varepsilon(k)| \geq 2sup|e(k)| \tag{5-25}$$

The estimation of the parameters will not be updated in the ‘dead zone’. where $\varepsilon(k)$ is the residual value of the model, $e(k)$ is the estimation error of the sensors.

3) System error

In addition to the observation errors that have been taken into account, the selected battery model has errors itself. Furthermore, the curve fitting of the SoC-OCV has errors, which include the errors of experimental measurement and the acquisition signal error from sensor. Therefore, error models are often introduced in the algorithm.

4) Magnitude difference of measurement

The issues of magnitude difference of measurement cannot be avoided in the process of parameter identification. The parameters cannot often be accurately estimated if the magnitudes differ greatly. Hence, there is a homogenization

procedure, such as difference equation, when large orders of magnitude in the estimation process.

5) Time-variable parameters

In practical battery applications, the chemical reactions inside the battery will change with time. To ensure the accuracy of the parameters, it is necessary to make the identified parameters come from the latest time point when the parameters are identified online by the adaptive or recurrence algorithm. A 'forgetting factor' can be introduced into RLS algorithm to reduce the impact of the information from previous generations of measured value on the current measured value. For inputs with weak stimulus signals, the covariance matrix might be updated according to the original information during the iterative update of the parameter estimation of the algorithm, thereby causing large deviations with the phenomenon of 'saturation'. Thus, estimating the parameters in batches using different estimating methods, such as Adaptive Kalman Filter (AKF) and EKF, to improve the accuracy, then, reduce calculation burden.

For the issues discussed above, a comparative and improved model for SoC estimation is proposed and demonstrated in Figure 5.16 and Table 5.7. In Figure 5.16, the comparative model includes a second-order RC (2-RC) ECM and a Thevenin model. The initial input signals include current $I$, temperature $T$, and the relationship of SoC-OCV obtained by polynomial fitting. Based on the second-order RC ECM with preset parameters, it will give outputs of estimated $SoC_0$ and open circuit voltage of $U$, which

are the input signals for the Thevenin model to identify the parameters. Meanwhile, the $SoC_0$ is seen as the primitive truth value to compare with the estimated SoC from the Thevenin model.

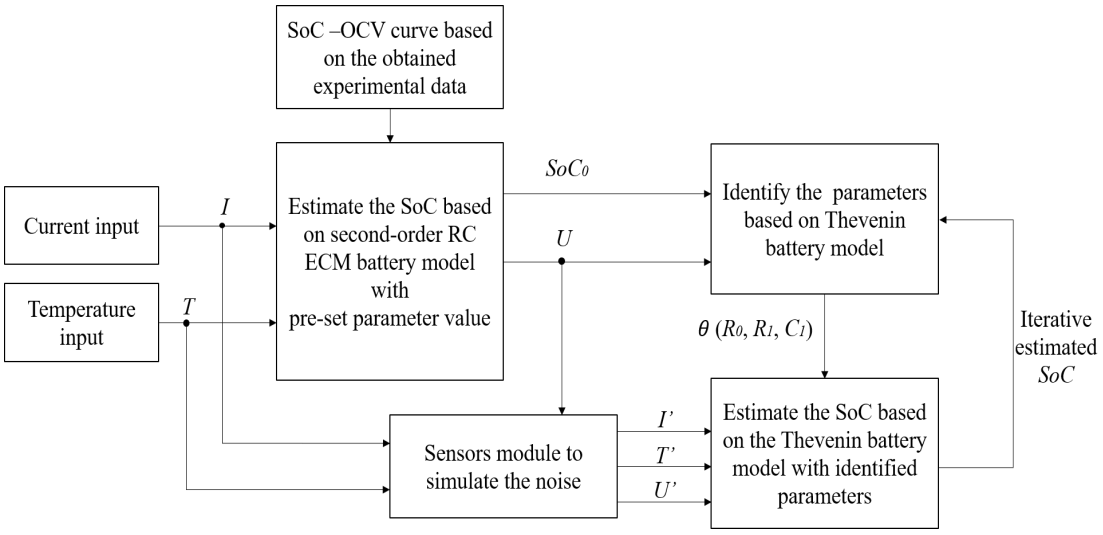


Figure 5.16 The comparative and improved estimation model

Table 5.7 The methodology of comparative and improved estimation model

| **Comparative and improved SoC estimation model** | | |
|---|---|---|
| Preparation | SoC-OCV relationship: Polynomial fitting of experimental data | |
| Thevenin model | Basic method | Improved method |
| Parameters identification | Identify the parameters ($R_0$, $R_1$, $C_1$) by RLS | Identify the parameters $R_0$ by RLS, ($R_1$, $C_1$) by AKF |
| SoC estimation | Iterative estimation by EKF | Iterative estimation by EKF |

As listed in table 5.7, the basic approach of the parameters' identification in Thevenin battery model is all using RLS. The identified parameters $\theta$ $(R_0, R_1, C_1)$ are referring the components in Figure 2.10. In addition, the input signals for Thevenin model are added with the errors from sensor block, (*I'*, *T'*, *U'*). Based on the inputs, the SoC is estimated by EKF, which could be compared to the $SoC_0$. For the improved estimation model, the parameters are identified in batches: the $R_0$ is identified by RLS, while using AKF to identify the $R_1$ and $C_1$, then estimate the *SoC* by EKF.

The example code for model parameter identification using RLS, AKF and EKF for SoC estimation is in the attachment. In this comparative and improved model, the second-order EC ECM and Thevenin model has less parameters to be identified, which reduced the dimension and calculational complexity. The introduction of 'forgetting factor' avoid the saturation effect of the covariance matrix, while the homogenization coefficient of the voltage and current is used to improve the accuracy of parameter identification.

## 5.6 Concluding Remarks

This Chapter has provided an analytical comparison of various SoC estimation methods. A well-designed SoC estimator includes the parameter identification of the battery model and the iterative estimation methods. A composite battery model using iEKF has been proposed in this Chapter. Four groups of real experiments and parameter identifications were conducted to build a reliable battery model for the achieving a credible estimator. A composite battery model was built using offline parameter identification using MATLAB. Based on this composite battery model, a mathematical model of the improved EKF was built. OCV method provided the initial

estimation inaccuracy and the Ah method provided a rough estimate of the SoC. The cumulative error of SoC estimation in Ah method was precisely corrected by the EKF algorithm. The iEKF algorithm provides successful simulation results for accurate SoC estimation under both static and dynamic operation conditions. The iEKF algorithm shows an outstanding advantage in the estimation accuracy while being less complex than other methods. In terms of the simplicity and feasibility, the iEKF is an excellent candidate for BMS implementation to promote the battery performance. To this end, the issues for the implementation of the SoC estimation have discussed, a comparative and improved model is proposed to solve the practical difficulties.

# Chapter 6 Conclusion and Future Work

This Chapter provides a summary of the work carried out in this thesis, discussing the role of each Chapter in achieving the main objective of the thesis and the contributions made to the body of knowledge as a whole. An overall conclusion is then drawn and the scope for the future work which expands on this thesis is also set out.

## 6.1 Summary

The main technical objective of this thesis was to develop an EMS with effective control strategy and smart optimization for HEVs. A novel iEKF algorithm is proposed based on a composite battery model to provide an accurate State of Charge (SoC) estimation for monitoring module in BMS.

As set out in Chapter 1, the motivation for the work carried out in this thesis is to increase the future uptake of battery energy storage devices in effective and safety-critical applications, such as in electric/hybrid-electric vehicles (EV/HEVs). The energy management system (EMS) with the control strategy and its optimization is identified as one the main areas of research for improving the future adoption of these delicate energy storage devices in a wider range of power and automotive applications. Hence, this thesis puts its focus on developing a novel hybrid EMS, whereby optimizing the rule-based control strategy, not only the aspect of decreasing emission will be achieved but also a better driving performance when achieving the optimization objectives with constrains.

Subsequently, to complete a coherent piece of research, the state-of-the-art of the EMS and the monitoring technologies, including the various battery models, as presented in

literature, is reviewed in Chapter 2. At first, to familiarise the reader with the common EVs topologies. Thereafter, to provide the reader with appreciation for attributions of each chapter, a comprehensive review of different types of EMS with applicable techniques are explained. The accuracy of SoC estimation is significantly relying on the different adoptions of battery models, the algorithms used for SoC estimation and the battery models are finally discussed.

Chapter 3 discussed the importance of EMS in the control of HEVs. Subsequently, a rule-based control strategy of premeditate EMS is proposed to increase the efficiency of battery usage in HEVs. For the purpose of reducing the emission, then increasing the fuel economy, the rule-based control strategy invented a new state based on the analysis of the engine and motor working modes. The designed rule-based control strategy was finally verified through simulation. Simulation conducted for this research adopted the vehicle model with practical data of Toyota-Prius. The simulation results show that the design of rule-based control strategy for premeditated EMS successfully achieved emission reduction and increased fuel economy.

The premeditated EMS has the advantage of simple application in practical usage, but loss of efficiency confronting complex working conditions. Therefore, a hybrid EMS combined the designed rule-based control strategy and the GA optimization was discussed in Chapter 4. A mathematical model associated the logic of rule-based control strategy and GA optimization was built and subsequently verified in a dynamic and bidirectional simulation. With the same input of working condition used in

Chapter 3, the simulation results show that the hybrid EMS significantly improved the fuel economy and reduced the emission.

The SoC is the decisive information for the execution of the designed EMS in Chapters 3 and 4. An adaptive algorithm of online SoC estimation was proposed in Chapter 5 to include a novel battery model and estimation algorithm to obtain a dynamic SoC value. The parameter identification of the proposed composite battery model adopted five groups of battery performance testing experiments. The experiments used the battery using $LiFePO_4$ cells and each set of experiments was discussed in detail.

The estimation algorithm combines the OCV, Ah method and EKF algorithm and is verified through a simulation in MATLAB_Simulink. The simulation results show that the iEKF estimator based on composite battery model maintained very high accuracy on SoC estimation in both static condition with constant current and temperature inputs and dynamic condition with changed current and temperature. Chapter 5 proposed a comparison framework for SoC estimator based on a 2-RC network battery model and developed the estimation algorithm and the method of parameters identification in pursuit of a higher accuracy estimator through comparison model.

Although the techniques developed in this thesis were verified through the simulation, the vehicle model adopted in the simulation for hybrid EMS is based on the practical data to improve the practicability. To enhance the reliability, the parameters identification of the composite battery for SoC estimator in this thesis conducted groups of experiments of $LiFePO_4$ battery. Therefore, the techniques of hybrid EMS

presented herein can be applied to the generic HEVs, and the iEKF algorithm could be applied in generic scenarios for SoC estimation.

## 6.2 Scope for Future Work

Although a conclusive body of work has been presented herein and benefits offered over the state of the art, there are areas which this thesis can expand on. The techniques presented in this thesis can be employed to solve some research issues raised in other scheduling and controlling hybrid electric area, especially in the technologies of vehicle applications. The list below summarises the scope for future work which can lead on from this thesis.

- The method to optimize the rule-based control strategy for hybrid EMS could be developed smarter and more effective and could use other models such as neural network model, *etc.*
- The hybrid EMS and the SoC estimator could be applied and verified through hardware-in-loop to increase the feasibility.
- A connection could be developed that the estimated SoC value obtained by the proposed estimator in monitoring module as the decisive factor used in the hybrid EMS module for BMS applications.
- In addition to the SoC, the techniques of estimating SoP and SoH could also be expanded in similar framework in monitoring module.
- A well-functioning BMS could be developed by combining the hybrid EMS and monitoring module with SoC estimation, the active cell equalization, and the cooling system.

# Bibliography


[1] B. Sharma, *Environmental chemistry*. Krishna Prakashan Media, 2014.

[2] R. K. Maurya, *Characteristics and control of low temperature combustion engines: Employing gasoline, ethanol and methanol*. Springer, 2017.

[3] A. Fotouhi, D. J. Auger, K. Propp, S. Longo, and M. Wild, "A review on electric vehicle battery modelling: From Lithium-ion toward Lithium–Sulphur," *Renewable and Sustainable Energy Reviews,* vol. 56, pp. 1008-1021, 2016.

[4] Z. Rezvani, J. Jansson, and J. Bodin, "Advances in consumer electric vehicle adoption research: A review and research agenda," *Transportation research part D: transport and environment,* vol. 34, pp. 122-136, 2015.

[5] M. Knez, G. K. Zevnik, and M. Obrecht, "A review of available chargers for electric vehicles: United States of America, European Union, and Asia," *Renewable and Sustainable Energy Reviews,* vol. 109, pp. 284-293, 2019.

[6] S. Li, P.-C. Sui, J. Xiao, and R. Chahine, "Policy formulation for highly automated vehicles: Emerging importance, research frontiers and insights," *Transportation Research Part A: Policy and Practice,* vol. 124, pp. 573-586, 2019.

[7] C. Breyer, S. Khalili, and D. Bogdanov, "Solar photovoltaic capacity demand for a sustainable transport sector to fulfil the Paris Agreement by 2050," *Progress in Photovoltaics: Research and Applications,* 2019.

[8] H. Hao, Y. Geng, and J. Sarkis, "Carbon footprint of global passenger cars: scenarios through 2050," *Energy,* vol. 101, pp. 121-131, 2016.

[9] R. Irle, "Global EV Sales for 2018–Final Results," ed, 2019.

[10] E. Nordic, "Outlook 2018," *International Energy Agency,* 2018.

[11] R. Salvucci, S. Petrović, K. Karlsson, M. Wråke, T. P. Uteng, and O. Balyk, "Energy scenario analysis for the Nordic transport sector: A critical review," *Energies,* vol. 12, no. 12, p. 2232, 2019.

[12] K. Hauff, S. Pfahl, and R. Degenkolb, "Taxation of Electric Vehicles in Europe: A Methodology for Comparison," *World Electric Vehicle Journal,* vol. 9, no. 2, p. 30, 2018.

[13] A. Elgowainy *et al.*, "Current and future United States light-duty vehicle pathways: Cradle-to-grave lifecycle greenhouse gas emissions and economic assessment," *Environmental science & technology,* vol. 52, no. 4, pp. 2392-2399, 2018.

[14] R. Gilbert and A. Perl, *Transport revolutions: moving people and freight without oil*. Routledge, 2018.

[15] Y. Ma, T. Shi, W. Zhang, Y. Hao, J. Huang, and Y. Lin, "Comprehensive policy evaluation of NEV development in China, Japan, the United States, and Germany based on the AHP-EW model," *Journal of cleaner production,* vol. 214, pp. 389-402, 2019.

[16] H. Ito and N. Kawazoe, "Assessing and promoting eco-policies in Toyota City, Japan," *Policy Design and Practice,* vol. 2, no. 1, pp. 35-52, 2019.

[17] D. Zhili, L. Boqiang, and G. Chunxu, "Development path of electric vehicles in China under environmental and energy security constraints," *Resources, Conservation and Recycling,* vol. 143, pp. 17-26, 2019.
[18] G. Yeung, "'Made in China 2025': the development of a new energy vehicle industry in China," *Area Development and Policy,* vol. 4, no. 1, pp. 39-59, 2019.
[19] B. Nykvist, F. Sprei, and M. Nilsson, "Assessing the progress toward lower priced long range battery electric vehicles," *Energy policy,* vol. 124, pp. 144-155, 2019.
[20] D. Coffin and J. Horowitz, "The Supply Chain for Electric Vehicle Batteries," *J. Int'l Com. & Econ.,* p. 1, 2018.
[21] M. Bauer, T. T. Nguyen, A. Jossen, and J. Lygeros, "Evaluating frequency regulation operated on two stationary energy systems with batteries from electric vehicles," *Energy Procedia,* vol. 155, pp. 32-43, 2018.
[22] D. Myall, D. Ivanov, W. Larason, M. Nixon, and H. Moller, "Accelerated reported battery capacity loss in 30 kWh variants of the Nissan Leaf," 2018.
[23] F. An, A. Vyas, J. Anderson, and D. Santini, "Evaluating commercial and prototype HEVs," *SAE Transactions,* pp. 769-780, 2001.
[24] G. Duarte, R. Varella, G. Gonçalves, and T. Farias, "Effect of battery state of charge on fuel use and pollutant emissions of a full hybrid electric light duty vehicle," *Journal of Power Sources,* vol. 246, pp. 377-386, 2014.
[25] N. Kawamoto, K. Naiki, T. Kawai, T. Shikida, and M. Tomatsuri, "Development of new 1.8-liter engine for hybrid vehicles," SAE Technical Paper0148-7191, 2009.
[26] R. Xiong and W. Shen, *Advanced Battery Management Technologies for Electric Vehicles*. John Wiley & Sons, 2019.
[27] Y. Ding, Z. P. Cano, A. Yu, J. Lu, and Z. Chen, "Automotive Li-ion batteries: Current status and future perspectives," *Electrochemical Energy Reviews,* vol. 2, no. 1, pp. 1-28, 2019.
[28] N. Picciano, "Battery aging and characterization of nickel metal hydride and lead-acid batteries," The Ohio State University, 2007.
[29] S. K. Dhar, F. Albano, S. Venkatesan, and D. Townsend, "Hybrid battery system for electric and hybrid electric vehicles," ed: Google Patents, 2014.
[30] D. Doerffel, "Testing and characterisation of large high-energy lithium-ion batteries for electric and hybrid electric vehicles," University of Southampton, 2007.
[31] X. Liu, K. Li, and X. Li, "The Electrochemical Performance and Applications of Several Popular Lithium-ion Batteries for Electric Vehicles-A Review," in *Advances in Green Energy Systems and Smart Grid*: Springer, 2018, pp. 201-213.
[32] J. Meng *et al.*, "Low-complexity online estimation for LiFePO4 battery state of charge in electric vehicles," *Journal of Power Sources,* vol. 395, pp. 280-288, 2018.
[33] W. Cao, Y. Zhang, and B. Antony, "Belt and Road: A New Journey for Foreign Investment-A Case Study of the Internationalization Strategy of BYD," in *3rd*

*International Symposium on Asian B&R Conference on International Business Cooperation (ISBCD 2018)*, 2018: Atlantis Press.

[34] M. H. Lipu *et al.*, "A review of state of health and remaining useful life estimation methods for lithium-ion battery in electric vehicles: Challenges and recommendations," *Journal of cleaner production,* vol. 205, pp. 115-133, 2018.

[35] Z. Gao, X. Zhang, Y. Xiao, H. Gao, H. Wang, and C. Piao, "Influence of Low-Temperature Charge on the Mechanical Integrity Behavior of 18650 Lithium-Ion Battery Cells Subject to Lateral Compression," *Energies,* vol. 12, no. 5, p. 797, 2019.

[36] M. Li, J. Lu, Z. Chen, and K. Amine, "30 years of lithium‐ion batteries," *Advanced Materials,* vol. 30, no. 33, p. 1800561, 2018.

[37] J. Du *et al.*, "Boundaries of high-power charging for long-range battery electric car from the heat generation perspective," *Energy,* 2019.

[38] W. Choi and H. H. Song, "Well-to-wheel greenhouse gas emissions of battery electric vehicles in countries dependent on the import of fuels through maritime transportation: A South Korean case study," *Applied energy,* vol. 230, pp. 135-147, 2018.

[39] S. J. Visco, B. D. Katz, Y. S. Nimon, and L. C. De Jonghe, "Protected active metal electrode and battery cell structures with non-aqueous interlayer architecture," ed: Google Patents, 2007.

[40] M. Kendall, "Fuel cell development for New Energy Vehicles (NEVs) and clean air in China," *Progress in Natural Science: Materials International,* vol. 28, no. 2, pp. 113-120, 2018.

[41] Q. Qiao, F. Zhao, Z. Liu, and H. Hao, "Recycling-Based Reduction of Energy Consumption and Carbon Emission of China's Electric Vehicles: Overview and Policy Analysis," SAE Technical Paper0148-7191, 2018.

[42] M. M. Thackeray, C. Wolverton, and E. D. Isaacs, "Electrical energy storage for transportation—approaching the limits of, and going beyond, lithium-ion batteries," *Energy & Environmental Science,* vol. 5, no. 7, pp. 7854-7863, 2012.

[43] M. A. Hannan, M. M. Hoque, A. Hussain, Y. Yusof, and P. J. Ker, "State-of-the-art and energy management system of lithium-ion batteries in electric vehicle applications: Issues and recommendations," *Ieee Access,* vol. 6, pp. 19362-19378, 2018.

[44] M. Brandl *et al.*, "Batteries and battery management systems for electric vehicles," in *2012 Design, Automation & Test in Europe Conference & Exhibition (DATE)*, 2012, pp. 971-976: IEEE.

[45] H. Rahimi-Eichi, U. Ojha, F. Baronti, and M.-Y. Chow, "Battery management system: An overview of its application in the smart grid and electric vehicles," *IEEE Industrial Electronics Magazine,* vol. 7, no. 2, pp. 4-16, 2013.

[46] K. W. E. Cheng, B. Divakar, H. Wu, K. Ding, and H. F. Ho, "Battery-management system (BMS) and SOC development for electrical vehicles," *IEEE transactions on vehicular technology,* vol. 60, no. 1, pp. 76-88, 2010.

[47] M. Hannan, F. Azidin, and A. Mohamed, "Multi-sources model and control algorithm of an energy management system for light electric vehicles," *Energy Conversion and Management,* vol. 62, pp. 123-130, 2012.
[48] Z. Song, H. Hofmann, J. Li, J. Hou, X. Han, and M. Ouyang, "Energy management strategies comparison for electric vehicles with hybrid energy storage system," *Applied Energy,* vol. 134, pp. 321-331, 2014.
[49] S. Chakraborty *et al.*, "Embedded systems and software challenges in electric vehicles," in *Proceedings of the conference on design, automation and test in Europe*, 2012, pp. 424-429: EDA Consortium.
[50] T. Stuart, F. Fang, X. Wang, C. Ashtiani, and A. Pesaran, "A modular battery management system for HEVs," SAE Technical Paper0148-7191, 2002.
[51] A. M. Andwari, A. Pesiridis, S. Rajoo, R. Martinez-Botas, and V. Esfahanian, "A review of Battery Electric Vehicle technology and readiness levels," *Renewable and Sustainable Energy Reviews,* vol. 78, pp. 414-430, 2017.
[52] S. S. Lv, Q. Q. Chen, X. Chen, and H. J. Ni, "Research Progress of Energy Management System for new energy vehicles," in *Applied Mechanics and Materials*, 2015, vol. 727, pp. 896-899: Trans Tech Publ.
[53] G. Pistoia, *Electric and hybrid vehicles: Power sources, models, sustainability, infrastructure and the market*. Elsevier, 2010.
[54] P. Lawlor, P. Dowling, and N. R. Lynam, "Accessory mounting system for a vehicle," ed: Google Patents, 2015.
[55] M. Akamatsu, P. Green, and K. Bengler, "Automotive technology and human factors research: Past, present, and future," *International journal of vehicular technology,* vol. 2013, 2013.
[56] J. Morgan and J. K. Liker, *The Toyota product development system: integrating people, process, and technology*. Productivity press, 2006.
[57] H. Pohl and M. Yarime, "Integrating innovation system and management concepts: The development of electric and hybrid electric vehicles in Japan," *Technological Forecasting and Social Change,* vol. 79, no. 8, pp. 1431-1446, 2012.
[58] N. Ding, K. Prasad, and T. Lie, "The electric vehicle: a review," *International Journal of Electric and Hybrid Vehicles,* vol. 9, no. 1, pp. 49-66, 2017.
[59] C. D. Anderson and J. Anderson, *Electric and hybrid cars: A history*. McFarland, 2010.
[60] J. T. Warner, *The handbook of lithium-ion battery pack design: chemistry, components, types and terminology*. Elsevier, 2015.
[61] M. Hannan, F. Azidin, and A. Mohamed, "Hybrid electric vehicles and their challenges: A review," *Renewable and Sustainable Energy Reviews,* vol. 29, pp. 135-150, 2014.
[62] K. Chau and W. Li, "Overview of electric machines for electric and hybrid vehicles," *International Journal of Vehicle Design: journal of vehicle engineering, automotive technology and components,* 2014.
[63] Z. Rao and S. Wang, "A review of power battery thermal energy management," *Renewable and Sustainable Energy Reviews,* vol. 15, no. 9, pp. 4554-4571, 2011.

[64] W. Lee, L. Xiang, R. Schober, and V. W. Wong, "Analysis of the behavior of electric vehicle charging stations with renewable generations," in *2013 IEEE International Conference on Smart Grid Communications (SmartGridComm)*, 2013, pp. 145-150: IEEE.

[65] R. B. Schainker, "Executive overview: energy storage options for a sustainable energy future," in *IEEE Power Engineering Society General Meeting, 2004.*, 2004, pp. 2309-2314: Ieee.

[66] H. Chen, T. N. Cong, W. Yang, C. Tan, Y. Li, and Y. Ding, "Progress in electrical energy storage system: A critical review," *Progress in natural science,* vol. 19, no. 3, pp. 291-312, 2009.

[67] Z. Song *et al.*, "Multi-objective optimization of a semi-active battery/supercapacitor energy storage system for electric vehicles," *Applied Energy,* vol. 135, pp. 212-224, 2014.

[68] I. Hadjipaschalis, A. Poullikkas, and V. Efthimiou, "Overview of current and future energy storage technologies for electric power applications," *Renewable and sustainable energy reviews,* vol. 13, no. 6-7, pp. 1513-1522, 2009.

[69] P. Gananchchelvi, J. Yu, and M. S. Pukish, "Current trends in in-vehicle electrical engineering applications," in *IECON 2012-38th Annual Conference on IEEE Industrial Electronics Society*, 2012, pp. 6268-6273: IEEE.

[70] A. van Velzen, J. A. Annema, G. van de Kaa, and B. van Wee, "Proposing a more comprehensive future total cost of ownership estimation framework for electric vehicles," *Energy policy,* vol. 129, pp. 1034-1046, 2019.

[71] N. Ortar and M. Ryghaug, "Should All Cars Be Electric by 2025? The Electric Car Debate in Europe," *Sustainability,* vol. 11, no. 7, p. 1868, 2019.

[72] Z. Wei, S. Yu, G. Sun, Y. Sun, Y. Yuan, and D. Wang, "Concept and development of virtual power plant," *Automation of Electric Power Systems,* vol. 37, no. 13, pp. 1-9, 2013.

[73] T. F. Wilton, J. J. Anderson, and R. W. Schmitz, "Method and apparatus for selective operation of a hybrid electric vehicle powerplant," ed: Google Patents, 2005.

[74] B. Scrosati, J. Garche, and W. Tillmetz, *Advances in battery technologies for electric vehicles*. Woodhead Publishing, 2015.

[75] Z. Song, K. Song, and T. Zhang, "State-of-the-Art and Development Trends of Energy Management Strategies for Intelligent and Connected New Energy Vehicles: A Review," SAE Technical Paper0148-7191, 2019.

[76] B. Lokeshgupta and S. Sivasubramani, "Multi-objective home energy management with battery energy storage systems," *Sustainable Cities and Society,* vol. 47, p. 101458, 2019.

[77] C. Musardo, G. Rizzoni, Y. Guezennec, and B. Staccia, "A-ECMS: An adaptive algorithm for hybrid electric vehicle energy management," *European Journal of Control,* vol. 11, no. 4-5, pp. 509-524, 2005.

[78] S. Ebbesen, P. Elbert, and L. Guzzella, "Battery state-of-health perceptive energy management for hybrid electric vehicles," *IEEE Transactions on Vehicular technology,* vol. 61, no. 7, pp. 2893-2900, 2012.

[79] T. Nüesch, M. Wang, C. Voser, and L. Guzzella, "Optimal energy management and sizing for hybrid electric vehicles considering transient emissions," *IFAC Proceedings Volumes,* vol. 45, no. 30, pp. 278-285, 2012.

[80] F. Yan, J. Wang, and K. Huang, "Hybrid electric vehicle model predictive control torque-split strategy incorporating engine transient characteristics," *IEEE transactions on vehicular technology,* vol. 61, no. 6, pp. 2458-2467, 2012.

[81] H. Moghbeli, A. H. Niasar, and N. Fallahi, "Fuzzy energy control strategy of through-to-road hybrid electric vehicle," in *2014 IEEE 23rd International Symposium on Industrial Electronics (ISIE)*, 2014, pp. 1660-1665: IEEE.

[82] S. Di Cairano, W. Liang, I. V. Kolmanovsky, M. L. Kuang, and A. M. Phillips, "Power smoothing energy management and its application to a series hybrid powertrain," *IEEE Transactions on control systems technology,* vol. 21, no. 6, pp. 2091-2103, 2012.

[83] H. He, R. Xiong, H. Guo, and S. Li, "Comparison study on the battery models used for the energy management of batteries in electric vehicles," *Energy Conversion and Management,* vol. 64, pp. 113-121, 2012.

[84] N. Ding, T. Lie, and K. Prasad, "The Design of Control Strategy for Blended Series-Parallel Power-Split PHEV–a Simulation Study," *International Journal of Transportation Systems,* vol. 2, pp. 21-24, 2017.

[85] Y. L. Murphey *et al.*, "Intelligent hybrid vehicle power control—Part II: Online intelligent energy management," *IEEE Transactions on Vehicular Technology,* vol. 62, no. 1, pp. 69-79, 2012.

[86] Y. L. Murphey, J. Park, Z. Chen, M. L. Kuang, M. A. Masrur, and A. M. Phillips, "Intelligent hybrid vehicle power control—Part I: Machine learning of optimal vehicle power," *IEEE Transactions on Vehicular Technology,* vol. 61, no. 8, pp. 3519-3530, 2012.

[87] B. Vural, S. Dusmez, M. Uzunoglu, E. Ugur, and B. Akin, "Fuel consumption comparison of different battery/ultracapacitor hybridization topologies for fuel-cell vehicles on a test bench," *IEEE Journal of Emerging and Selected Topics in Power Electronics,* vol. 2, no. 3, pp. 552-561, 2014.

[88] J.-S. Won and R. Langari, "Intelligent energy management agent for a parallel hybrid vehicle-part II: torque distribution, charge sustenance strategies, and performance results," *IEEE transactions on vehicular technology,* vol. 54, no. 3, pp. 935-953, 2005.

[89] S. F. Tie and C. W. Tan, "A review of energy sources and energy management system in electric vehicles," *Renewable and sustainable energy reviews,* vol. 20, pp. 82-102, 2013.

[90] C. M. Anderson-Cook, "Practical genetic algorithms," ed: Taylor & Francis, 2005.

[91] P. S. Georgilakis and N. D. Hatziargyriou, "A review of power distribution planning in the modern power systems era: Models, methods and future research," *Electric Power Systems Research,* vol. 121, pp. 89-100, 2015.

[92] S. Das, A. Biswas, S. Dasgupta, and A. Abraham, "Bacterial foraging optimization algorithm: theoretical foundations, analysis, and applications," in

*Foundations of Computational Intelligence Volume 3*: Springer, 2009, pp. 23-55.

[93] A. Sciarretta, M. Back, and L. Guzzella, "Optimal control of parallel hybrid electric vehicles," *IEEE Transactions on control systems technology,* vol. 12, no. 3, pp. 352-363, 2004.

[94] V. Marano, P. Tulpule, S. Stockar, S. Onori, and G. Rizzoni, "Comparative study of different control strategies for plug-in hybrid electric vehicles," SAE Technical Paper0148-7191, 2009.

[95] H. Ramadan, M. Becherif, and F. Claude, "Energy management improvement of hybrid electric vehicles via combined GPS/rule-based methodology," *IEEE Transactions on Automation Science and Engineering,* vol. 14, no. 2, pp. 586-597, 2017.

[96] H. Borhan, A. Vahidi, A. M. Phillips, M. L. Kuang, I. V. Kolmanovsky, and S. Di Cairano, "MPC-based energy management of a power-split hybrid electric vehicle," *IEEE Transactions on Control Systems Technology,* vol. 20, no. 3, pp. 593-603, 2011.

[97] G. K. Prasad and C. D. Rahn, "Model based identification of aging parameters in lithium ion batteries," *Journal of power sources,* vol. 232, pp. 79-85, 2013.

[98] A. Foucquier, S. Robert, F. Suard, L. Stéphan, and A. Jay, "State of the art in building modelling and energy performances prediction: A review," *Renewable and Sustainable Energy Reviews,* vol. 23, pp. 272-288, 2013.

[99] K. Sun and Q. Shu, "Overview of the types of battery models," in *Proceedings of the 30th Chinese Control Conference*, 2011, pp. 3644-3648: IEEE.

[100] X. Hu, F. Sun, and Y. Zou, "Comparison between two model-based algorithms for Li-ion battery SOC estimation in electric vehicles," *Simulation Modelling Practice and Theory,* vol. 34, pp. 1-11, 2013.

[101] C. Qiu, G. He, W. Shi, M. Zou, and C. Liu, "The polarization characteristics of lithium-ion batteries under cyclic charge and discharge," *Journal of Solid State Electrochemistry,* vol. 23, no. 6, pp. 1887-1902, 2019.

[102] R. Xiong, L. Li, and J. Tian, "Towards a smarter battery management system: A critical review on battery state of health monitoring methods," *Journal of Power Sources,* vol. 405, pp. 18-29, 2018.

[103] I. Bloom *et al.*, "An accelerated calendar and cycle life study of Li-ion cells," *Journal of power sources,* vol. 101, no. 2, pp. 238-247, 2001.

[104] D. W. Dees, V. S. Battaglia, and A. Bélanger, "Electrochemical modeling of lithium polymer batteries," *Journal of power sources,* vol. 110, no. 2, pp. 310-320, 2002.

[105] L. Jaegul, L. Soonjae, and E. Namgoong, "Dynamic state battery model with self-adaptive aging factor for EV and HEV applications," in *Proceedings of the 15th International Electric Vehicle Symposium*, 1998.

[106] K. Morio, H. Kazuhiro, and P. Anil, "Battery SOC and distance to empty meter of the honda EV plus," in *Proc. International Electric Vehicle Symposium*, 1997, pp. 1-10.

[107] J. Li, J. K. Barillas, C. Guenther, and M. A. Danzer, "A comparative study of state of charge estimation algorithms for LiFePO4 batteries used in electric vehicles," *Journal of power sources,* vol. 230, pp. 244-250, 2013.

[108] Z. Li, L. Lu, and M. Ouyang, "Comparison of methods for improving SOC estimation accuracy through an ampere-hour integeration approach [J]," *Journal of Tsinghua University (Science and Technology),* vol. 8, no. 038, 2010.

[109] F. Xuyun and S. Zechang, "A battery model including hysteresis for State-of-Charge estimation in Ni-MH battery," in *2008 IEEE Vehicle Power and Propulsion Conference*, 2008, pp. 1-5: IEEE.

[110] M. A. Hannan, M. H. Lipu, A. Hussain, and A. Mohamed, "A review of lithium-ion battery state of charge estimation and management system in electric vehicle applications: Challenges and recommendations," *Renewable and Sustainable Energy Reviews,* vol. 78, pp. 834-854, 2017.

[111] J. Meng, G. Luo, and F. Gao, "Lithium polymer battery state-of-charge estimation based on adaptive unscented Kalman filter and support vector machine," *IEEE Transactions on Power Electronics,* vol. 31, no. 3, pp. 2226-2238, 2015.

[112] P. Zhang, F. Yan, and C. Du, "A comprehensive analysis of energy management strategies for hybrid electric vehicles based on bibliometrics," *Renewable and Sustainable Energy Reviews,* vol. 48, pp. 88-104, 2015.

[113] L. Kumar and S. Jain, "Electric propulsion system for electric vehicular technology: A review," *Renewable and Sustainable Energy Reviews,* vol. 29, pp. 924-940, 2014.

[114] J. Cao and A. Emadi, "A new battery/ultracapacitor hybrid energy storage system for electric, hybrid, and plug-in hybrid electric vehicles," *IEEE Transactions on power electronics,* vol. 27, no. 1, pp. 122-132, 2011.

[115] C.-C. Lin, H. Peng, and J. Grizzle, "A stochastic control strategy for hybrid electric vehicles," in *Proceedings of the 2004 American control conference*, 2004, vol. 5, pp. 4710-4715: IEEE.

[116] Z. Filipi, "Hydraulic and pneumatic hybrid powertrains for improved fuel economy in vehicles," in *Alternative Fuels and Advanced Vehicle Technologies for Improved Environmental Performance*: Elsevier, 2014, pp. 505-540.

[117] J. Peng, H. He, and R. Xiong, "Rule based energy management strategy for a series–parallel plug-in hybrid electric bus optimized by dynamic programming," *Applied Energy,* vol. 185, pp. 1633-1643, 2017.

[118] D. Wang, C. Guan, S. Pan, M. Zhang, and X. Lin, "Performance analysis of hydraulic excavator powertrain hybridization," *Automation in construction,* vol. 18, no. 3, pp. 249-257, 2009.

[119] F. Feng, X. Hu, J. Liu, X. Lin, and B. Liu, "A review of equalization strategies for series battery packs: variables, objectives, and algorithms," *Renewable and Sustainable Energy Reviews,* vol. 116, p. 109464, 2019.

[120] A. Afram, F. Janabi-Sharifi, A. S. Fung, and K. Raahemifar, "Artificial neural network (ANN) based model predictive control (MPC) and optimization of HVAC systems: A state of the art review and case study of a residential HVAC system," *Energy and Buildings,* vol. 141, pp. 96-113, 2017.

[121] Ç. Iris and J. S. L. Lam, "A review of energy efficiency in ports: Operational strategies, technologies and energy management systems," *Renewable and Sustainable Energy Reviews,* vol. 112, pp. 170-182, 2019.
[122] M. Kumar, M. Husian, N. Upreti, and D. Gupta, "Genetic algorithm: Review and application," *International Journal of Information Technology and Knowledge Management,* vol. 2, no. 2, pp. 451-454, 2010.
[123] R. Cheng, *Genetic algorithms and engineering optimization*. Wiley-Interscience, 2000.
[124] M. Gen, R. Cheng, and L. Lin, *Network models and optimization: Multiobjective genetic algorithm approach*. Springer Science & Business Media, 2008.
[125] K. Deb, A. Anand, and D. Joshi, "A computationally efficient evolutionary algorithm for real-parameter optimization," *Evolutionary computation,* vol. 10, no. 4, pp. 371-395, 2002.
[126] J. rey Horn, N. Nafpliotis, and D. E. Goldberg, "A niched Pareto genetic algorithm for multiobjective optimization," in *Proceedings of the first IEEE conference on evolutionary computation, IEEE world congress on computational intelligence*, 1994, vol. 1, pp. 82-87: Citeseer.
[127] N. Srinivas and K. Deb, "Muiltiobjective optimization using nondominated sorting in genetic algorithms," *Evolutionary computation,* vol. 2, no. 3, pp. 221-248, 1994.
[128] M. Nesbeit *et al.*, *Comparative Study on the Differences Between the EU and US Legislation on Emissions in the Automotive Sector: Study*. European Parliament, 2016.
[129] C. A. C. Coello, G. B. Lamont, and D. A. Van Veldhuizen, *Evolutionary algorithms for solving multi-objective problems*. Springer, 2007.
[130] Ö. Yeniay, "Penalty function methods for constrained optimization with genetic algorithms," *Mathematical and computational Applications,* vol. 10, no. 1, pp. 45-56, 2005.
[131] T. Markel *et al.*, "ADVISOR: a systems analysis tool for advanced vehicle modeling," *Journal of power sources,* vol. 110, no. 2, pp. 255-266, 2002.
[132] K. L. Mills, J. J. Filliben, and A. Haines, "Determining relative importance and effective settings for genetic algorithm control parameters," *Evolutionary computation,* vol. 23, no. 2, pp. 309-342, 2015.
[133] C. Segura, C. A. C. Coello, and A. G. Hernández-Díaz, "Improving the vector generation strategy of differential evolution for large-scale optimization," *Information Sciences,* vol. 323, pp. 106-129, 2015.
[134] F. R. Salmasi, "Control strategies for hybrid electric vehicles: Evolution, classification, comparison, and future trends," *IEEE Transactions on vehicular technology,* vol. 56, no. 5, pp. 2393-2404, 2007.
[135] R. M. Jarvis and R. Goodacre, "Genetic algorithm optimization for pre-processing and variable selection of spectroscopic data," *Bioinformatics,* vol. 21, no. 7, pp. 860-868, 2004.
[136] K. Deb, A. Pratap, S. Agarwal, and T. Meyarivan, "A fast and elitist multiobjective genetic algorithm: NSGA-II," *IEEE transactions on evolutionary computation,* vol. 6, no. 2, pp. 182-197, 2002.

[137] T. Bäck, D. B. Fogel, and Z. Michalewicz, *Evolutionary computation 1: Basic algorithms and operators*. CRC press, 2018.
[138] S. Sivanandam and S. Deepa, "Genetic algorithm optimization problems," in *Introduction to genetic algorithms*: Springer, 2008, pp. 165-209.
[139] E. Falkenauer, *Genetic algorithms and grouping problems*. John Wiley & Sons, Inc., 1998.
[140] C. M. Fonseca and P. J. Fleming, "Genetic Algorithms for Multiobjective Optimization: FormulationDiscussion and Generalization," in *Icga*, 1993, vol. 93, no. July, pp. 416-423: Citeseer.
[141] A. Konak, D. W. Coit, and A. E. Smith, "Multi-objective optimization using genetic algorithms: A tutorial," *Reliability Engineering & System Safety,* vol. 91, no. 9, pp. 992-1007, 2006.
[142] K. Deb and J. Sundar, "Reference point based multi-objective optimization using evolutionary algorithms," in *Proceedings of the 8th annual conference on Genetic and evolutionary computation*, 2006, pp. 635-642: ACM.
[143] J. Vasconcelos, J. A. Ramirez, R. Takahashi, and R. Saldanha, "Improvements in genetic algorithms," *IEEE Transactions on magnetics,* vol. 37, no. 5, pp. 3414-3417, 2001.
[144] H. Tamaki, H. Kita, and S. Kobayashi, "Multi-objective optimization by genetic algorithms: A review," in *Proceedings of IEEE international conference on evolutionary computation*, 1996, pp. 517-522: IEEE.
[145] N. Higashi and H. Iba, "Particle swarm optimization with Gaussian mutation," in *Proceedings of the 2003 IEEE Swarm Intelligence Symposium. SIS'03 (Cat. No. 03EX706)*, 2003, pp. 72-79: IEEE.
[146] G. Mao-Guo, J. Li-Cheng, Y. Dong-Dong, and M. Wen-Ping, "Evolutionary multi-objective optimization algorithms," 2009.
[147] K. Deb, L. Thiele, M. Laumanns, and E. Zitzler, "Scalable multi-objective optimization test problems," in *Proceedings of the 2002 Congress on Evolutionary Computation. CEC'02 (Cat. No. 02TH8600)*, 2002, vol. 1, pp. 825-830: IEEE.
[148] I. Rahman, P. M. Vasant, B. S. M. Singh, M. Abdullah-Al-Wadud, and N. Adnan, "Review of recent trends in optimization techniques for plug-in hybrid, and electric vehicle charging infrastructures," *Renewable and Sustainable Energy Reviews,* vol. 58, pp. 1039-1047, 2016.
[149] J. P. Trovão, P. G. Pereirinha, H. M. Jorge, and C. H. Antunes, "A multi-level energy management system for multi-source electric vehicles–an integrated rule-based meta-heuristic approach," *Applied Energy,* vol. 105, pp. 304-318, 2013.
[150] K. Mets, T. Verschueren, W. Haerick, C. Develder, and F. De Turck, "Optimizing smart energy control strategies for plug-in hybrid electric vehicle charging," in *2010 IEEE/IFIP Network Operations and Management Symposium Workshops*, 2010, pp. 293-299: IEEE.
[151] P. Jinhuan, Y. Chengliang, and Z. Jianwu, "Application of genetic algorithm in optimization of control strategy for hybrid electric vehicles," *Chinese Journal of Mechanical Engineering,* vol. 16, no. 07, pp. 87-91, 2005.

[152] K. Sim, S.-M. Oh, C. Namkoong, J.-S. Lee, K.-S. Han, and S.-H. Hwang, "Control strategy for clutch engagement during mode change of plug-in hybrid electric vehicle," *International Journal of Automotive Technology,* vol. 18, no. 5, pp. 901-909, 2017.

[153] R. Xiong, Y. Zhang, J. Wang, H. He, S. Peng, and M. Pecht, "Lithium-ion battery health prognosis based on a real battery management system used in electric vehicles," *IEEE Transactions on Vehicular Technology,* vol. 68, no. 5, pp. 4110-4121, 2018.

[154] L. Lu, X. Han, J. Li, J. Hua, and M. Ouyang, "A review on the key issues for lithium-ion battery management in electric vehicles," *Journal of power sources,* vol. 226, pp. 272-288, 2013.

[155] F. Un-Noor, S. Padmanaban, L. Mihet-Popa, M. N. Mollah, and E. Hossain, "A comprehensive study of key electric vehicle (EV) components, technologies, challenges, impacts, and future direction of development," *Energies,* vol. 10, no. 8, p. 1217, 2017.

[156] S. M. Rezvanizaniani, Z. Liu, Y. Chen, and J. Lee, "Review and recent advances in battery health monitoring and prognostics technologies for electric vehicle (EV) safety and mobility," *Journal of Power Sources,* vol. 256, pp. 110-124, 2014.

[157] M. Berecibar, I. Gandiaga, I. Villarreal, N. Omar, J. Van Mierlo, and P. Van den Bossche, "Critical review of state of health estimation methods of Li-ion batteries for real applications," *Renewable and Sustainable Energy Reviews,* vol. 56, pp. 572-587, 2016.

[158] C. Hu, G. Jain, P. Zhang, C. Schmidt, P. Gomadam, and T. Gorka, "Data-driven method based on particle swarm optimization and k-nearest neighbor regression for estimating capacity of lithium-ion battery," *Applied Energy,* vol. 129, pp. 49-55, 2014.

[159] J. Á. Antón, P. G. Nieto, F. de Cos Juez, F. S. Lasheras, M. G. Vega, and M. R. Gutiérrez, "Battery state-of-charge estimator using the SVM technique," *Applied Mathematical Modelling,* vol. 37, no. 9, pp. 6244-6253, 2013.

[160] S. Malkhandi, "Fuzzy logic-based learning system and estimation of state-of-charge of lead-acid battery," *Engineering Applications of Artificial Intelligence,* vol. 19, no. 5, pp. 479-485, 2006.

[161] Y. Zheng, L. Lu, X. Han, J. Li, and M. Ouyang, "LiFePO4 battery pack capacity estimation for electric vehicles based on charging cell voltage curve transformation," *Journal of power sources,* vol. 226, pp. 33-41, 2013.

[162] J. Xu, B. Cao, Z. Chen, and Z. Zou, "An online state of charge estimation method with reduced prior battery testing information," *International Journal of Electrical Power & Energy Systems,* vol. 63, pp. 178-184, 2014.

[163] H. Dai, X. Wei, Z. Sun, J. Wang, and W. Gu, "Online cell SOC estimation of Li-ion battery packs using a dual time-scale Kalman filtering for EV applications," *Applied Energy,* vol. 95, pp. 227-237, 2012.

[164] D. Simon, "Kalman filtering with state constraints: a survey of linear and nonlinear algorithms," *IET Control Theory & Applications,* vol. 4, no. 8, pp. 1303-1318, 2010.

[165] R. Xiong, H. He, F. Sun, and K. Zhao, "Evaluation on state of charge estimation of batteries with adaptive extended Kalman filter by experiment approach," *IEEE Transactions on Vehicular Technology,* vol. 62, no. 1, pp. 108-117, 2012.
[166] D. Pavković, M. Krznar, A. Komljenović, M. Hrgetić, and D. Zorc, "Dual EKF-based state and parameter estimator for a LiFePO4 battery cell," *Journal of Power Electronics,* vol. 17, no. 2, pp. 398-410, 2017.
[167] S. Yousefizadeh, J. D. Bendtsen, N. Vafamand, M. H. Khooban, T. Dragičević, and F. Blaabjerg, "EKF-based predictive stabilization of shipboard DC microgrids with uncertain time-varying load," *IEEE Journal of Emerging and Selected Topics in Power Electronics,* vol. 7, no. 2, pp. 901-909, 2018.
[168] Y. Fang, R. Xiong, and J. Wang, "Estimation of Lithium-Ion Battery State of Charge for Electric Vehicles Based on Dual Extended Kalman Filter," *Energy Procedia,* vol. 152, pp. 574-579, 2018.
[169] F. Guo, G. Hu, S. Xiang, P. Zhou, R. Hong, and N. Xiong, "A multi-scale parameter adaptive method for state of charge and parameter estimation of lithium-ion batteries using dual Kalman filters," *Energy,* vol. 178, pp. 79-88, 2019.
[170] F. Sun, X. Hu, Y. Zou, and S. Li, "Adaptive unscented Kalman filtering for state of charge estimation of a lithium-ion battery for electric vehicles," *Energy,* vol. 36, no. 5, pp. 3531-3540, 2011.
[171] Z. He, M. Gao, C. Wang, L. Wang, and Y. Liu, "Adaptive state of charge estimation for Li-ion batteries based on an unscented Kalman filter with an enhanced battery model," *Energies,* vol. 6, no. 8, pp. 4134-4151, 2013.
[172] J. Zhang and C. Xia, "State-of-charge estimation of valve regulated lead acid battery based on multi-state Unscented Kalman Filter," *International Journal of Electrical Power & Energy Systems,* vol. 33, no. 3, pp. 472-476, 2011.
[173] S. Gao, M. Kang, L. Li, and X. Liu, "Estimation of state-of-charge based on unscented Kalman particle filter for storage lithium-ion battery," *The Journal of Engineering,* vol. 2019, no. 16, pp. 1858-1863, 2019.
[174] J. Xu, C. C. Mi, B. Cao, J. Deng, Z. Chen, and S. Li, "The state of charge estimation of lithium-ion batteries based on a proportional-integral observer," *IEEE Transactions on Vehicular Technology,* vol. 63, no. 4, pp. 1614-1621, 2013.
[175] A. Barré, B. Deguilhem, S. Grolleau, M. Gérard, F. Suard, and D. Riu, "A review on lithium-ion battery ageing mechanisms and estimations for automotive applications," *Journal of Power Sources,* vol. 241, pp. 680-689, 2013.
[176] H. He, R. Xiong, X. Zhang, F. Sun, and J. Fan, "State-of-charge estimation of the lithium-ion battery using an adaptive extended Kalman filter based on an improved Thevenin model," *IEEE Transactions on vehicular technology,* vol. 60, no. 4, pp. 1461-1469, 2011.
[177] J. K. Barillas, J. Li, C. Günther, and M. A. Danzer, "A comparative study and validation of state estimation algorithms for Li-ion batteries in battery management systems," *Applied Energy,* vol. 155, pp. 455-462, 2015.

[178] R. Xiong, X. Gong, C. C. Mi, and F. Sun, "A robust state-of-charge estimator for multiple types of lithium-ion batteries using adaptive extended Kalman filter," *Journal of Power Sources,* vol. 243, pp. 805-816, 2013.
[179] S. Piller, M. Perrin, and A. Jossen, "Methods for state-of-charge determination and their applications," *Journal of power sources,* vol. 96, no. 1, pp. 113-120, 2001.
[180] G. Plett, "LiPB dynamic cell models for Kalman-filter SOC estimation," in *The 19th international battery, hybrid and fuel electric vehicle symposium and exhibition*, 2002, pp. 1-12: Citeseer.
[181] H. Han, H. Xu, Z. Yuan, and Y. Zhao, "Modeling for lithium-ion battery used in electric vehicles," in *2014 IEEE Conference and Expo Transportation Electrification Asia-Pacific (ITEC Asia-Pacific)*, 2014, pp. 1-5: IEEE.
[182] H. He, R. Xiong, and J. Fan, "Evaluation of lithium-ion battery equivalent circuit models for state of charge estimation by an experimental approach," *energies,* vol. 4, no. 4, pp. 582-598, 2011.
[183] X. Hu, S. Li, and H. Peng, "A comparative study of equivalent circuit models for Li-ion batteries," *Journal of Power Sources,* vol. 198, pp. 359-367, 2012.
[184] W.-Y. Chang, "The state of charge estimating methods for battery: A review," *ISRN Applied Mathematics,* vol. 2013, 2013.
[185] G. Hunt and C. Motloch, "Freedom car battery test manual for power-assist hybrid electric vehicles," *INEEL, Idaho Falls,* 2003.
[186] D. H. Doughty and C. C. Crafts, "FreedomCAR: electrical energy storage system abuse test manual for electric and hybrid electric vehicle applications," Sandia National Laboratories2006.
[187] Y. Hu and S. Yurkovich, "Battery cell state-of-charge estimation using linear parameter varying system techniques," *Journal of Power Sources,* vol. 198, pp. 338-350, 2012.
[188] S. J. Julier and J. K. Uhlmann, "New extension of the Kalman filter to nonlinear systems," in *Signal processing, sensor fusion, and target recognition VI*, 1997, vol. 3068, pp. 182-193: International Society for Optics and Photonics.
[189] B. Ristic, S. Arulampalam, and N. Gordon, *Beyond the Kalman filter: Particle filters for tracking applications*. Artech house, 2003.
[190] M. C. Best, T. Gordon, and P. Dixon, "An extended adaptive Kalman filter for real-time state estimation of vehicle handling dynamics," *Vehicle System Dynamics,* vol. 34, no. 1, pp. 57-75, 2000.
[191] G. Pérez, M. Garmendia, J. F. Reynaud, J. Crego, and U. Viscarret, "Enhanced closed loop State of Charge estimator for lithium-ion batteries based on Extended Kalman Filter," *Applied Energy,* vol. 155, pp. 834-845, 2015.
[192] T. Wang, S. Chen, H. Ren, and Y. Zhao, "Model‐based unscented Kalman filter observer design for lithium‐ion battery state of charge estimation," *International Journal of Energy Research,* vol. 42, no. 4, pp. 1603-1614, 2018.
[193] A. M. Bizeray, S. Zhao, S. R. Duncan, and D. A. Howey, "Lithium-ion battery thermal-electrochemical model-based state estimation using orthogonal collocation and a modified extended Kalman filter," *Journal of Power Sources,* vol. 296, pp. 400-412, 2015.

[194] H. He, H. Qin, X. Sun, and Y. Shui, "Comparison study on the battery SoC estimation with EKF and UKF algorithms," *Energies,* vol. 6, no. 10, pp. 5088-5100, 2013.

[195] C. Liu, W. Liu, L. Wang, G. Hu, L. Ma, and B. Ren, "A new method of modeling and state of charge estimation of the battery," *Journal of Power sources,* vol. 320, pp. 1-12, 2016.

[196] G. L. Plett, "Extended Kalman filtering for battery management systems of LiPB-based HEV battery packs: Part 3. State and parameter estimation," *Journal of Power sources,* vol. 134, no. 2, pp. 277-292, 2004.

# Attachment

**RLS Parmeter identification EKF SOC estimation**

```
clear;clc;
%%% all parameters are estimated using RLS, and SoC estimation uses EKF
load('I');
load('U');
load('time');
load('SOC');
load('R0');
% Input the reference value of experimental data，SOC and R0
%%% noise added
% I1=zeros(1,12580);
% u1=zeros(12580,1);
% for i=1:12580
%       I1(i)=I(i)+normrnd(0,0.0061);
%       u1(i)=U(i)+normrnd(0,0.015);
% end
% I=I1;
% U=u1;
%%% EKF algorithm for Thevenin model
% I_midvalue=zeros(1,12580);
% U_midvalue=zeros(12580,1);
% U_midvalue(1)=U(1);
% I_midvalue(1)=I(1);
% for i=2:1:12580
%       U_midvalue(i)=U(i)*1/(0.1+5)+U_midvalue(i-1)*5/(1+5);
%       I_midvalue(i)=I(i)*1/(0.1+5)+I_midvalue(i-1)*5/(1+5);
% end
% U=U_midvalue; num=length(I); delta_t=1;        %sampling period
%%
%% data preparation，assign initial value
%%
%====================================%
%RC R0 parameter estimation and data processing
lamda_rc=0.98;          %forgetting factor
y=zeros(1,num);                 %terminal voltage
theta_rc=[0.01 0.01 0.0001];          %parameter initialization
P_rc=1e-4*eye(3,3);   %covariance matrix
result_R0=zeros(1,num);
result_R1=zeros(1,num);      result_C1=zeros(1,num);      result_tao1=zeros(1,num);      result_rc
=ones(3,num); result_rc(:,1)=theta_rc';
epsilon=zeros(1,num);          %residual value
true_R1=0.03755*ones(1,num);    %R1truth
true_C1=100*ones(1,num);          %C1truth
true_tao1=3.755*ones(1,num);    %tao1truth
%====================================%
```

```
%SOC estimated data processing
initial_U1=0;
initial_soc=0.933;      %SOCassign initial value
x_soc=[initial_U1;initial_soc];  %state matrix
A_soc=zeros(2,2);
B_soc=zeros(2,1); C_soc=zeros(1,2);
Q_soc=1e-4*eye(2);      %state noise covariance matrix
R_soc=  eye(1)*1e-5;    %observation noise covariance matrix
P_soc=1e-4*eye(2);      %covariance matrix
e_soc=zeros(1,num);     %residual
result_SOC=zeros(1,num); result_SOC(2)=initial_soc;
%%
for      k=3:num
%==============RLS====================%
%RC   R0 parameter iteration process

y(k-1)=U(k-1)-(3.704-1.594*result_SOC(k-1)+20.61*result_SOC(k-1)^2-92.9*result_SOC          (k-
1)^3+208.7*result_SOC(k-1)^4-247*result_SOC(k-1)^5+147.7*result_SOC(k-1)^6-35.0
5*result_SOC(k-1)^7);
fai_rc=[y(k-2)  I(k-1)  I(k-2)];  K_rc=P_rc*fai_rc'/(lamda_rc+fai_rc*P_rc*fai_rc');   epsilon(k-
1)=y(k-1)-fai_rc*theta_rc';  theta_rc=theta_rc+K_rc'*epsilon(k-1);
P_rc=(P_rc-K_rc*fai_rc*P_rc)/lamda_rc;          result_rc(:,k-1)=theta_rc';          result_R0(k-
1)=result_rc(2,k-1);

result_R1(k-1)=(result_rc(3,k-1)+result_rc(1,k-1)*result_rc(2,k-1))/(1-result_rc(1
,k-1));
result_tao1(k-1)=-delta_t/log(result_rc(1,k-1)); result_C1(k-1)=result_tao1(k-1)/result_R1(k-1);
%==============EKF====================%
%SOC iteration process
A_soc(1,1)=exp(-delta_t/result_tao1(k-1)); A_soc(2,2)=1;
B_soc(1)=result_R1(k-1)*(1-exp(-delta_t/result_tao1(k-1))); B_soc(2)=delta_t/(3600*2.3);
C_soc(1)=-1;  x_soc_1=A_soc*x_soc+B_soc*I(k-1);

C_soc(2)=-1.594+41.22*x_soc_1(2)-278.7*x_soc_1(2)^2+834.8*x_soc_1(2)^3-1235*x_soc_
1(2)^4+886.2*x_soc_1(2)^5-245.35*x_soc_1(2)^6;
P_soc_1=A_soc*P_soc*A_soc'+Q_soc;

Voc_soc=3.704-1.594*x_soc_1(2)+20.61*x_soc_1(2)^2-92.9*x_soc_1(2)^3+208.7*x_soc_1(    2)^4-
247*x_soc_1(2)^5+147.7*x_soc_1(2)^6-35.05*x_soc_1(2)^7;
e_soc(k)=U(k)-(Voc_soc+x_soc_1(1)+result_R0(k-1)*I(k));
K_soc=P_soc_1*C_soc'*(C_soc*P_soc_1*C_soc'+R_soc)';  x_soc=x_soc_1+K_soc*e_soc(k);
P_soc=(eye(2)-K_soc*C_soc)*P_soc_1;  result_SOC(k)=x_soc(2); disp(k/num*100);
end
%EKF algorithm
R0_START=result_R0;
R1_START=result_R1;
C1_START=result_C1;
R0_midvalue=zeros(1,num);
R1_midvalue=zeros(1,num);
C1_midvalue=zeros(1,num);
R0_midvalue(1)=result_R0(1);
R1_midvalue(1)=result_R1(1);
```

```
C1_midvalue(1)=result_C1(1);
for i=2:1:10000
R0_midvalue(i)=result_R0(i)*0.1/(0.1+9)+R0_midvalue(i-1)*9/(0.1+9);
R1_midvalue(i)=result_R1(i)*0.1/(0.1+9)+R1_midvalue(i-1)*9/(0.1+9);
C1_midvalue(i)=result_C1(i)*0.1/(0.1+9)+C1_midvalue(i-1)*9/(0.1+9);
end result_R0=R0_midvalue; result_R1=R1_midvalue; result_C1=C1_midvalue;
result_R0(num)=result_R0(num-1);
result_R1(num)=result_R1(num-1);
result_C1(num)=result_C1(num-1);
result_tao1=result_R1.*result_C1;
result_R0_erro_RLS=abs(R0-result_R0);    %R0error identification
result_R1_erro_RLS=abs(true_R1-result_R1);      %R1      error      identification
result_C1_erro_RLS=abs(true_C1-result_C1);      %C1      error      identification
result_tao1_erro_RLS=abs(true_tao1-result_tao1);      %tao1   error   identification
result_SOC_erro_RLS=abs(SOC-result_SOC);      %SOC errorestimation
%%
%results in figure
%%
figure(1);
plot(time,R0,time,result_R0);
xlabel('time/s','FontSize',14);
ylabel('R0','FontSize',14);
legend('model','estimate');
title('R0 comparison of estimated value and the true value');
grid;
figure(2);
plot(time,true_R1,time,result_R1);
xlabel('time/s','FontSize',14);
ylabel('R1','FontSize',14);
legend('model','estimate');
title('R1 comparison of estimated value and the true value ');
grid;
figure(3);
plot(time,true_C1,time,result_C1);
xlabel('time/s','FontSize',14);
ylabel('C1','FontSize',14);
legend('model','estimate');
title('C1 comparison of estimated value and the true value ');
grid;
figure(4);
plot(time,true_tao1,time,result_tao1);
xlabel('time/s','FontSize',14);
ylabel('tao1','FontSize',14);
legend('model','estimate');
title('tao1 comparison of estimated value and the true value ');
grid; figure(5);
plot(time,SOC,time,result_SOC);
xlabel('time/s','FontSize',14);
```

```
ylabel('SOC','FontSize',14);
legend('model','estimate');
title('SOC comparison of estimated value and the true value ');
grid;
```

**Improved SoC estimation**

```
clear;clc;
%%% using RLS identify R0,using AKF identify the polarization parameters R1 and C1， using
EKF estimate SOC load('I');
load('U');
load('time');
load('SOC');
load('R0');      %input the experimental data， reference value of SOC and R0
%noise added
% I1=zeros(1,12580);
% u1=zeros(12580,1);
% for i=1:12580
%       I1(i)=I(i)+normrnd(0,0.0061);
%       u1(i)=U(i)+normrnd(0,0.015);
% end
% I=I1;
% U=u1;
%%%EKF algorithm
% I_midvalue=zeros(1,12580);
% U_midvalue=zeros(12580,1);
% U_midvalue(1)=U(1);
% I_midvalue(1)=I(1);
% for i=2:1:12580
%       U_midvalue(i)=U(i)*0.1/(0.1+0.00005)+U_midvalue(i-
1)*0.00005/(0.1+0.00005);
%       I_midvalue(i)=I(i)*0.1/(0.1+0.00005)+I_midvalue(i-
1)*0.00005/(0.1+0.00005);
% end
% U=U_midvalue; num=length(I); delta_t=1;        %sampling period
%%
%%data praperation， initial value assignment
%%
%=====================================%
% estimation data processing of R0 %
I_r0=zeros(1,num); U_r0=zeros(1,num);
for  i=2:1:num
I_r0(i)=I(i)-I(i-1);
U_r0(i)=U(i)-U(i-1);
end
P_r0 =  10^6;      % covariance matrix
lamda=0.98;       % forgetting factors
theta_r0=0.15*ones(1,num);%R0initial value
result_R0 =theta_r0(1)*ones(1,num); delta_deadzone=0;
% threshold values of dead zone
```

```
%==================================%
%RC data processing of parameter estimation
y=zeros(1,num);
ku=24;% homogenization coefficient of the voltage
ki=-1/min(I);     % homogenization coefficient of the current
theta_rc=[0.01  0.01  0.0001];        % assign the initial value of the parameters
P_rc=1e-5*eye(3,3);                   % covariance matrix
Rv_rc =  eye(1)*1e-5;      % covariance matrix of observation noise
result_R1=zeros(1,num);
result_C1=zeros(1,num);
result_tao1=zeros(1,num);
result_rc =ones(3,num);
result_rc(:,1)=theta_rc';
epsilon=zeros(1,num);     % error of the model
epsilon1=zeros(1,num);    % residual values
true_R1=0.02*ones(1,num);%R1truth value
true_C1=1000*ones(1,num);%C1truth value
true_tao1=20*ones(1,num);%tao1truth value
%==================================%
%SOC estimation data processing
initial_U1=0;
initial_soc=0.8;          %SOCassign initial values
x_soc=[initial_U1;initial_soc];% state matrix
A_soc=zeros(2,2);
B_soc=zeros(2,1);
C_soc=zeros(1,2);
Q_soc=1e-4*eye(2);        % covariance matrix of state noise
R_soc=  eye(1)*1e-5;      % observation matrix of state noise
P_soc=1e-4*eye(2);        % covariance matrix
e_soc=zeros(1,num);       % residual
result_SOC=zeros(1,num);
%%
for       k=2:num
%=============RLS=====================%
%R0 iterative process
if abs(I_r0(k))>delta_deadzone K_r0(k)=(P_r0*I_r0(k))/(lamda+I_r0(k)^2*P_r0);
else  K_r0(k)=0;  end
theta_r0(k)          =          theta_r0(k-1)+K_r0(k)*(U_r0(k)-theta_r0(k-1)*I_r0(k));          P_r0=(1-
K_r0(k)*I_r0(k))*P_r0/lamda;
result_R0(k)= theta_r0(k);

%================EKF==================%
%SOC iterative process
A_soc(1,1)=exp(-delta_t/result_tao1(k-1));  A_soc(2,2)=1;
B_soc(1)=result_R1(k-1)*(1-exp(-delta_t/result_tao1(k-1))); B_soc(2)=delta_t/(3600*2.3);
C_soc(1)=-1;  x_soc_1=A_soc*x_soc+B_soc*I(k-1);
C_soc(2)=-1.594+41.22*x_soc_1(2)-278.7*x_soc_1(2)^2+834.8*x_soc_1(2)^3-1235*x_soc_
1(2)^4+886.2*x_soc_1(2)^5-245.35*x_soc_1(2)^6;
P_soc_1=A_soc*P_soc*A_soc'+Q_soc;

Voc_soc=3.704-1.594*x_soc_1(2)+20.61*x_soc_1(2)^2-92.9*x_soc_1(2)^3+208.7*x_soc_1(     2)^4-
247*x_soc_1(2)^5+147.7*x_soc_1(2)^6-35.05*x_soc_1(2)^7;
```

```
e_soc(k)=U(k)-(Voc_soc+x_soc_1(1)+result_R0(k)*I(k));
K_soc=P_soc_1*C_soc'*(C_soc*P_soc_1*C_soc'+R_soc)'; x_soc=x_soc_1+K_soc*e_soc(k);
P_soc=(eye(2)-K_soc*C_soc)*P_soc_1; result_SOC(k)=x_soc(2);
%==============AKF====================%
%RC identification of iterative process

y(k)=U(k)-(3.704-1.594*result_SOC(k)+20.61*result_SOC(k)^2-92.9*result_SOC(k)^3+20
8.7*result_SOC(k)^4-247*result_SOC(k)^5+147.7*result_SOC(k)^6-35.05*result_SOC(k)^ 7)-
I(k)*result_R0(k);
if k==2
epsilon(1)=0.0001; end
fai_rc=[ku*y(k-1) ki*I(k-1) epsilon(k-1)]; K_rc=P_rc*fai_rc'/(Rv_rc+fai_rc*P_rc*fai_rc');
epsilon1(k)=ku*y(k)-fai_rc*theta_rc';
% The coefficients of the U1 and U2 are estimated here, so the error expression here
should be the sum of U1 and U2
theta_rc=theta_rc+K_rc'*epsilon1(k);
epsilon(k)=ku*y(k)-fai_rc*theta_rc'+ fai_rc(3)*theta_rc(3);% epsilon here represents U2
Rw=((P_rc*fai_rc')*fai_rc*P_rc)/(Rv_rc+fai_rc*P_rc*fai_rc');
P_rc=P_rc-K_rc*fai_rc*P_rc+Rw;
result_rc(:,k)=theta_rc';
result_R1(k)=ki*result_rc(2,k)/(ku*(1-result_rc(1,k)));

result_C1(k)=ku*delta_t*(result_rc(1,k)-1)/(ki*result_rc(2,k)*log(result_rc(1,k)));
    result_tao1(k)=result_R1(k)*result_C1(k);
disp(k/num*100)
end
```

```
% EKF algorithm
R0_START=result_R0;
R1_START=result_R1;
C1_START=result_C1;
R0_midvalue=zeros(1,num);
R1_midvalue=zeros(1,num);
C1_midvalue=zeros(1,num);          R0_midvalue(1)=result_R0(1);          R1_midvalue(1)=result_R1(1);
C1_midvalue(1)=result_C1(1); for  i=2:1:10000
R0_midvalue(i)=result_R0(i)*0.1/(0.1+20)+R0_midvalue(i-1)*20/(0.1+20);
R1_midvalue(i)=result_R1(i)*0.1/(0.1+20)+R1_midvalue(i-1)*20/(0.1+20);
C1_midvalue(i)=result_C1(i)*0.1/(0.1+20)+C1_midvalue(i-1)*20/(0.1+20);
end result_R0=R0_midvalue;  result_R1=R1_midvalue;  result_C1=C1_midvalue;
result_tao1=result_R1.*result_C1;                    result_R0_erro_AKF=abs(R0-result_R0);
result_R1_erro_AKF=abs(true_R1-result_R1);           result_C1_erro_AKF=abs(true_C1-
result_C1);                                  result_tao1_erro_AKF=abs(true_tao1-result_tao1);
result_SOC_erro_AKF=abs(SOC-result_SOC);
%%
% Results in figure
%%
figure(1);
plot(time,R0,time,result_R0);
xlabel('time/s','FontSize',14);
ylabel('R0','FontSize',14);
legend('model','estimate');
title('R0 comparison of estimated value and the true value ');
grid;
figure(2);
plot(time,true_R1,time,result_R1);
xlabel('time/s','FontSize',14);
ylabel('R1','FontSize',14);
legend('model','estimate');
title('R1 comparison of estimated value and the true value ');
grid;
figure(3);
plot(time,true_C1,time,result_C1);
xlabel('time/s','FontSize',14);
ylabel('C1','FontSize',14);
legend('model','estimate');
title('C1 comparison of estimated value and the true value ');
grid;
figure(4);
plot(time,true_tao1,time,result_tao1);
xlabel('time/s','FontSize',14);
ylabel('tao1','FontSize',14);
legend('model','estimate');
title('tao1 comparison of estimated value and the true value ');
grid;
figure(5);
plot(time,SOC,time,result_SOC);
xlabel('time/s','FontSize',14);
```